NEW METHODS OF MASS ANALYSIS WITH QUADRUPOLES WITH ADDED OCTOPOLE FIELDS

by

ANNIE MORADIAN

B.Sc., Sharif University of Technology, 1994
M.Sc., University of British Columbia, 2002

A THESIS SUBMITTED IN PARTIAL FULFILMENT OF
THE REQUIREMENTS FOR THE DEGREE OF

DOCTOR OF PHILOSOPHY

in

THE FACULTY OF GRADUATE STUDIES

(Chemistry)

THE UNIVERSITY OF BRITISH COLUMBIA

December 2007

Abstract

Mass selective axial ejection of ions and mass analysis with a stability island with linear quadrupoles with added octopole fields are described. With mass selective axial ejection, quadrupoles with 2.0% and 2.6% added octopole fields have been tested and compared to a conventional quadrupole. The effects of trapping ions at different q values, excitation voltage, scan direction, balanced and unbalanced rf voltages on the rods, and dc applied between the rods have been investigated. The highest scan speeds and highest resolution are obtained with resonant excitation and ejection at high q ($q = 0.8$). With axial ejection, the quadrupole with a 2.0% added octopole field provides mass resolution and ejection efficiencies similar to a conventional rod set. Quadrupole, dipole and simultaneous dipole-dipole excitation between the x and y rod pairs were compared and no advantage was found with quadrupole or dipole-dipole excitation. The effects of scan speed were investigated and a resolution at half height of about 1600 is possible at scan speeds up to 5000 Th/s.

Mass analysis using islands of stability was investigated with a quadrupole with 2.0% added octopole field. The island of stability is formed with auxiliary excitation. The experiments confirm the predictions of the simulations. With the resolving dc applied to the quadrupole so that the Mathieu parameter a>0, conventional mass analysis with applied rf and dc and no auxiliary excitation is possible. In this case use of an island of stability yields similar peak shape and resolution. However with the polarity of the resolving dc reversed so that a<0, only very low resolution can be obtained; the added octopole prevents conventional mass analysis. By using a stability island when a<0, the resolution is substantially improved.

Table of Contents

List of Tables

List of Figures

List of Symbols and Abbreviations

Symbol or Abbreviation	Definition
rf	Radio frequency
dc	Direct current
3-D	Three dimensional
ESI	Electrospray ionization
MALDI	Matrix assisted laser desorption ionization
$R_{1/2}$	Resolution at half peak height
LIT	Linear ion trap
FTICR	Fourier transform ion cyclotron resonance
LC	Liquid chromatography
MS	Mass spectrometry
TOF	Time of flight
MS/MS	Mass spectrometry/mass spectrometry
2-D	Two dimensional
RIT	Rectilinear ion trap
MSAE	Mass selective axial ejection
Q0	Quadrupole ion guide
Q1	First quadrupole
Q2	Collision cell
Q3	Third quadrupole

DAC	Digital to analog converter
MCS	Multichannel scaler
CEM	Channel electron multiplier
GUI	Graphic user interface
QPS	Quadrupole power supply
CAD	Collisionally activated dissociation
CPS	Counts per second
U	Direct current voltage
V	Radio frequency voltage
x, y, z	Cartesian co-ordinates
Ω	Angular frequency
r_0	Field radius
z	Number of charges
e	Electron charge
m	Ion mass
t	Time
a, q	Mathieu parameters
α', α''	Integration Constants
u_0	Initial velocity
$\dot{u}_0$	Initial radial velocity
β	Function of a and q parameters
ω_u	Ion oscillation frequency

m/z	Mass to charge ratio
n	Number of rf cycles
h	Constant for each stability region
d	Distance from the end of the rods
ω_{ex}	Quadrupole excitation frequency
K	Quadrupole excitation resonance order
A_N	Dimensionless amplitude of the electric potential multipole
N	The electric potential multipole order
r_{norm}	Normalization radius
$\mathrm{Re}[f(\zeta)]$	Real part of the complex function $f(\zeta)$
R_y, R_x	Radius of y-pole and x-pole pairs
Th/s	Thomson per second
IG	Ionization gauge
PG	Pirani gauge
E_0	Initial ion kinetic energy
E	Ion kinetic energy after collisions
C_D	Drag coefficient
A	Collision cross section
n	Gas number density
m_1	Ion mass
m_2	Collision gas mass
l	Length that an ion travels

Φ_{FF}	Potential in the fringing region
$E_{z,quad}$	Axial component of the electric field
$E_{z,lens}$	Electric field of the exit lens
$\langle E_z \rangle_{rf}$	Averaged total axial field
V_{eff}	Effective potential
ω_0	Secular frequency
$\Delta\omega$	Frequency shift
V'	Amplitude of quadrupole excitation voltage
ν	Ratio of angular frequencies of excitation to drive rf
q'	Ratio of excitation voltage to rf voltage
A,B,C,D	Stability islands

Acknowledgement

My graduate years in Don Douglas' lab have been one of the best experiences in my life. Don is the best advisor and teacher I could have wished for. I'm grateful to Don for his commitment to helping see my project through to its final completion, and his equally generous and wise guidance during every step of the work from experiments to publishing papers. I also thank Don for prompt reading of this thesis with lots of comments and advice.

I would like to express my gratitude to my supervisory committee members, especially Dr. Michael Blades for his help throughout my studies and for review of this thesis. I'm grateful to all members of Chemistry mechanical and electronic engineering services for their help especially Dave Tonkin for his technical expertise and great assistance with quadrupole power supply electronics.

I gratefully acknowledge NSERC and SCIEX through an Industrial chair for financial support of this research. I would also like to acknowledge Dr. Jim Hager and Dr. Bruce Collings from MDS-SCIEX for their helpful comments and suggestions throughout the course of this research.

I express my gratitude to Douglas' lab former and present members for their help and support throughout my studies in the lab. My heartfelt thanks go to Chuanfan for assisting me through first stages of my experiments and for always being ready to help. I would like to thank Xianzhen for initiating the simulation studies of "Stability islands for quadrupoles with added octopole fields", which provided me the opportunity to investigate them experimentally. I thank Winnie (Z.) for calculating the stability boundary that was needed for my paper and thesis. I'm grateful to Milica, Kevin,

Dedication

To Ara, Beaina and Lara

and in loving memory of my father Ardzrooni Moradian.

Chapter 1 Introduction

In 1989 the Nobel Prize in Physics was awarded one half to Norman Ramsey, for the invention of the separated oscillatory fields method and its use in the hydrogen maser and other atomic clocks, and one half jointly to Hans Dehmelt and Wolfgang Paul, for the development of ion trapping techniques. The first experiments on trapping ions were performed by Paul and his collaborators in the 1950s [1, 2], who showed that ions with different mass to charge ratios could be separated by a four-pole static (dc) electric field with a superimposed radio frequency field. This was developed into a standard method for mass separation, now widely used, the quadrupole mass filter. The three-dimensional (3-D) quadrupole ion trap, also included in Paul's original patent [3], was first developed as a mass selective detector by Fischer in 1959 [4].

This work was representative of a turning point in the development of ion traps and the technology associated with them. The 3-D quadrupole ion trap and its linear counterpart, the quadrupole mass filter became extremely useful instruments. Over the past two decades, the development of soft ionization techniques such as electrospray ionization (ESI) [5] and matrix-assisted laser desorption ionization (MALDI) [6] have turned mass spectrometry into a powerful method for the characterization of biological molecules. A flourishing industry has been developed around these instruments and the demand for higher performance systems has driven research in this area. Today, high precision mass spectrometry has become a billion-dollar industry, with a vast and expanding market in the biomedical and pharmaceutical sectors.

1.1 Theory and background

1.1.1 Quadrupole Mass Filter

The basics of quadrupole mass filter operation including the quadrupole potential
and ion motion, have been described in detail by Dawson [7], and March and Hughes [8].
A quadrupole field is produced by a set of four parallel hyperbolic rods. Many mass
filters employ circular rods instead of hyperbolic rods due to the difficulty of
manufacturing hyperbolic rods to high precision [7]. This introduces slight perturbations
to the pure quadrupole field but it has been shown that these are insignificant near the
axis of the beam [9] and can be minimized with the proper selection of the rod radius r.

A constant direct current (dc) voltage U and a radio frequency (rf) voltage $V \cos \Omega t$
are applied to the rods as shown in Figure 1.1.

$+ (U - V\cos\Omega t)$

$- (U - V\cos\Omega t)$
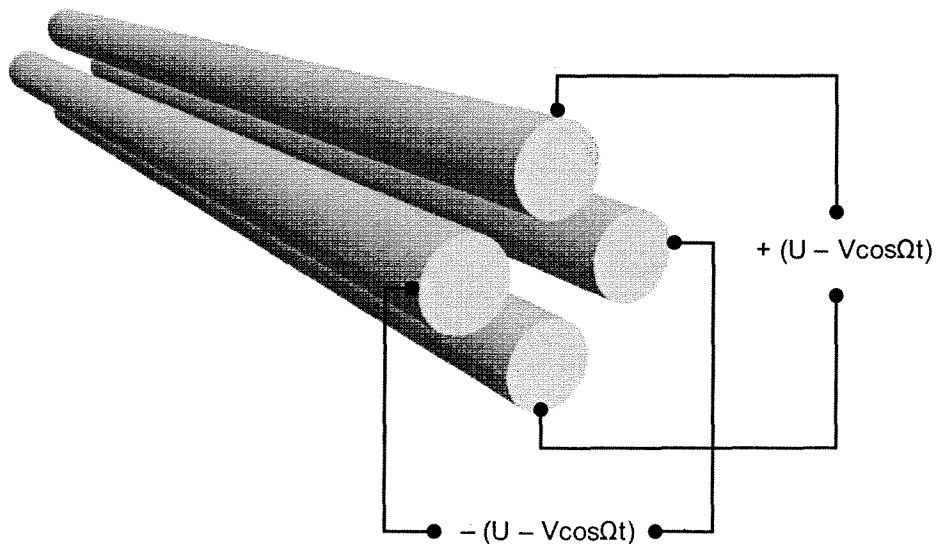
Figure 1.1 Conventional circular quadrupole rods in a quadrupole mass filter.

The potential $\Phi(x,y)$ at any point inside the quadrupole is described by

$$\Phi(x, y, t) = \frac{x^2 - y^2}{r_0^2} \Phi(t) \tag{1.1}$$

where x and y are Cartesian co-ordinates and r_0, the field radius, is the distance from the

centre of the quadrupole to any rod. The potential $\Phi(t)$ is given by:

$$\Phi(t) = (U - V \cos \Omega t) \tag{1.2}$$

where U is the dc voltage, V is the zero-to-peak amplitude of the rf voltage applied

from each quadrupole rod to ground, and Ω is the angular frequency of the rf voltage.

The ion motions in the x and y directions in the quadrupole field are independent and

are determined by the following equations:

$$\ddot{x} + \frac{2ze}{mr_0^2}(U - V \cos \Omega t)x = 0$$
$$\ddot{y} - \frac{2ze}{mr_0^2}(U - V \cos \Omega t)y = 0 \tag{1.3}$$

where $\ddot{x} = \frac{d^2 x}{dt^2}$ and $\ddot{y} = \frac{d^2 y}{dt^2}$, z is the number of charges on an ion, e is the electron

charge, m is the ion mass and t is time. These differential equations can be written with

dimensionless parameters, and are then the Mathieu equation:

$$\frac{d^2 u}{d\xi^2} + (a_u - 2q_u \cos 2\xi)u = 0 \tag{1.4}$$

$$\xi = \frac{\Omega t}{2} \quad u = x \text{ or } y \tag{1.5}$$

By comparison with equation (1.3) a and q are:

$$a_x = -a_y = \frac{8eU}{mr_0^2 \Omega^2} \qquad q_x = -q_y = \frac{4eV}{mr_0^2 \Omega^2} \tag{1.6}$$

The Mathieu equation has been discussed in many books [7, 8], and only the solutions to the equation will be presented here:

$$u(\xi) = \alpha' e^{\mu\xi} \sum_{n=-\infty}^{\infty} C_{2n} e^{2ni\xi} + \alpha'' e^{-\mu\xi} \sum_{n=-\infty}^{\infty} C_{2n} e^{-2ni\xi} \qquad (1.7)$$

where α' and α'' are integration constants depending on the initial position u_0 and initial radial velocity $\dot{u}_0$. The constants C_{2n} and μ depend only on the a and q values. Therefore the nature of an ion's motion is determined by its (a,q) value, regardless of the initial conditions.

The solutions represented by equation (1.7) can further be divided into two subcategories; stable and unstable. Stable solutions arise only when μ is imaginary such that $\mu = i\beta$ and β is not an integer. In this case ions oscillate in the $x - y$ plane with limited amplitudes and pass through the quadrupole field without hitting the rods. Integer values of β form a series of solutions, which are periodic and unstable. Ion amplitudes grow exponentially in the x, y or in both directions, and ions are lost. Substituting $\mu = i\beta$ into equation (1.7) and simplifying it, gives the equation of motion for stable ions

$$u(\xi) = A \sum_{n=-\infty}^{\infty} C_{2n} \cos(2n+\beta)\xi + B \sum_{n=-\infty}^{\infty} C_{2n} \sin(2n+\beta)\xi \qquad (1.8)$$

where $A = \alpha' + \alpha''$ and $B = i(\alpha' + \alpha'')$. From equation (1.8), β is an important parameter that determines the oscillation frequencies of the ions. The relation of β to (a,q) is given by the recursion formula [8].

4

$$\beta^2 = a + \cfrac{q^2}{(2+\beta)^2 - a - \cfrac{q^2}{(4+\beta)^2 - a - \cfrac{q^2}{(6+\beta)^2 - a - \cdots}}}$$

$$+ \cfrac{q^2}{(\beta-2)^2 - a - \cfrac{q^2}{(\beta-4)^2 - a - \cfrac{q^2}{(\beta-6)^2 - a - \cdots}}} \qquad (1.9)$$

When $q \leq 0.4$, β can be approximated by [7, 8].

$$\beta^2 \approx a + \frac{q^2}{2} \qquad (1.10)$$

For given rf and dc voltages, ions in a quadrupole field have oscillatory motion (according to equation (1.8)) that is characterized by frequencies unique to their mass-to-charge ratio. The lowest frequency is termed the "secular frequency". Higher frequencies are not simple harmonics of the lowest frequency. These frequencies can be calculated using equation (1.11).

$$\omega_u = (2n + \beta)\frac{\Omega}{2}, n = 0, \pm 1, \pm 2, \ldots \qquad (1.11)$$

The stability of solutions to the Mathieu equation depends on the a and q values. Therefore a diagram in the a and q plane consists of regions of stability and instability. This is called the stability diagram. In the stability diagram there is an infinite number of regions where ion motion is stable in both the x and y directions. The first overlapping region for combined x and y stability with iso-β lines is plotted in Figure 1.2. Because a_x and a_y (and equally q_x and q_y) are symmetric with respect to the origin of the $a - q$ plane as shown in equation (1.5), the first quadrant is enough to represent the entire

stability diagram. Almost all commercial quadrupole mass filters are operated in first stability region.

1.2 Mass Analysis with Quadrupole rod sets

1.2.1 Mass Filter

In a quadrupole mass analyzer for fixed values of r_0, Ω, U and V all ions with the same m/z have the same operating point ((a,q) values) in the stability diagram. Since a/q is equal to $2U/V$ and does not depend on m, all masses lie along an operating or scan line a/q = constant as shown in Figure 1.2. By scanning the U and V values along this line (i.e. with a fixed ratio), ions with different masses will be transmitted in sequence of mass-to-charge ratio and will reach a detector in order, producing a mass spectrum. Each operating line with specific slope (a/q) corresponds to one resolution setting. In theory the resolution is calculated from the width of the stability region for each of the operating lines. By increasing the U/V ratio, the operating line approaches closer to the tip of the stability region and only a small range of m/z values will be stable. This corresponds to higher resolution. Usually resolution is defined as $R_{1/2} = m/\Delta m_{1/2}$, where $\Delta m_{1/2}$ refers to a measured peak width at half height.
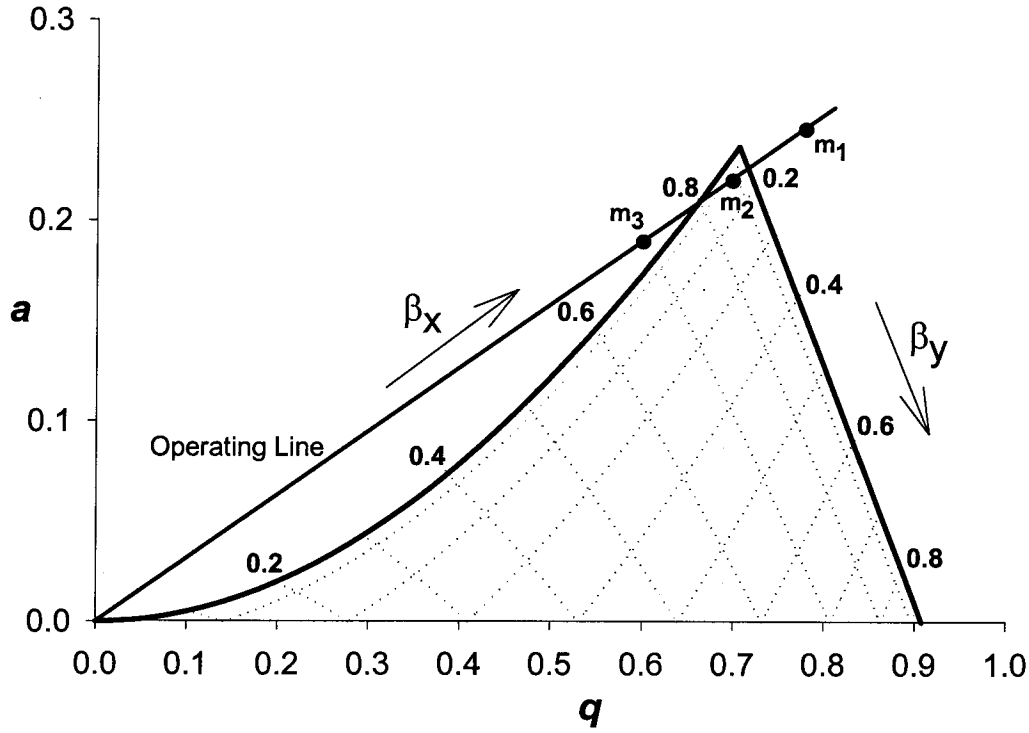
Figure 1.2 First stability region of a quadrupole mass filter with iso-β lines. The points m_1, m_2, m_3 represent ions with different masses on an operating line.

In theory, as the operating line in the stability diagram approaches the tip of the stability region, the resolution will increase without limit. In these theoretical treatments two assumptions have been made which cannot be completely valid. These are (1) all ions stay in the quadrupole field for a sufficiently long time, i.e. the rods are infinitely long and (2) circular rods give an adequate approximation to a hyperbolic field. Considering the finite length of a real quadrupole rod set, the resolution can be expressed as [10, 11]

$$R_{1/2} = n^2 / h \qquad (1.12)$$

where n is the number of rf cycles that ions spend in the quadrupole field and the h is a constant that is different for different stability regions. For the first stability region $h \approx 10 - 20$ [11].

An rf − only quadrupole is a quadrupole which is operated with no dc voltage between the pole pairs ($U = 0$). This allows the largest possible range of mass-to-charge ratios to pass through the quadrupole. An ion has a stable trajectory when $0 \leq q_u \leq 0.908$. Therefore, if V and Ω are fixed, there is a lower limit to the mass-to-charge ratio of ions which have stable trajectories in the quadrupole. Consequently rf − only quadrupoles are used as ion guides and high pass mass filters.

1.2.2   Fringing fields

In a practical quadrupole mass analyzer the field does not end abruptly at the ends of the quadrupole rods. Usually an end plate is positioned at a distance, d, from the ends of the rods. Penetration of the potential of the end plate into the region between the quadrupole rods will cause a distortion of the ideal quadrupole field. The field in this region is referred to as the fringing field [12]. The quadrupole field grows from zero (on the end plates) to its full value within the quadrupole. In the fringing field region, x, y, and z motion become coupled and the ion motion is very complicated. Normally, this fringing field might be expected to extend over a distance of at least the order of the field radius of the quadrupole rod set [13].

Brubaker first recognized the importance of fringing fields in the mass filter. From his studies two qualitative results were drawn for the effects of the entrance fringing fields on the amplitudes of ion motion [12].

1. Short fringing fields give lower amplitudes of ion oscillation, than perfect fields for both the x and y directions.

2. Long fringing fields (many rf cycles) give large amplitudes of oscillation in the y direction. In this case fringing field defocuses the ions.

Brubaker described the fringing field with a linear model and proposed a "delayed dc ramp" to avoid the defocusing of the ions caused by the large y trajectories [12]. With operation in the first stability region and without the "delayed dc ramp", there is an optimum fringing field length of about two rf cycles which was verified theoretically and experimentally to increase the transmission [14, 15]. Hunter and McIntosh modeled the fringing field and concluded that an exponential function describes the field more realistically than a linear model [16].

All the above-mentioned studies for fringing fields were focused on the entrance fringing fields for rf/dc mass filters. Little work has been done to investigate the effect of the exit fringing fields on ion motion. Brinkman reported the first rf-only operation of a quadrupole rod set as a mass spectrometer. The method was based on the exit fringing fields [17]. Others expanded on his work. Details of this will be given in Section 1.5.2.

1.3 Quadrupole Ion Traps

1.3.1 The Three Dimensional Quadrupole Ion Trap

The quadrupolar field in a 3-D ion trap can be produced by three hyperbolic electrodes, a ring electrode in the middle with cap electrodes on each end as shown in

Figure 1.3. The electric potential $\Phi(x, y, z)$ in the 3-D ion trap is similar to the electric

potential in the quadrupole mass filter

$$\Phi(x, y, z, t) = \frac{(x^2 + y^2 - 2z^2)}{r_0^2} \Phi(t)$$

(1.13)
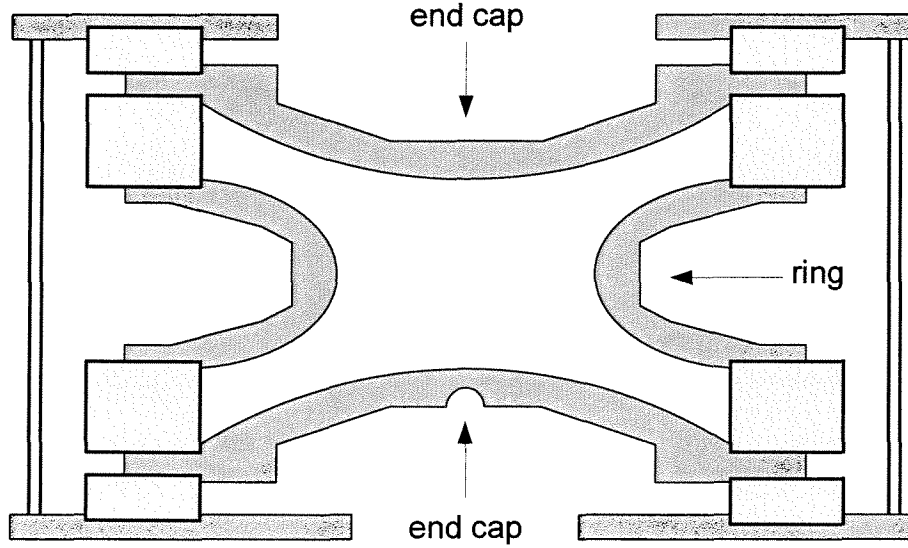
Figure 1.3 Schematic cross section of a 3-D quadrupole ion trap.

where x, y and z are Cartesian co-ordinates and r_0 is the distance from the centre of the

trap to the ring electrode. The potential $\Phi(t)$ is given by equation 1.2. The quadrupole

field still depends on the square of the distance from a reference point, in this case the

center of the trap. Ion motion in the x, y and z directions are independent. The

equations of motion can be written and solved as in section 1.1. In the quadrupole ion

trap, the rf voltage is typically applied to the ring electrode and the two end cap

electrodes are typically held at ground potential. Within a selected range of m/z ratios,

determined by the applied voltages, the device traps ions within the space bounded by the

electrodes. Typically, a mass spectrum is produced by scanning the applied rf voltages to

eject ions in the axial direction through an end cap opening, sequentially, with increasing m/z ratio, for detection [8]. This scanning method is called a "mass selective instability scan" and it was introduced by Stafford and co-workers in the first commercial 3-D ion trap [18]. Because the mass-to-charge ratio of the ion that is ejected from the ion trap is directly proportional to the rf voltage (for a given r_0 and Ω) an upper limit to the mass-to-charge range of the ion trap is imposed by the magnitude of the rf voltage that can be applied to the electrodes.

1.3.2 Linear Ion Traps

. In 1969 Church described "ring" ion trap and "racetrack" ion trap geometries [19]. Bending the two-dimensional quadrupole rod electrodes into a circle formed the ring ion trap. He was able to trap and measure the presence of H^+ ($m/z=1$) and $^3He^+$ ($m/z = 3$).

If a linear (two – dimensional) quadrupole is operated with rf-only voltages, and if stopping potentials are applied to electrodes at the ends of the quadrupole, ions of a broad range of m/z can be trapped in the quadrupole. Ions are confined in the radial (x, y) direction by the quadrupolar potential and in the axial (z) direction by the electrostatic potentials at the ends of the quadrupole.

There are several advantages associated with the trapping of ions in linear ion traps [20]. Since there is no quadrupole field along the z-axis, linear traps have higher injection efficiencies than 3-D traps. The larger volume of the linear trap compared to a 3-D trap enables storage of more ions without space charge effects. This can be attributed to strong focusing of ions along the centerline of the linear ion trap, increasing the volume occupied by ions.

Linear ion traps first were used purely as traps. In 1988 Dolonikowski and co-workers [21] trapped ions in an rf – only quadrupole to study ion/molecule reactions. After reactions occurred in the linear ion trap, these ions were pulsed into a quadrupole mass filter for mass analysis. Beaugrand et al. [22] also studied the chemical equilibria and kinetic and thermodynamic parameters of selected ion/molecule reactions in a triple quadrupole instrument where the central quadrupole served as a linear ion trap and collision cell. This technique has subsequently been used by others to study ion/molecule chemistry [23]. At about the same time, Prestage et al. [24] presented a novel linear ion trap, which increased the number of laser cooled atomic ions that could be trapped in a fixed volume with minimal effects from Doppler shifting caused by the rf confining fields. The success of this instrument has led to the application of linear ion traps in frequency standards experiments [25].

Linear ion traps have been used in combination with other mass analyzers. The external accumulation of ions in multipole traps allows higher trapping efficiency and space charge capacity. Thus they can be used as storage devices with ion manipulation capabilities. Douglas [26] described coupling a linear trap to a 3-D ion trap. In this instrument the linear trap can be used to pre-concentrate analyte ions and remove unwanted ions prior to mass analysis in the 3-D trap [27, 28]. This improves the duty cycle significantly and allows detection of trace analyte ions in a large excess of other ions.

The storage capabilities of multipole and linear ion traps provide a convenient method for interfacing a continuous ion source like electrospray ionization (ESI) to Time of Flight (TOF) [29] and Fourier Transform Ion Cyclotron Resonance (FTICR) mass

spectrometers. The ion trap acts as a front-end storage device for these instruments. Ions are continuously stored as they are injected into the trap, and are subsequently pulsed out into these mass analyzers for detection. Hardman et al. [30] showed that an "electrostatic" trap mass analyzer (Orbitrap) can be coupled to a continuous electrospray ion source by accumulating ions in an rf – only quadrupole prior to their injection into the "electrostatic" trap.

Liquid Chromatography/ Mass Spectrometry (LC/MS) analysis with FTICR instruments become more practical with the increase in sensitivity made possible by accumulation of electrosprayed ions in a linear octopole ion trap, prior to their transfer to the FTICR cell [31]. In some instruments linear hexapole or segmented linear quadrupole ion traps are used for the same purpose. A linear trap can be used for dissociation or hydrogen exchange of ions prior to ion detection by FTICR [20, 32].

By coupling linear ion traps to TOF mass spectrometers, different research groups also used traps for ion isolation and fragmentation through ion excitation [33-35]. This adds tandem mass spectrometry capability to TOF mass spectrometers.

1.3.3 The Secular Frequency and Resonant Excitation

Ions in a linear quadrupole ion trap can be resonantly excited when an auxiliary ac voltage at a frequency ω_{ex} is added to the drive rf frequency Ω. The amplitude of the excitation voltage is several orders of magnitude lower than the amplitude of the drive rf voltage. Dipole and quadrupole excitation are possible. For dipole excitation, the auxiliary ac is applied between two opposite poles of the quadrupole rod set and the electric field of the excitation is constant (independent of position). Resonance takes

place when the frequency ω_{ex} coincides with one of the secular frequencies given by equation (1.11).

Quadrupole excitation occurs when the auxiliary ac is applied to all four poles of a quadrupole rod set. In this case the magnitude of the electric field is linearly proportional to the coordinates x and y. Sudakov et al. [36] calculated the excitation frequencies of ions with quadrupole excitation and showed ions are excited when

$$\omega_{ex} = |l + \beta_u| \frac{\Omega}{K} \tag{1.14}$$

where $K = 1,2,3,...$, $l = 0,\pm1 \pm2,...$ and $\beta_u = \beta_x$ or β_y.

When ions are resonantly excited, the amplitude of their oscillation begins to increase. If the amplitude of the supplemental ac voltage is sufficient, ions can be ejected from the ion trap. This process is referred to as resonant ejection. Resonant excitation of ions has been effectively used for isolating, fragmenting and mass-selectively ejecting ions at different q values in quadrupole ion traps.

1.4 Quadrupoles with Added Multipoles

1.4.1 Multipole Potentials

A potential, Φ, within a region free of charge, must satisfy Laplace's equation

$$\nabla^2 \Phi = 0 \tag{1.15}$$

Multiple solutions to the Laplace equation that satisfy the above condition exist. If each individual solution is considered to be a component (or fraction) of the overall potential, one additional solution is the linear combination of the component potentials. The

component potentials may be expressed in terms of a multipole expansion. In Cartesian coordinates a two-dimensional electric potential $\Phi(x, y, t)$ can be expanded in multipoles, $\phi_N(x, y)$, as [20] :

$$\Phi(x, y, t) = V(t) \sum_{N=0}^{\infty} A_N \phi_N(x, y) \qquad (1.16)$$

where $V(t)$ is a time dependent amplitude of the potential, and A_N is the dimensionless amplitude of the multipole $\phi_N(x, y)$. The term $\phi_N(x, y)$ can be derived from:

$$\phi_N(x, y) = \mathrm{Re}\left[\frac{x + iy}{r_{norm}} \right]^N \qquad (1.17)$$

where r_{norm} is a normalization radius and $\mathrm{Re}[f(\zeta)]$ means the real part of the complex function $f(\zeta)$, $(\zeta = x + iy)$ and $i^2 = -1$ [37]. Analytical expressions for the multipoles in Cartesian coordinates are given by Szilagyi [38]. The term $\phi_0(x, y) = 1$ represents a constant potential that is independent of x and y, $\phi_1(x, y)$ corresponds to a linear dipole potential, $\phi_2(x, y)$ is a quadrupole potential, $\phi_3(x, y)$ is a hexapole potential, $\phi_4(x, y)$ is an octopole potential, etc. The values of the coefficients A_N depend on boundary conditions. For a system of four parallel rods, these can be calculated with the method of effective charges [39]. Even order multipoles (N=2, 4, 6 ...) are symmetric with respect to reflection in the x and y axes and odd order multipoles (N=1, 3, 5 ...) are antisymmetric with respect to reflection in the x axis and symmetric with respect to reflection in the y axis. In quadrupoles, electric field components higher than those from ϕ_2 are non-linear and are termed higher order fields. A summary of the multipoles is given in Table 1.1.

Table 1.1 Summary of the potential for each multipole.

Multipole	Potential
Dipole (N=1)	$\phi_1 = x / r_{norm}$
Quadrupole (N=2)	$\phi_2 = (x^2 - y^2) / r_{norm}^2$
Hexapole (N=3)	$\phi_3 = (x^3 - 3xy^2) / r_{norm}^3$
Octopole (N=4)	$\phi_4 = (x^4 - 6x^2y^2 + y^4) / r_{norm}^4$
Decapole (N=5)	$\phi_5 = (x^5 - 10x^3y^2 + 5xy^4) / r_{norm}^5$
Dodecapole (N=6)	$\phi_6 = (x^6 - 15x^4y^2 + 15x^2y^4 - y^6) / r_{norm}^6$

1.4.2 Higher Order Fields in 3-D and Linear Ion Traps

Non-idealities in the electrode geometry of the quadrupole mass analyzer and the 3-D quadrupole ion trap result in the presence of higher order fields. These non-idealities result from the necessary truncation of the electrodes in the quadrupole mass filter and the quadrupole ion trap, using round rods for the quadrupole mass filter, holes in the end caps of ion traps for ion injection or ejection, and imperfections in the machining and manufacturing of electrodes [40].

Several groups have studied the effects of mechanical errors on quadrupole mass filter performance and recommended that quadrupole mass filters be manufactured to very high precision to avoid field distortions [10, 13, 41]. Other studies showed that it is

possible to adjust the contributions of higher multipoles in a round rod quadrupole mass filter by changing the ratio of rod radius, r, to field radius, r_0, to optimize the peak shape and resolution [9, 42-44]. In all these studies the amplitudes of the higher multipole fields were about 10^{-3} or less of the quadrupole term.

The presence of higher order fields in the 3-D quadrupole ion trap has both advantages and disadvantages. In the early years of research, ion losses, shifts in the observed mass-to charge-ratio of ions and some "ghost" peaks (peaks observed at spurious mass-to-charge values) were attributed to the effects of higher order fields [8]. Later work showed methods to minimize all of these phenomena by intentionally introducing weak higher order multipole fields [45-47]. Franzen [48, 49] described the distortions caused by these fields mathematically. Addition of a positive even-order higher multipole to the field in the z direction of a 3-D trap introduces non-linear effects; the most important is a shift of the frequency of ion oscillation with the amplitude of oscillation [49]. Later it was recognized that higher order fields could be beneficial to ion trap performance because they increase the ion fragmentation efficiency in mass spectrometry/mass spectrometry (MS/MS) experiments, and give higher resolution in ion ejection or isolation [48, 50, 51]. These benefits might also be expected to apply to linear quadrupole traps.

Douglas and coworkers have investigated methods to add higher order multipole fields to linear quadrupoles [52-54]. They have shown that higher order multipole fields can be added to linear round rod quadrupoles by modifications to the electrode dimensions. These modifications to the quadrupole rod structures were calculated to produce 2 – 12% octopole or hexapole fields while the amplitudes of other higher

multipoles remained relatively small. The percentage of added multipole field is calculated from

$$\frac{A_N}{A_2} \times 100 = \% \ \text{Added multipole} \qquad (1.17)$$

where N is the order of the multipole. Therefore with a 2.0% added octopole field

$\frac{A_4}{A_2} = 0.02$. Octopole fields of 2 – 4% were added to linear quadrupoles by making one

pair of rods greater in diameter than the other pair [52, 53] and 2 – 12% hexapole fields

were added by rotating two rods (the y rods) towards an x rod [54, 55]. In both cases all

rods are equally spaced from the central axis. Figure 1.4 shows a photograph of a round

rod quadrupole with a 2.0% added octopole field. The ratio $\frac{R_y}{R_x}$ is 1.22. Surprisingly it

was also found that conventional mass analysis with applied dc and rf fields is possible

with this rod set, despite the large field distortions, provided the dc is applied with the

correct polarity, i.e. the positive dc applied to the smaller rods [56]. The positive dc on

the smaller rods is for positive ions but is reversed for negative ions. Experiments where

trapped ions were resonantly excited to induce fragmentation showed that a rod set with a

4% added octopole field can give higher efficiency in dissociating ions than a

conventional rod set [57], especially at pressures of 1×10^{-4} Torr or less.
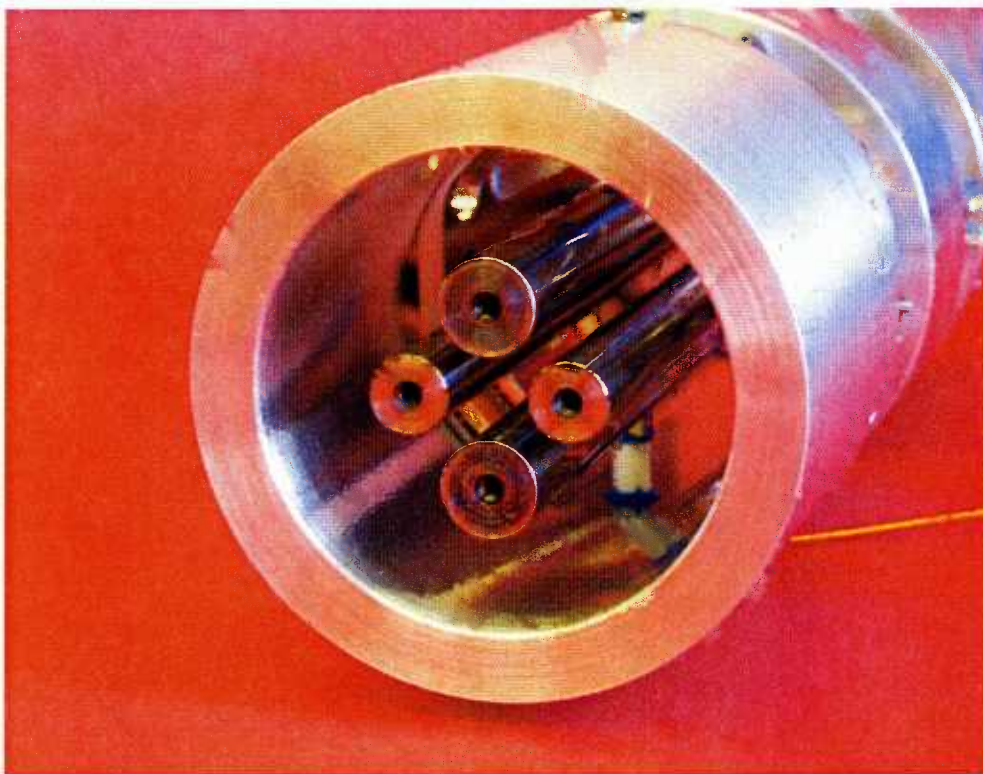
Figure 1.4 A round rod quadrupole with a 2.0% added octopole field.

1.5 Linear Ion Traps as Mass Analyzers

Despite the previously described advantages of 2-D ion traps in hybrid instruments, only recently have they been commercialized as stand-alone mass analyzers. Some earlier examples of 2-D ion traps used as mass spectrometers are presented here briefly.

Senko et al. demonstrated image current detection with Fourier transform (FT) analysis with a 2-D trap, which utilized independent detection electrodes between the quadrupole rods [58]. Although the results were promising, space charge effects were found to limit the sensitivity. Welling et al. demonstrated two alternative methods for mass selective instability scans in a linear quadrupole ion trap [59]. The first relied on the manipulation of the q-value of the trapped ions and provided fast scans of about 1000

Th/s with low resolution ($m / \Delta m \approx 6$) that was relatively mass independent over large mass ranges of 20-1000 Th. The second used frequency swept parametric excitation to eject ions between the quadrupole rods. With lower scan rates of 15-30 Th/s, resolution of 800 at m/z 130 was obtained.

1.5.1 Linear Quadrupole Ion Trap with Radial Ejection

Bier and Syka described several forms of linear and circular 2-D ion traps that can be used as mass spectrometers [60]. They suggested using the mass selective instability scan mode of operation (with resonance excitation) for scanning these 2-D ion traps. Schwartz and co-workers [61] described a working instrument based on this. They used hyperbolic rods cut in three sections as their quadrupole linear ion trap. Ions are confined radially in the central section by the rf voltage and axially by dc potentials on the end sections. The ion trap section has slots cut into the x-rods through which ions are ejected. These slots cause imperfections in the fields. To improve performance, the x-rods were moved 0.75 mm beyond their normal spacing. Dipole excitation with auxiliary ac voltages on the x rods is used to isolate, excite, and eject ions. Ions are isolated by a broadband waveform with frequencies 5-500 kHz, with a notch at the frequency of the target ions usually at q = 0.83. For MS/MS, ions are activated by resonant excitation at a q of $0.25 - 0.35$. The detection efficiency can be doubled because a detector can be put on either side of the 2-D ion trap to detect ions that are ejected through either x-rod. A mass resolution of greater than 30,000 at a scan rate of 27 Th/s was obtained and MS[4] was demonstrated [61].

In 2004 Cooks and co-workers introduced a miniaturized linear ion trap called a rectilinear ion trap (RIT) [62]. The RIT has two pairs (x, y) of rectangular electrodes, where the x-rectangles have slots in them for ion ejection. The RIT uses two flat electrodes at either end of the ion trap to confine ions. The rf signal is applied between the x, y electrode pairs and this field is approximately quadrupolar, at least near the trap center. The basics of operation of the RIT are very similar to the linear quadrupole ion trap described by Schwartz and co-workers [61]. The demonstrated capabilities of the RIT include tandem mass spectrometry, a mass resolution of around 1000, and a m/z range of 650 Th.

1.5.2 Linear Quadrupole Ion Trap with Axial Ejection

In 1970's and 1980's research was focused on developing an rf-only mass spectrometer, which would overcome some of the shortcomings of rf/dc mass filters. Among these, the important inherent problem of conventional rf/dc mass filters was considered the dependence of achievable resolution and good peak shape on the precision of the quadrupole field [63]. Another limitation of the mass filter is the discrimination by the fringing fields against slow ions (high mass or low energy) [13] and also the loss of transmission, which occurs at high resolution.

The rf-only quadrupoles offer some promise with regard to the above limitations. Without the dc component of the fringing fields at the entrance of the quadrupole there is no discrimination against high mass ions. This means that the transmission efficiency is independent of mass for any particular instrument. Its exact geometry should be less important since ions spend less time near the outer limits of the field [64].

Brinkmann reported the first rf-only operation of a linear quadrupole as a mass spectrometer [17]. Brinkmann made the fundamental point that ions leaving the quadrupole rods could gain considerable energy from the fringing fields. This is possible when the ions travel through the exit region with considerable radial amplitude where the fringing fields are close to their maximum. This condition applies when the rf-only quadrupole rod set operates with ions at the edge of the stability diagram. Ions on the verge of instability near $q = 0.908$ acquire large axial energies from the exit fringing fields; therefore they can be distinguished from stable ions with lower q-values, which oscillate near the field axis. An energy filtering technique based on a variable spherical retarding field was used for mass separation. Brinkmann obtained a resolution in excess of 1000 at $m/z = 500$, demonstrating ten times higher transmission than that obtained with the same instrument with rf/dc operation mode [17].

Others expanded Brinkmann's work in developing rf-only mass spectrometers by changing the geometry of the retarding field and accelerating ions at the ion exit [65-69] All reported the advantages of high tolerances for mechanical imperfections in the quadrupole rod assembly, higher sensitivity and higher resolution compared to conventional rf/dc mass analyzers. However there were some differences in the results presented by two groups of researchers regarding the dependence of resolution on the number of rf cycles ions spend in the quadrupole rod sets [64, 70]. It was clear that the rf-only mode operation was not well understood and further research was needed for its complete characterization.

In 1999 Hager [71] reported a new method of mass scanning with linear quadrupoles, called mass selective axial ejection (MSAE). This method is a further

development of Brinkmann's idea of using fringing fields at the exit of the quadrupole rod set. In the fringing field, the otherwise independent ion motions in x, y and z are coupled. The quadrupole is operated in rf-only mode with ions flowing continuously into the quadrupole. The end plate or exit lens is set at a stopping potential relative to the quadrupole rod offset. Within the fringing field, radial energy of the ions is converted into axial energy and ions can surmount the exit lens barrier to reach a detector. Ions with larger radial displacements in the fringing field receive greater axial kinetic energy increases than ions with smaller radial displacements. Thus some form of radial excitation of ions is required for ion ejection.

The same concept was then used for axial ejection of ions trapped in a linear quadrupole [72]. Experiments were done with a triple quadrupole mass spectrometer like that shown in Figure 1.5. Fragment ions produced in tandem mass spectrometry were trapped in the collision cell (Q2) or the last mass analyzing quadrupole (Q3), by applying stopping potentials to lenses at the ends of the quadrupoles. For axial ejection, ions were excited at their resonant frequencies by applying fixed-frequency auxiliary ac voltages to two or all four rods of a quadrupole or to the exit lens. By scanning the trapping rf amplitude, ions of different m/z ratios came into resonance and were ejected to produce a mass spectrum.
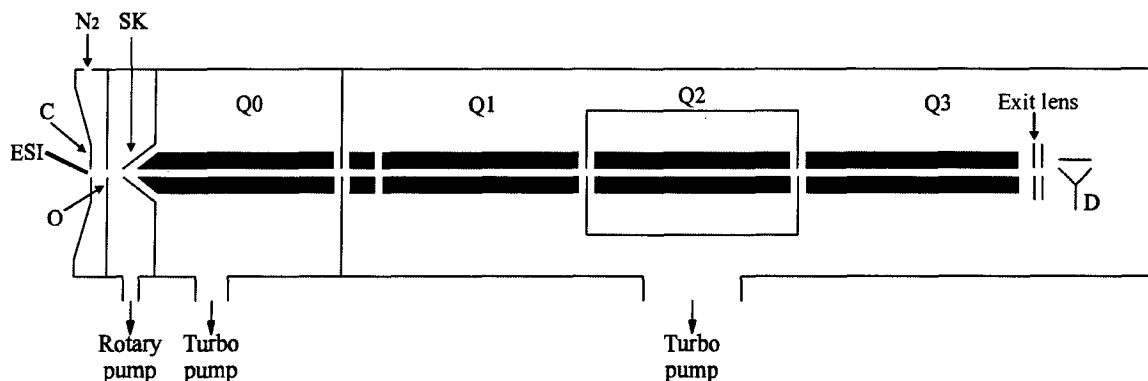
Figure 1.5 Schematic of the ESI-triple quadrupole mass spectrometer system: N_2, nitrogen curtain gas; C, curtain plate; O, sampling orifice; SK, skimmer; Q0, rf only quadrupole; Q1, mass-analyzing quadrupole; Q2, collision cell; Q3, mass-analyzing quadrupole; D, detector.

The resolution at half height ($R_{1/2}$) with axial ejection from Q2 (4×10^{-4} Torr) was typically about 1000 at m/z 609 with a scan rate of 1000 Th/s. Slower scans, 5 Th/s, resulted in much higher resolution, $R_{1/2}$= 6000 at m/z 609. It was found that, because of the lower pressure in Q3 (3×10^{-5} Torr), $R_{1/2}$= 6000 could be obtained at the higher scan speed of 100 Th/s. Experiments with fragment ions formed in Q2 and then trapped and axially ejected from Q3 showed 16 times greater sensitivity than a conventional triple quadrupole MS/MS scan [72].

Hopfgartner and co-workers [73] were first to employ this method in the drug discovery field. They described an increase in the sensitivity of MS/MS by a factor of 60 compared to running MS/MS in the normal triple quadrupole mode on the same instrument. Leblanc et al. [74] described applications of MSAE to proteomics. They showed that the combination of the triple quadrupole based MS/MS scans with the very sensitive ion trap product MSAE scans allows rapid identification of peptides at low concentrations. It was demonstrated that with this instrument it was possible to conduct a

variety of ion processing steps prior to performing a mass scan. Thus with a triple

quadrupole system, trapping in Q2 or Q3 with MSAE allows higher sensitivity in

MS/MS, but at the same time, all the scan modes of a triple quadrupole system such as

single reaction monitoring, multiple reaction monitoring and neutral loss scans are still

possible. These latter scan modes are not possible with other 2D or 3D trap systems.

Higher energy fragmentation patterns are generated with this instrument, leading to a

richer product ion spectrum without an inherent low mass cut off.

1.5.3   Islands of Stability

Sudakov et al. [36] derived the first and higher order resonance conditions for ions

confined in a quadrupole ion trap with auxiliary quadrupole excitation (equation (1.14)).

They also showed that auxiliary quadrupole excitation changes the stability conditions of

an ion in the quadrupole field. Collings and Douglas [75] demonstrated excitation of ions

in a pressurized linear ion trap (1.8-7.3 mTorr) using higher order resonances (up to

K=6).

With quadrupole excitation in a linear ion trap, multiple bands of instability appear

on the stability diagram due to the first and higher order resonances. Thus multiple

ejection conditions can occur for the same ion at a single excitation frequency [36].

Konenkov and co workers [76] showed that if the quadrupole excitation is applied to

an rf/dc mass filter, where the quadrupole field is characterized by the two different

values of β_x and β_y, then ions can be excited in two different directions (x, y) with the

same excitation frequency. As the excitation amplitude increases, the stability diagram

splits into a number of stable areas or islands, each with its own operating point and mass

resolving abilities. They investigated this phenomena theoretically and experimentally [76]. Using an inductively coupled plasma mass spectrometer, experimental mapping of the stability diagram confirmed the theory. Peak shape enhancements (i.e. low mass tail suppression) were demonstrated by measuring Ar ion isotope abundances. An operating point was found that gave almost a 1000 times increase in abundance sensitivity for $m/z = 39$ in the presence of $^{40}Ar^+$.

In principle using islands of stability for mass analysis in a quadrupole mass filter may be considered as a new method of mass analysis. Recently this method of mass analysis was investigated theoretically [77] and experimentally [78] for a quadrupole with an added octopole field. Details will be given in Chapter 6 of this thesis.

1.6 Outline of This Thesis

The results from the MS/MS performance and operation of quadrupoles with added octopole fields as mass filters are of interest for the following reasons. First, despite the added octopole field, the quadrupole rod sets can give resolution comparable to that of a conventional rod set, provided the dc voltage is applied with the correct polarity [56]. Second, the rod sets show increased fragmentation efficiency compared to conventional rod sets [57], especially at pressures of $1x10^{-4}$ Torr or less. Some triple quadrupole instruments operate both as a conventional triple quadrupole MS/MS system and with trapping of ions in Q3. Therefore the last quadrupole, Q3, when operated as mass filter must be capable of at least unit mass resolution. When the same Q3 rod set is used for trapping and resonant excitation, the mass scanning method is axial ejection. Therefore if a quadrupole rod set with added octopole field that provides higher MS/MS efficiencies

can also operate as a mass filter with axial ejection, then in principle it can replace the Q3 conventional rod set in such instruments. Investigation of this hypothesis is a major focus of this thesis.

Chapter 2 describes the instrumentation, experimental apparatus, sample preparation and methods of data acquisition and analysis used in this study. Chapter 3 describes the results obtained with MSAE of ions from a conventional linear quadrupole, and a quadrupole with 2.6% added octopole field without trapping. The focus of Chapter 4 is the MSAE of ions from a conventional linear quadrupole ion trap operating with different excitation modes. Chapter 5 describes, the results of the MSAE of ions from a linear quadrupole ion trap with 2.0 % added octopole field operating with different excitation modes. Some of the work described in this chapter is submitted to the Journal of the American Society for Mass Spectrometry for publication. Chapter 6 describes experimental investigation of mass analysis with islands of stability with a quadrupole mass filter with a 2.0% added octopole field. Most of Chapter 6 has been published in reference 78. Chapter 7 is a summary with suggestions for future work.

Chapter 2   Experimental Methods

2.1   Instrument

Experiments were done with the system shown in Figure 2.1. Details are given in Table 2.1. Ions formed by pneumatically assisted electrospray ionization pass through a 1.5 mm diameter aperture in a curtain plate, through a dry N_2 curtain gas, and enter the vacuum system through a 0.125 mm diameter orifice in the tip of a cone. Ions then travel through a quadrupole ion guide, Q_0 where they are collisionally cooled. The 20 cm long Q0 rods are capacitively coupled through two 25 pF capacitors to the Q1 drive rf voltage. The mass filter quadrupole, Q1, is separated from the ion guide by the entrance lens plate with a 1.0 mm diameter aperture. Ions leave Q1 and pass through two additional lenses, the first with a mesh covered 9 mm aperture, and the second with an open 9 mm aperture. The mesh-covered lens is referred to as exit lens 1 and the open aperture lens as exit lens 2. Exit lens 1 is located 3.5 mm from the end of the Q1 and exit lens 2 is separated from exit lens 1 by a 5 mm spacer.

The pumping system consists of two turbo pumps and two rotary pumps. A Pirani gauge and an ion gauge are used to measure the pressures in the first and second chambers. Rotary pump 1 and turbo pump 1 for the first vacuum stage have speeds of 7.14 and 360 L/s respectively. Rotary pump 2 and turbo pump 2 for the second vacuum stage have speeds of 6.67 and 50 L/s respectively. With these arrangements the first vacuum stage pressure was measured as 10×10^{-3} Torr and the second vacuum stage 3.2×10^{-5} Torr. This experimental set up was used for non-trapping experiments.
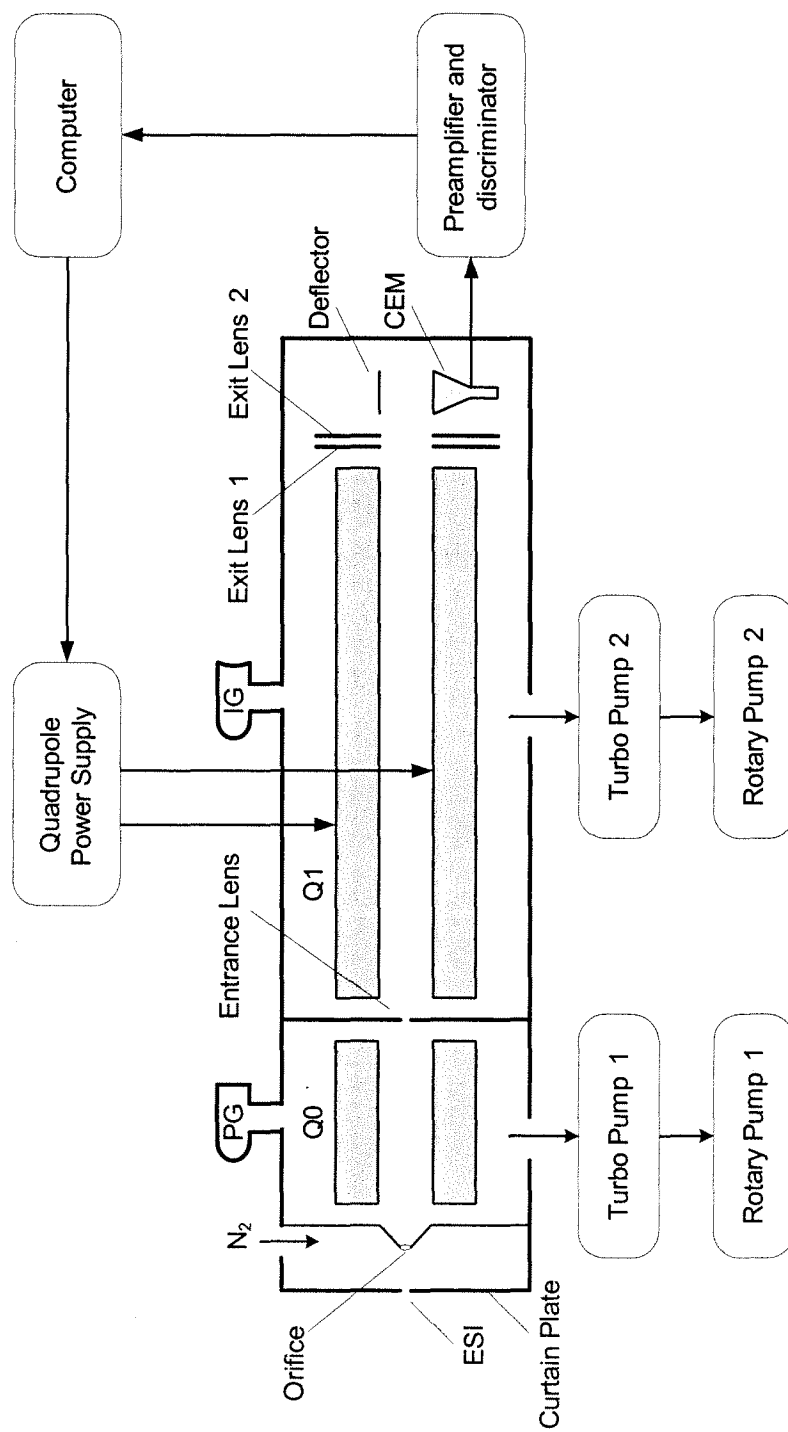
Figure 2.1 Schematic of the single quadrupole instrument. ESI, electrospray ionization; Q0, ion guide; Q1, quadrupole mass filter; IG, ionization gauge; PG, Pirani gauge; CEM, channel electron multiplier.

Table 2.1 Instrumentation.

Syringe pump	Harvard Apparatus, model 22, (South Natick, MA)
Quadrupole rod set	MDS SCIEX (Concord ON)
Quadrupole power supply	MDS SCIEX (Concord ON) API 3+
Pumping system	Rotary pump 1, Leybold (Germany) Trivac 25B
	Rotary pump 2, Leybold (Germany) Trivac 16A
	Turbo pump 1, Leybold (Germany) Turbovac 361
	Turbo pump 2, Leybold (Germany) Turbovac 50
Detector	Burle Electro-Optics channeltron electron multiplier, model 4822B, (Sturbridge, MA)
Computer	Power Macintosh 7100/80
Ion gauge	Kurt J. Lesker (Clairton, PA.), model G100F
Pirani gauge	Leybold (Germany), Thermovac TM230
Preamplifier	Ortec/Ametek (Oakridge, TN) 9302 fast amplifier
Discriminator	Tennelec TC453 constant fraction discriminator (leading edge mode)

For trapping experiments the entrance aperture diameter was changed to 3.0 mm to mimic the conditions used by Hager [72]. With this it was necessary to change the turbo pump 2 to a 360 L/s pump in order to maintain the second chamber pressure around 1.6×10^{-5} Torr. At the same time the cone orifice diameter was also changed to 0.0875 mm, which decreased the pressure in the Q0 chamber to 8×10^{-3} Torr.

The quadrupole power supply operates at 1.20 MHz. It has a maximum rf output voltage V_{max} (the zero to peak voltage between each rod and ground) of 5000 V and a maximum dc output voltage U (the voltage between each rod and ground) of $\pm$ 840 V. When operating the quadrupole as a mass filter, the quadrupole power supply was controlled by software (Tune 2.2, SCIEX, Concord, ON). The quadrupole power supply was connected to a Macintosh computer (PowerMac 7100/80) through a digital-to-analog converter (DAC). The mass ranges set in the software are converted to mass command voltages by the DAC. These mass command voltages set the required rf voltage levels to scan the quadrupole power supply. This method of scanning was used when the instrument was operated as an rf/dc mass filter and as an rf only quadrupole for MSAE experiments without trapping. To perform MSAE experiments in trapping mode the quadrupole power supply was modified to have an external scanning option and also modified so that low-level resolving dc ($< \pm$ 15) could be added between the rod pairs of the quadrupole. For external scanning, the drive rf voltages were set by an external analog voltage ramp provided by a multichannel scaler (MCS-pci, Ortec-Ametek, Oak Ridge, TN, USA). The ramp output voltage range is computer adjustable within the range of 0 to +10 V. The MCS was also used to collect spectra and is plugged into the pci-bus of an Intel Pentium III computer.

A channel electron multiplier (CEM) is used as the ion detector. The CEM is a continuous dynode device, which can detect either positive or negative ions. For positive ion detection the input is generally at a high negative potential and the output is at ground. An ion striking the input face of the CEM starts an electron cascade, resulting in a current pulse (30 ns, $\sim 10^{-6}$ A), which is amplified by a preamplifier. A discriminator is used to distinguish pulses caused by ions from background noise. The ion signal is recorded in ion counting mode. The recorded data are the total number of ions detected at different m/z ratios. The computer calculates the count rate (ions/s) for each scan and these data are used to construct a mass spectrum over a certain m/z range. To reduce the pick up of rf voltage by the detector circuit, two 1830 pF capacitors were added to the detector circuit as shown in Figure 2.2.
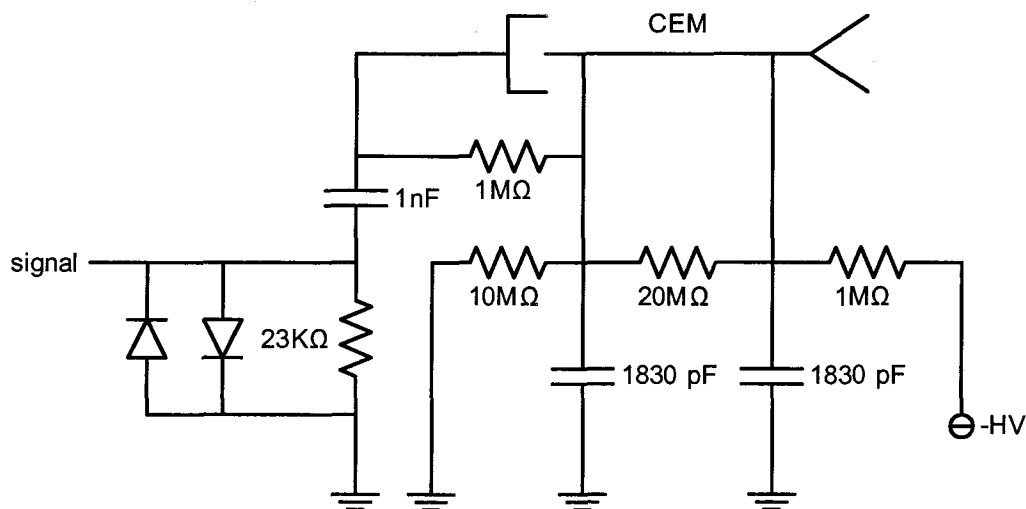
Figure 2.2 Circuit diagram of the detector circuit for detection of positive ions.

Experiments were done with a conventional quadrupole rod array with a field radius $r_0 = 4.17$ mm, and ratio of rod radius to field radius $R/r_0 = 1.126$, and with quadrupoles with

2.0 or 2.6 % added octopole fields with field radii $r_0 = 4.5$ mm (Figure 2.3). The octopole

fields are added by making the radius of the y rods, R_y, greater than the radius of the x rods,

R_x ($R_x = r_0$). For the quadrupole with a 2.0% added octopole field, $R_y/R_x = 1.220$, and for

the 2.6% added octopole $R_y / R_x = 1.300$. Table 2.2 shows the dimensionless amplitudes of

the even multipoles up to N = 10 calculated as described in Ref [35].

Table 2.2 Multipole amplitudes.

Rod set	A_0	A_2	A_4	A_6	A_8	A_{10}
Conventional	0.0000	1.00149	0.0000	0.001267	0.0000	-0.002431
2% Octopole	-0.02029	0.9994	0.01961	0.003281	0.0008604	-0.002345
2.6% Octopole	-0.02638	1.0014	0.02567	0.001286	0.0009514	-0.002358
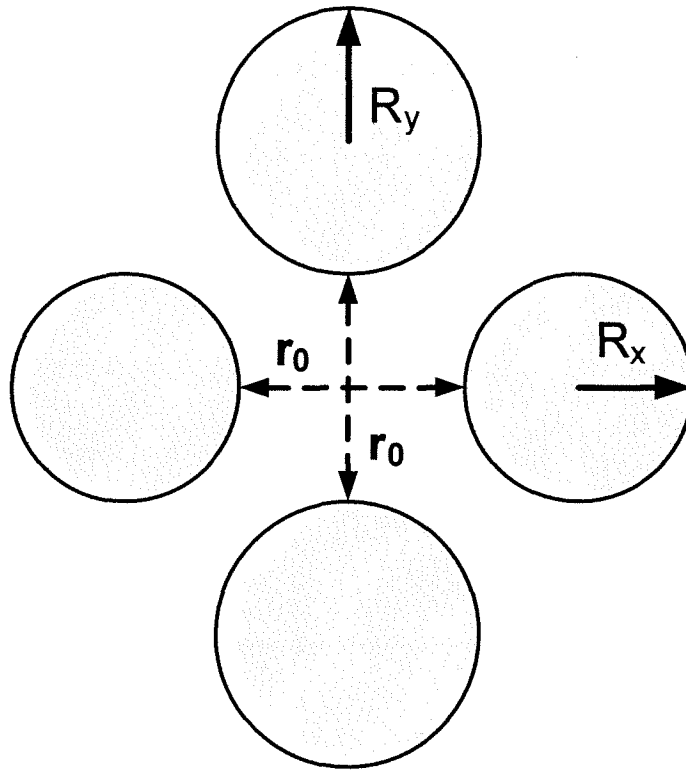
Figure 2.3 Cross sections of the electrodes of a quadrupole with an added octopole field.

2.2 Linear Ion Trap Experimental Set Up

The single-quadrupole instrument shown in Figure 2.1 was modified to operate as a

linear ion trap. A block diagram of the apparatus as used for trapping experiments is provided

in Figure 2.4. The entrance and exit lenses were connected to a two-channel arbitrary

waveform generator, (PC Instruments AWG-344, Twinsburg, OH, USA). Each channel

provides a maximum amplitude output (0 to peak) of 12 V, which is increased by homemade

amplifiers to the desired voltages. The master clock is provided by the arbitrary waveform

generator. First it was necessary to estimate the number of ions trapped in the linear ion trap

in each injection period. The timing parameters for this are shown in Figure 2.5. The

quadrupole power supply was operated in rf-only mode and the rf voltage was manually set to a voltage corresponding to the desired q value of ion injection. Ions were injected in the trap by lowering the entrance lens to -15 V in first experiments. During the injection period, the exit lens was held at a stopping potential (+120 V). Then the entrance lens was increased to the same stopping potential of (+120 V) and ions were cooled for 50-100 ms. Ions were detected by lowering the exit lens to (-15 V) to transmit ions. Ions were then detected by triggering the MCS to collect data. For this experiment it was expected that the injection time and number of detected ions should be linearly related until a plateau is reached. With this experimental set up the number of ions trapped in the LIT was found to decrease with injection time as shown in Figure 2.6. This strange result could be explained by following the ion path with the respective potentials step by step. Ions enter the LIT, travel towards the exit lens, approach the barrier of (+120 V), reflect back and proceed towards the entrance lens.
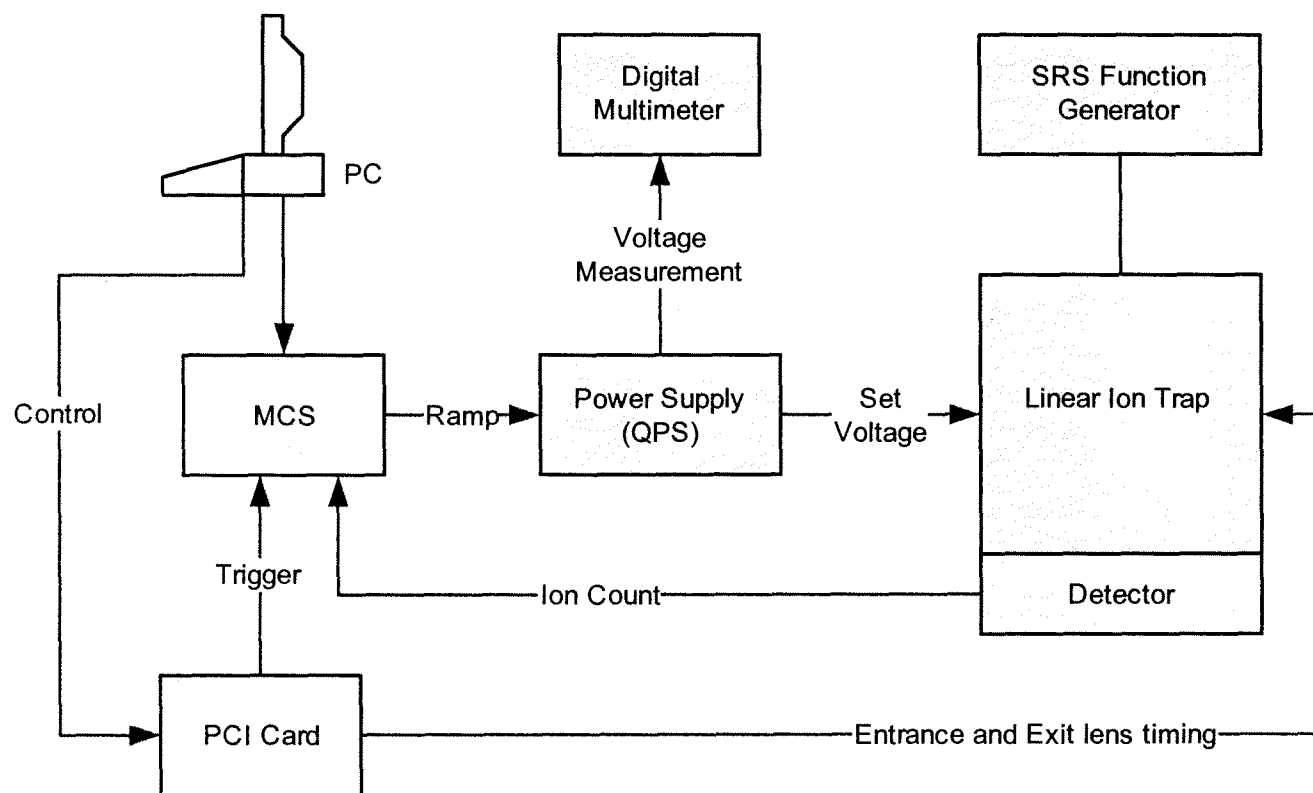
Figure 2.4 Block diagram of the ion trapping experimental set up.
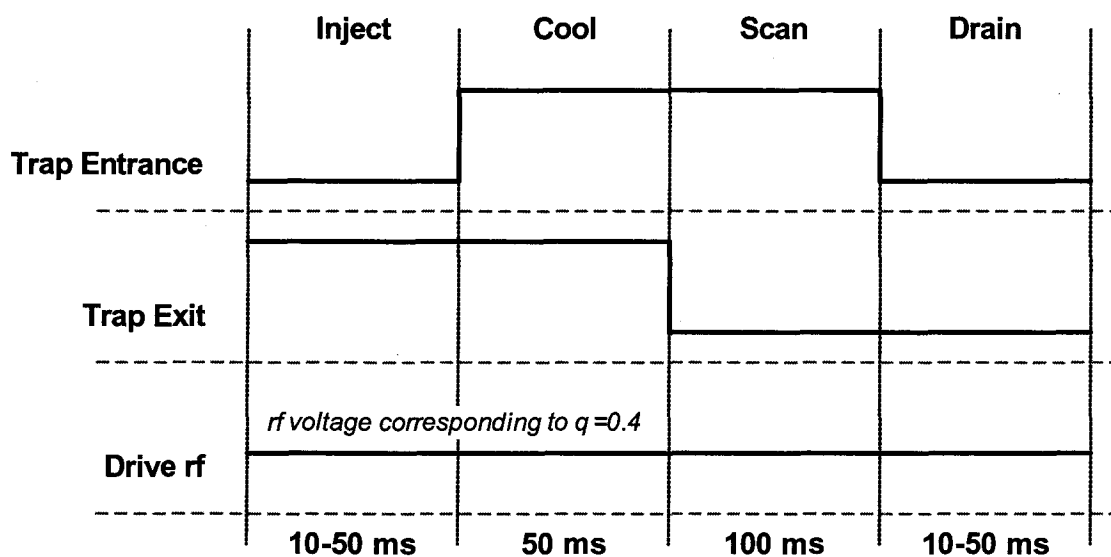
Figure 2.5 Pulse sequence for counting injected ions.
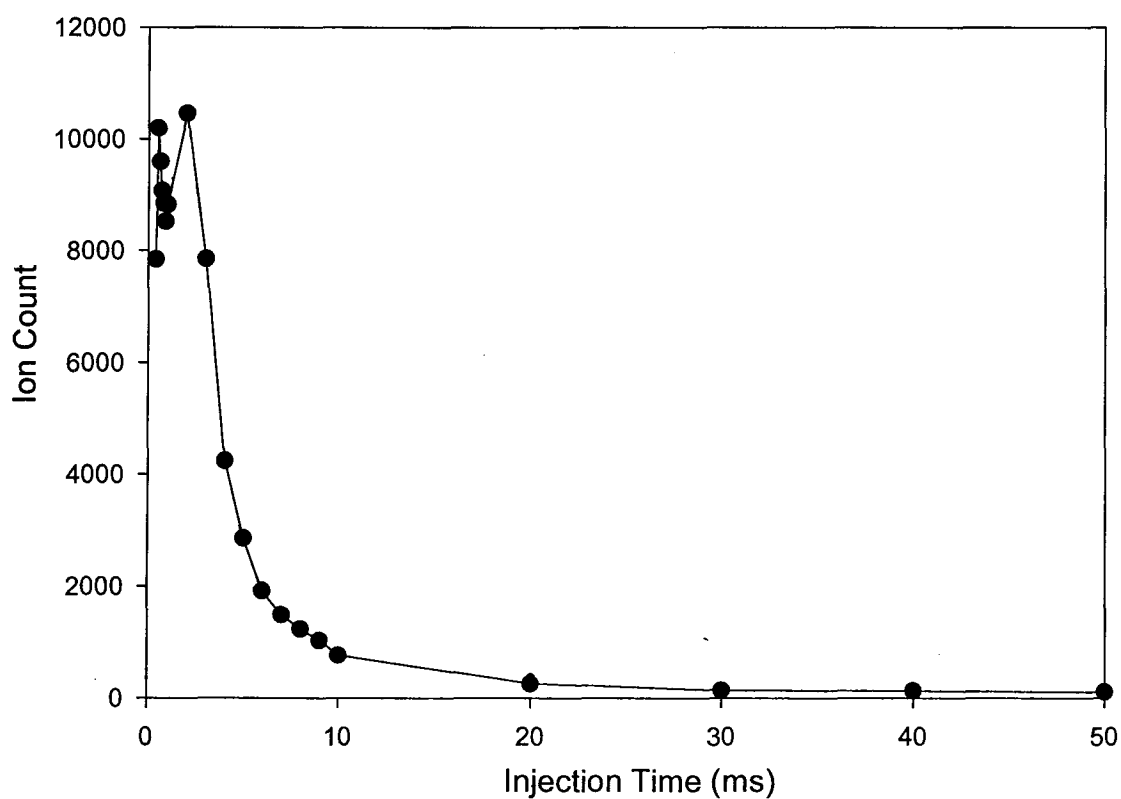
Figure 2.6 Injected ion count vs. injection time.

For the reflected ions, the entrance lens must also provide a potential barrier; otherwise ions can leave the trap. The entrance lens initially was held at (-15 V) during the injection time, which allowed ions to leave the trap. Only for the very shortest injection period was it possible to detect increasing numbers of ions with longer injection times. When the offset of the entrance lens was increased to a value that simultaneously allowed the passage of ions into the LIT and enabled trapping of reflected ions, the ion count increased with longer injection times as shown in Figure 2.7. This required that the lens voltage be one or two volts higher than the rod offset voltage of the Q1 rod set.

The trapping efficiency is low for these experiments because of the low pressure in the linear ion trap. The kinetic energy losses of ions in the ion trap can be estimated from [23]:

$$\frac{E}{E_0} = \exp\left(-\frac{C_D A n m_2 l}{m_1}\right) \tag{2.1}$$

where E_0 is the initial ion kinetic energy at the trap entrance, E is the energy after collisions with background gas, C_D is a drag coefficient, A is the collision cross section, n is the gas number density, m_1 is the ion mass, m_2 is the collision gas mass and l is the length that ions travel. For these experiments, $C_D = 2.2$, $n = 5.28 \times 10^{11}$ cm^{-3}, $A = 280$ Å, $l = 40$ cm, $m_2 = 28$ amu, $m_1 = 609$ amu, so that $E = 0.94 E_0$, after ions pass through the quadrupole and then back to the entrance. Ions lose only about 6% of their initial energy. With a Q0 rod offset of +2.0 V and a Q1 rod offset of −1.0 V, the initial energy of the ions is about 3 eV, and after one round trip the energy will be reduced to 2.82 eV. Therefore the entrance lens voltage of 0.0 or +1.0 volt is not sufficient to stop the ions from leaving Q1 and entering the Q0 chamber, where they are lost.
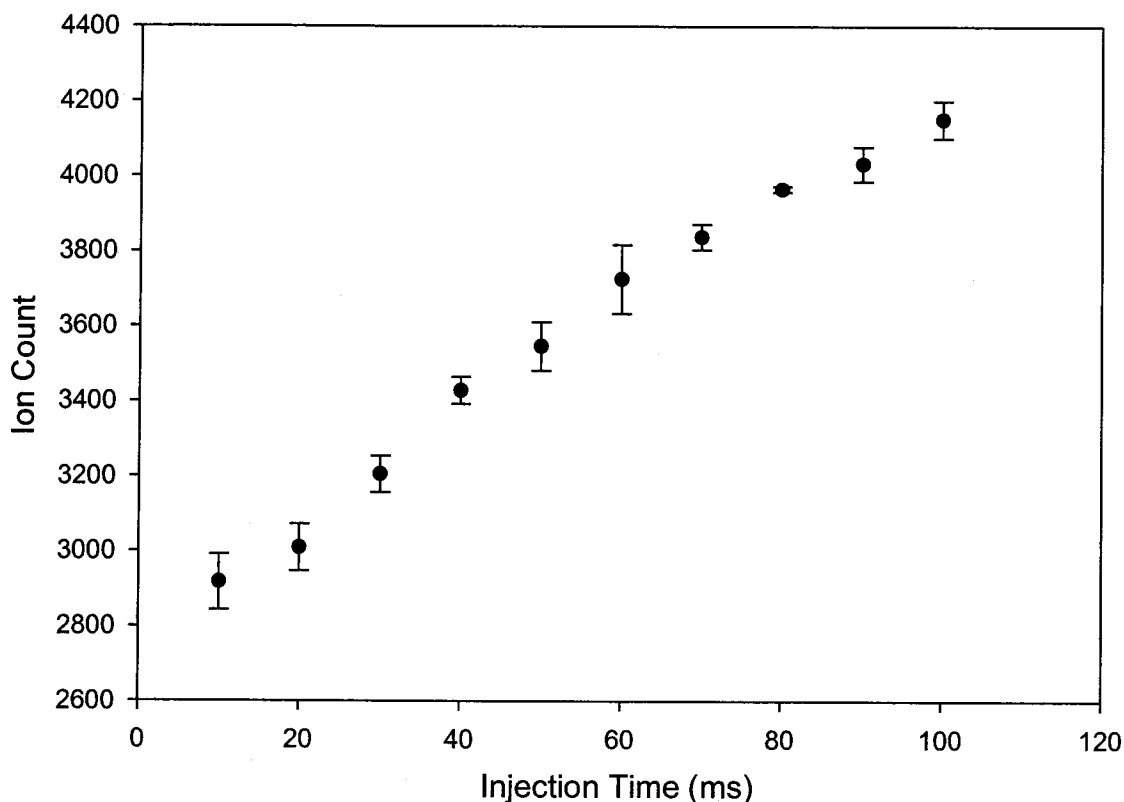
Figure 2.7 Injected ion count vs. injection time for injection at q = 0.4.

A schematic of the timing parameters for a typical MSAE scan with trapped ions is shown in Figure 2.8. First a variable length (10-50 ms) pulse, 1 volt higher than the Q1 rod offset but below the Q0 rod offset (+2 V), is applied to the entrance lens to allow ions to enter Q1, (Q1 offset −1 to -5 V). During this injection step the exit lens is held at +120 V. At the end of the injection pulse the entrance lens is raised to +120 V. Next, the trapped ions are cooled for 50 ms. Just prior to the mass scan the dc voltage applied to the exit lens is reduced to a scan value. For lower scan speeds this was 2-3 volts above the dc rod offset of Q1 and for higher scan speeds 10-25 volts above the Q1 rod offset. Auxiliary dipole or quadrupole excitation is applied at a fixed frequency, and the drive rf is ramped either up or down, over the chosen mass-to-charge range to eject ions from the

39

linear ion trap. Finally, the dc voltages applied to the entrance lens and the exit lens are lowered to -15 V for 10-50 ms to drain any residual ions from the linear ion trap and Q0. Operating voltages are shown in Table 2.3.
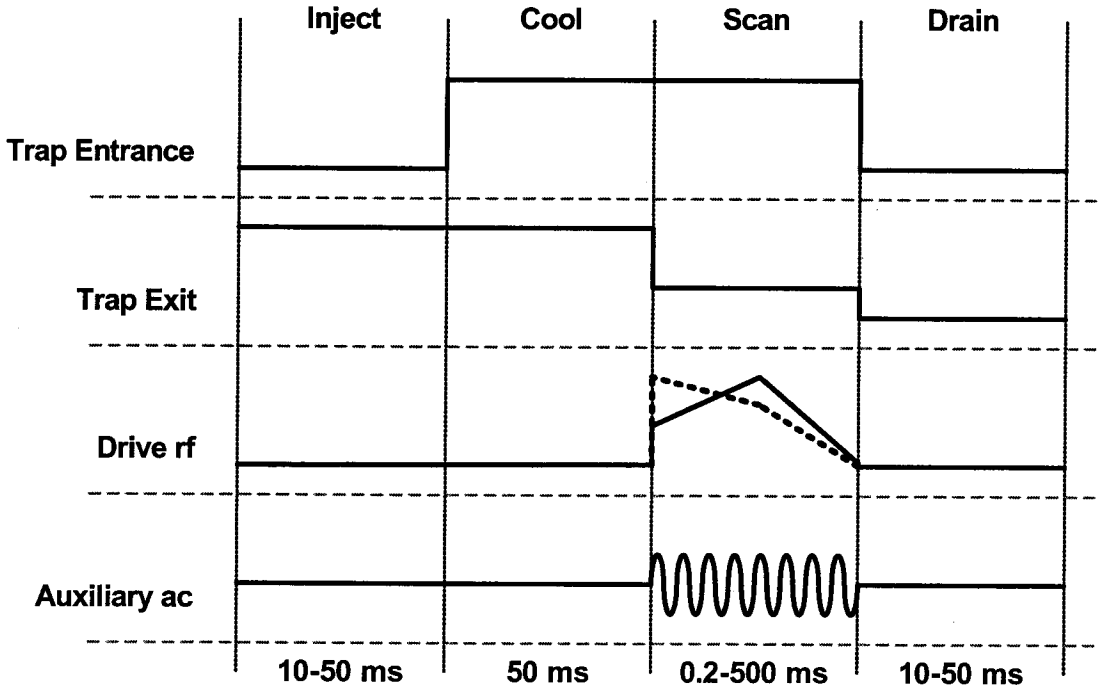
Figure 2.8 Schematic of the timing parameters for MSAE experiments.

Table 2.3 Operating voltages.

Sprayer	+3500
Curtain plate	+500
Orifice	+50; +30
Q0 rod offset	+2
Entrance lens	+1, 0, -1, -2 or +120
Q1 rod offset	0, -1, -2, -3, -4, -5
Exit lens 1	-15 or +120
Exit lens 2	-300

Auxiliary ac from an arbitrary waveform generator (SRS DS345, Stanford Instruments, Sunnyvale, CA) was applied between one pair of rods (x or y) as dipole excitation [33] or simultaneously between two pairs of rods as dipole-dipole excitation, or to all four rods as quadrupole excitation. For dipole excitation the electrical connection between the (x or y) pair of the rods was disconnected and the output from the main drive was connected to the center tap of the secondary winding of a bipolar transformer (1:1 turns ratio). The primary winding of the transformer was connected to the SRS arbitrary waveform generator and the two ends of the secondary were connected to a rod pair. Quadrupole excitation was applied through the quadrupole power supply through a circuit supplied by MDS-SCIEX.

For all the experiments with trapped ions reported here, approximately 23% of the drive rf (in phase with the pair of poles that has the auxiliary excitation) was added to the

exit lens by connecting the lens to the rf output of the quadrupole supply through a 15 pf

capacitor [79] as shown in the scale diagram in Figure 2.9.
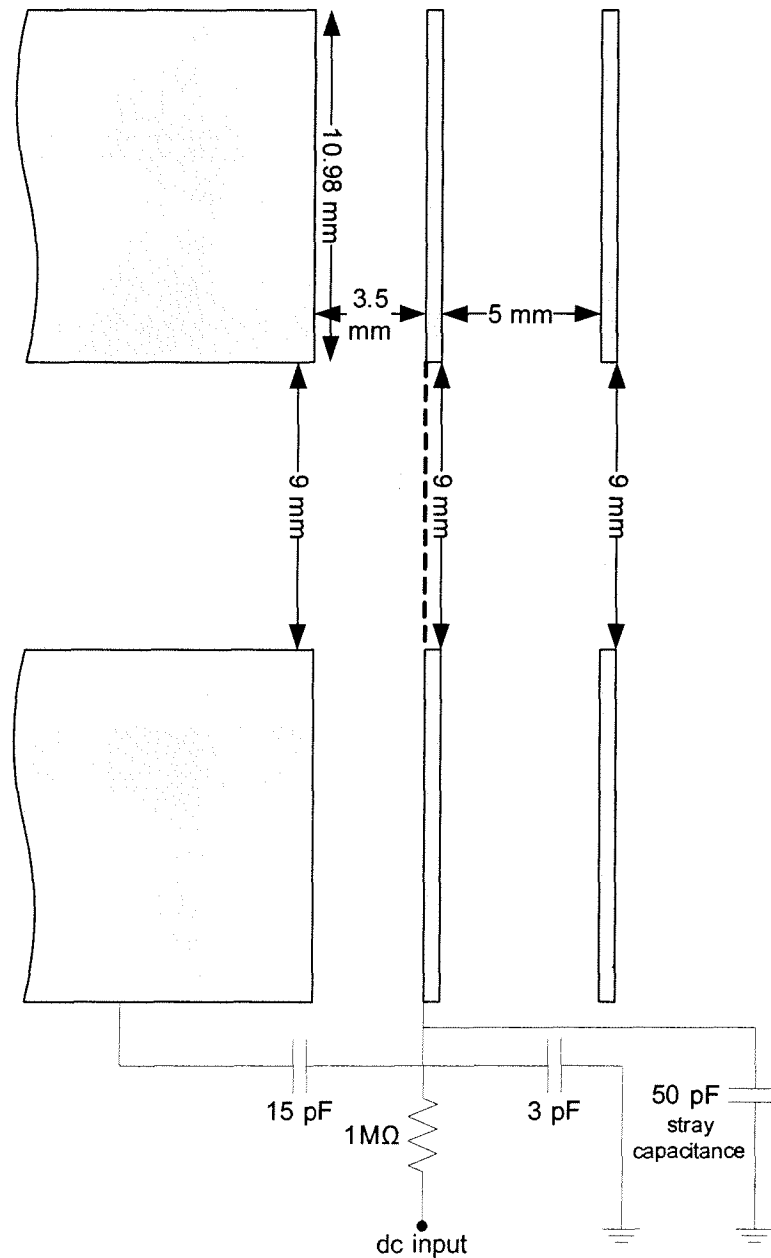
Figure 2.9 Cross section view of the two exit lenses and the pair of the quadrupole rods

that are capacitively coupled to exit lens 1.

2.2.1 Sample preparation

Reserpine ($C_{33}H_{40}N_2O_9$) (m.w. 609.7) and renin substrate tetradecapeptide (DRVYIHPFHLLVYS) (m.w. 1759.0), were from Sigma (St. Louis, MO, USA). Agilent tune mix was from Agilent technologies (Santa Clara, CA, USA). Methanol and acetic acid were from Fisher Scientific (Nepean, ON, Canada). UHP grade nitrogen was from Praxair (Vancouver, BC, Canada). Solutions were as follows: reserpine, 1-10 μM, renin substrate 10 –50 μM, all in 70% (V/V) methanol, 29.5% (V/V) water, 0.5% (V/V) acetic acid; Agilent tune mix as supplied. The solution flow rate for all experiments was 1 μL/min.

2.2.2 Data Analysis

Data analysis used in-house developed software. The software is designed to read MCS produced spectra with the corresponding parameters (e.g. rf voltage specifications) and save spectra in a database for later analysis and graphing. In a few steps a user can graph spectra as intensity vs. mass-to-charge ratio, find peaks and calculate resolution. The software is capable of storing and sorting thousands of spectra based on their collection date. Using this software it was possible to organize and quickly browse data from a large number of experiments. Figure 2.10 and 2.11 show the Graphic User Interface (GUI) of the MSAE data analysis software.
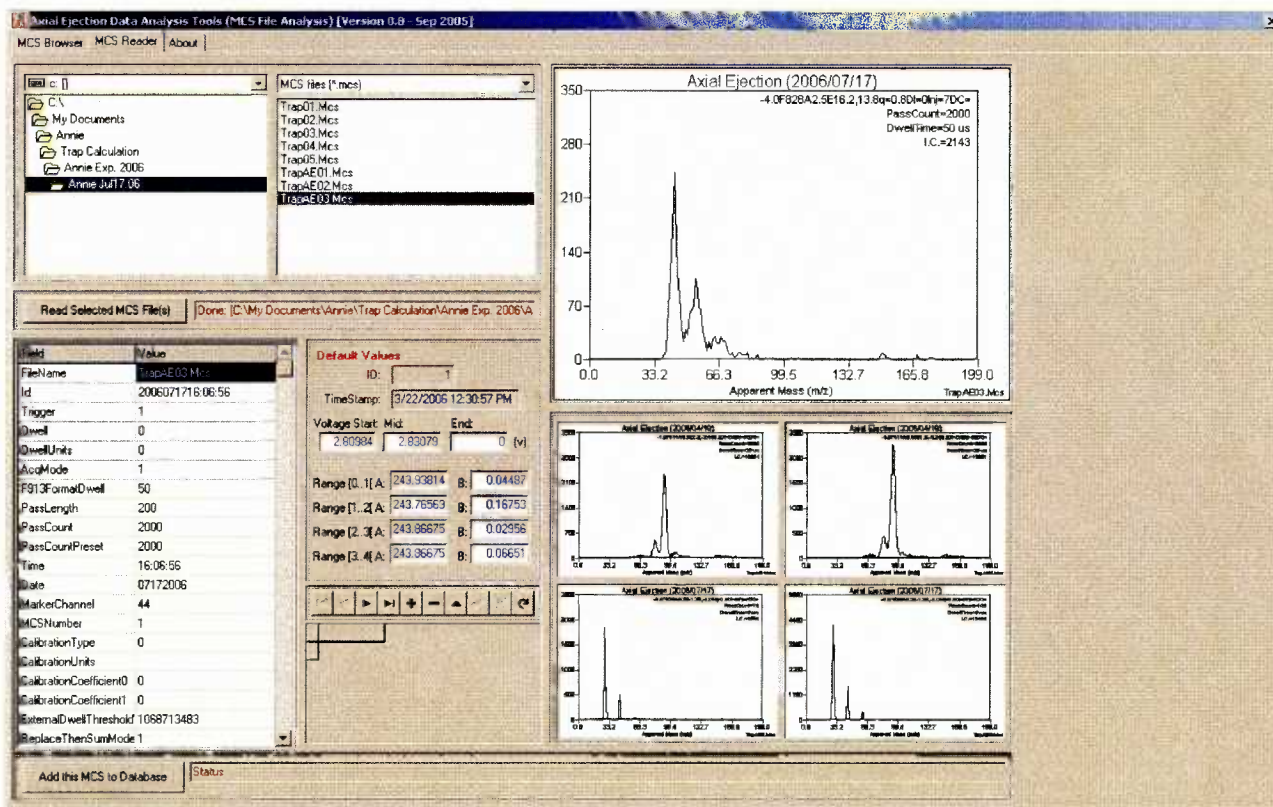
Figure 2.10 MSAE data analysis software GUI.
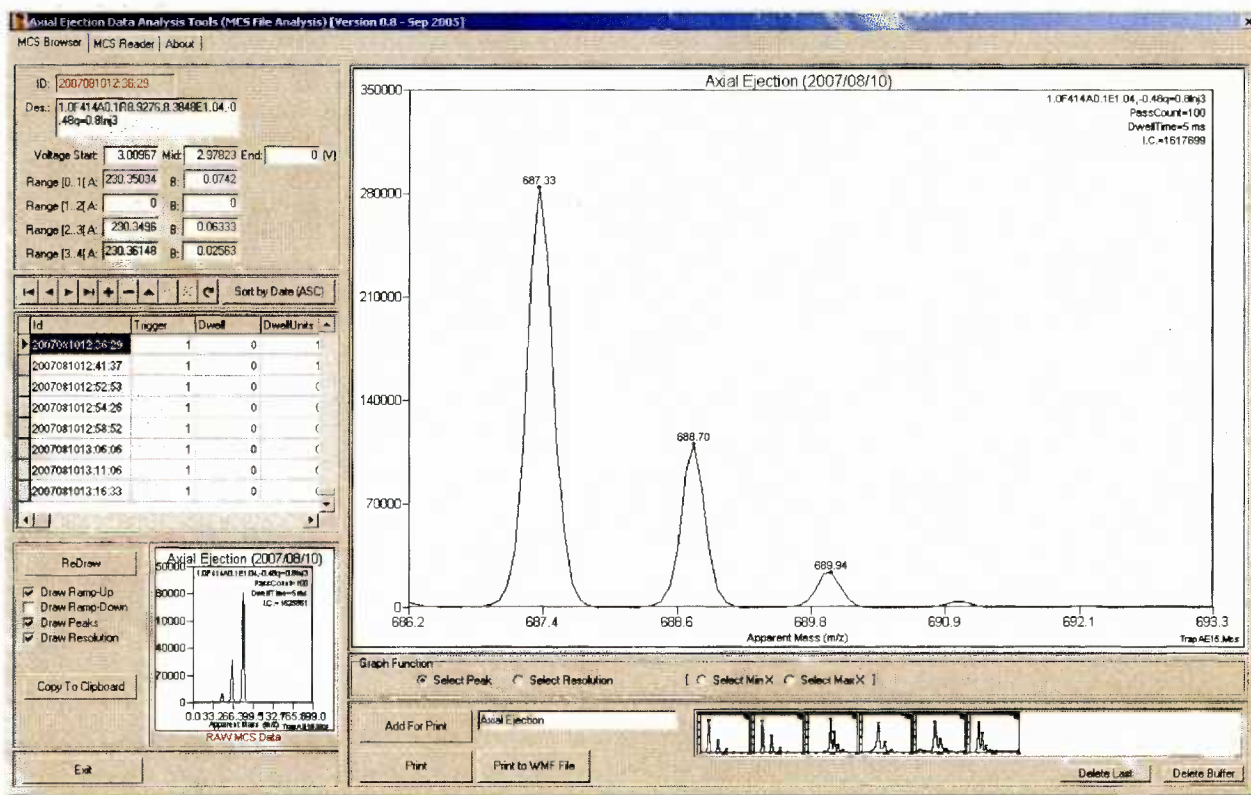
Figure 2.11 MSAE data analysis software GUI.

Chapter 3 Mass Selective Axial Ejection of Ions

Without Trapping

3.1 Introduction

This chapter describes the experimental set up and methods for performing MSAE of

ions from a conventional rod set and a 2.6% added octopole field quadrupole rod set

without trapping the ions. The purpose of this work was to reproduce Hager's results with

a conventional round-rod quadrupole for comparison to MSAE results from the

quadrupole rod set with a 2.6% added octopole field.

3.2 Experimental

The experimental apparatus is shown in Figure 2.1. The operating voltages are

summarized in Table 3.1. First, the quadrupole power supply was operated in rf/dc mass

filter mode and a spectrum of reserpine isotopic peaks was recorded. Then, in single ion

monitoring mode, the monoisotopic peak (609.3) was monitored while increasing the exit

lens voltage to stop the ions. With the operating voltages shown in Table 3.1 the exit lens

barrier to stop the ions was +300 volts. In order to decrease the required voltage, all the

dc voltages of the system were lowered such that +100 volts on the exit lens stopped the

ions. The final operating voltages are summarized in Table 3.2. Once the stopping

potential for the monoisotopic peak (609.3) of reserpine was determined, the instrument

was operated in rf-only mode with the stopping potential applied to the exit lens. The

amplitude of the drive rf was scanned to bring ions of different m/z ratios to the stability boundary ($a = 0$, $q = 0.908$). Ions near the boundary gain large amplitudes of oscillation.

Table 3.1 Initial operating voltages (V).

sprayer	+3700
curtain plate	+550
orifice	+200
Q0 rod offset	+110
interquad lens	+70
Q1 rod offset	+109
Exit lens 1	-10, +300
Exit lens 2	-10, +300

Table 3.2 Final operating voltages.

sprayer	+3700
curtain plate	+441
orifice	+91
Q0 rod offset	+1
interquad lens	-39
Q1 rod offset	0
Exit lens 1	-119, +100
Exit lens 2	-119, +100

These excited ions overcome the exit lens barrier and are ejected to produce a mass spectrum [71].

Initially experiments were done with a conventional quadrupole rod set using balanced and unbalanced (up to 15%) rf, with 7 V dc applied between the rods and with 50-110 V_{p-p} auxiliary rf (at the frequency of quadrupole power supply) applied to the exit lens. This rf was 1.8 to 3.9 % of the main rf and was in phase and phase locked with the drive rf. Figure 3.1 shows a block diagram of the experimental set up for applying rf to exit lens in this configuration.

The software (Tune 2.2, Sciex) used to count ions, indicates the number of counts per second of the most intense peak times the number of scans. To report the intensity as counts per second, the number taken from the software was divided by the number of scans.
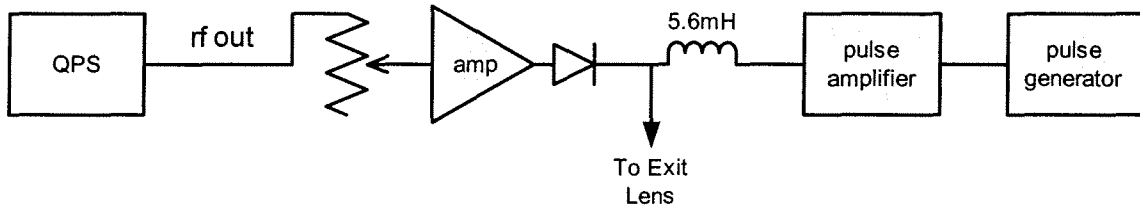
Figure 3.1 Block diagram of the experimental set up to add rf to the exit lens.

The stability boundaries for a quadrupole with a 2.6% added octopole field were calculated as in [13]. The transmission of the quadrupole for given a, q values was calculated from 6000 ion trajectories. The initial spatial distributions were Gaussian with standard deviations $\sigma_x = \sigma_y = 0.0020 r_0$. Initial velocity distributions were thermal for an ion of mass 390. Multipoles up to the 20 pole term ($N = 10$) were included in the

calculation. No fringing fields were included. Points with a transmission of 1% were taken as the stability boundaries.

3.3 Results and Discussion

3.3.1 Experiments with a Conventional Quadrupole Rod Set

Figure 3.2 shows a spectrum of reserpine isotopic peaks obtained by operating the quadrupole as a conventional rf/dc mass filter. The resolution ($R_{1/2}$) is about 2900 and the scan speed is 5 Th/s. Figure 3.3 shows a spectrum of the isotopic peaks of reserpine with MSAE, obtained with balanced rf and ejection at the stability boundary $q = 0.908$ with a scan speed of 0.8 Th/s. With MSAE scans, adjusting the rod offset and the exit lens voltages can optimize the resolution. For Figure 3.3 the exit lens voltage was 108 volts repulsive with respect to the dc rod offset of the quadrupole (–8.0 volts). This value yielded optimum signal-to-background levels. The resolution ($R_{1/2}$) is about 1900, more than sufficient to separate the isotopic peaks. The background level was 10 counts/sec on average and it was not possible to improve the signal-to-background ratio beyond what is shown in Figure 3.3.
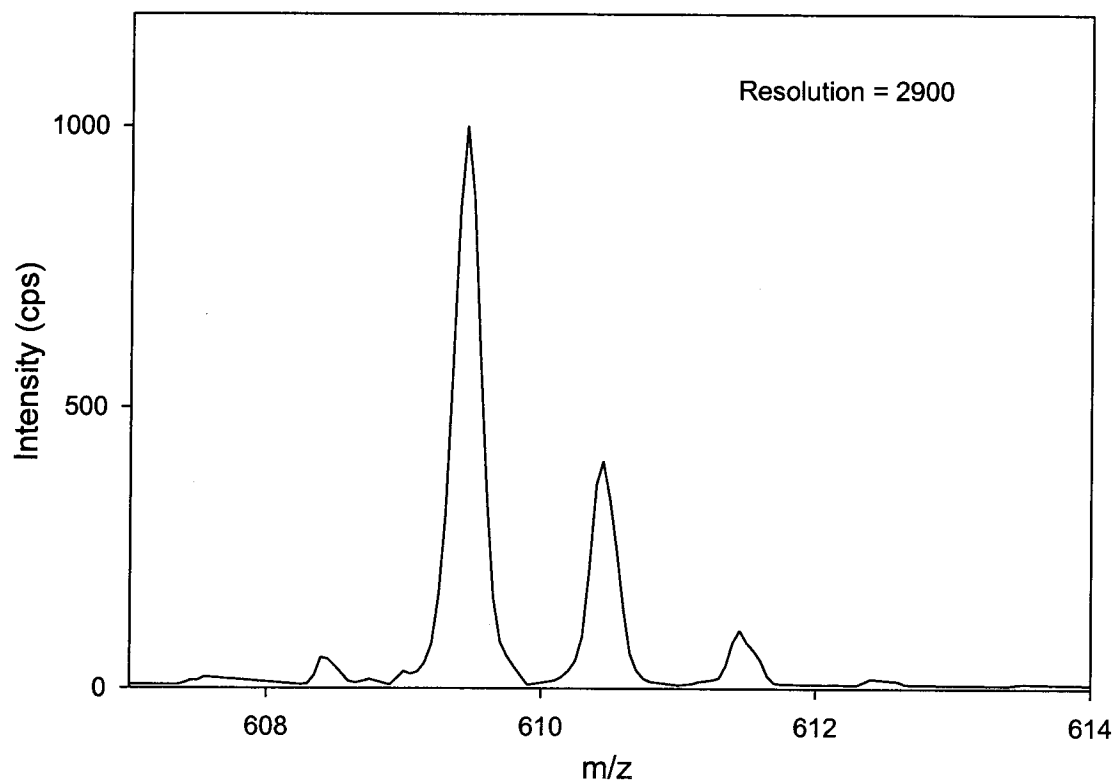
Figure 3.2 Mass analysis of reserpine ions with operation at the tip of the stability region with a conventional quadrupole rod set and a scan speed of 5 Th/s.
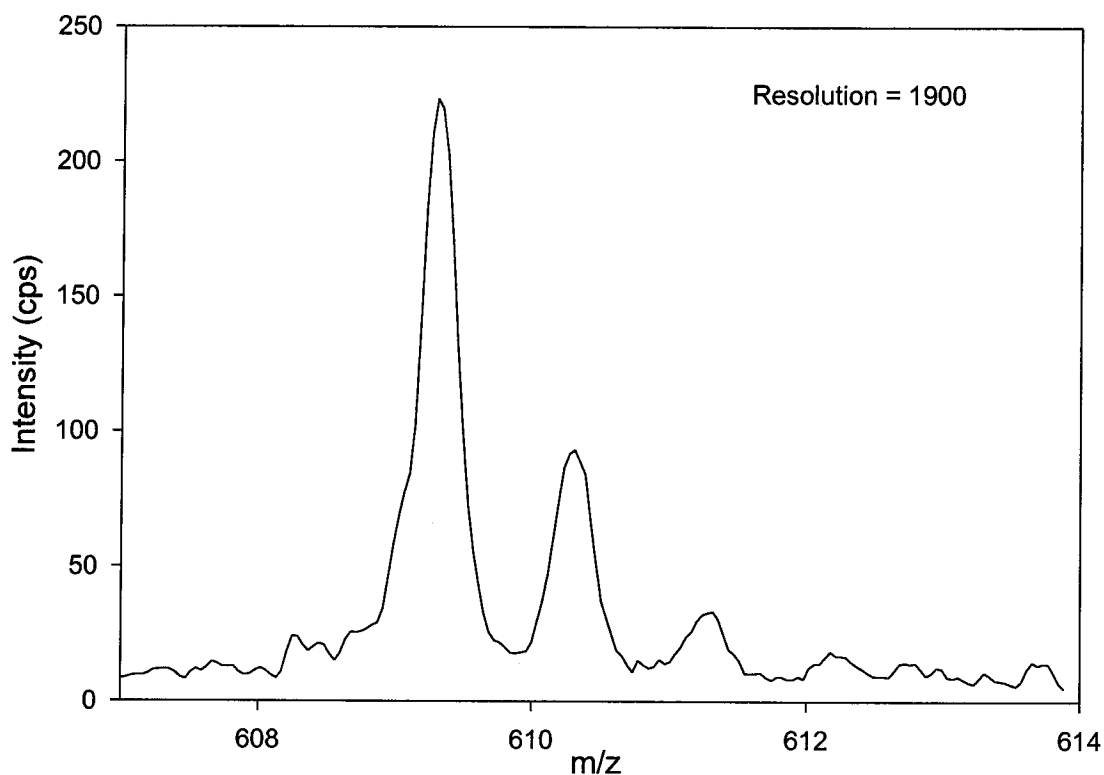
Figure 3.3 MSAE of reserpine ions at $q = 0.908$ obtained with balanced rf and a scan

speed of 0.8 Th/s.

As in Hager's experiments [71], unbalancing the drive rf by approximately ±15% has

a dramatic effect on MSAE performance. Both sensitivity and resolution increase. The

effect of an unbalanced rf is shown in Figure 3.4. A lower rf voltage (–15%) was applied

to the A-poles (the poles with positive dc, x-poles). The sensitivity is ca. 5 times greater

than with balanced rf (Figure 3.3). The resolution ($R_{1/2}$) is 2095. Figure 3.5 shows the

MSAE of reserpine ions when the A-poles have +15% rf unbalance and the resolution

($R_{1/2}$) is 2386. With unbalanced rf slightly better resolution is obtained when the A-pole

has the higher (+15%) rf voltage. When the ions enter the exit fringing field the ion

motions in the xz and yz planes are coupled and become very complex and there is no

theoretical treatment available. However, Hager argued [79] that when the rf is unbalanced the field gradient will be different in the xz and yz planes. If the rf is unbalanced such that the higher rf is on the x-pole (the positive dc pole) pair, then ions aligned with the y-pole (the negative dc pole) pair are slowed down and spend more time in the exit fringing field which improves the radial to axial coupling. Therefore for a given exit lens barrier voltage this results in significantly higher ion ejection energies and improved ejection efficiency.
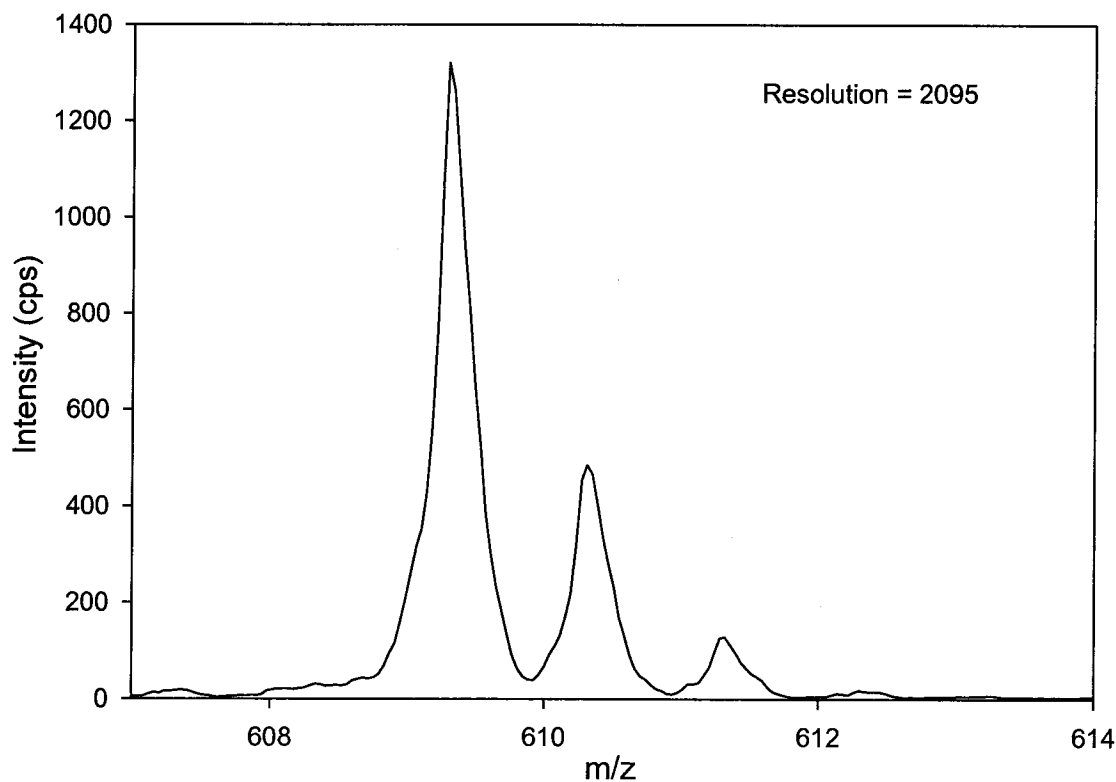
Figure 3.4 MSAE of reserpine ions at $q = 0.908$ with a scan speed of 0.8 Th/s. The rf is unbalanced so that the A-pole pair has 15% lower rf voltage than with balanced rf.
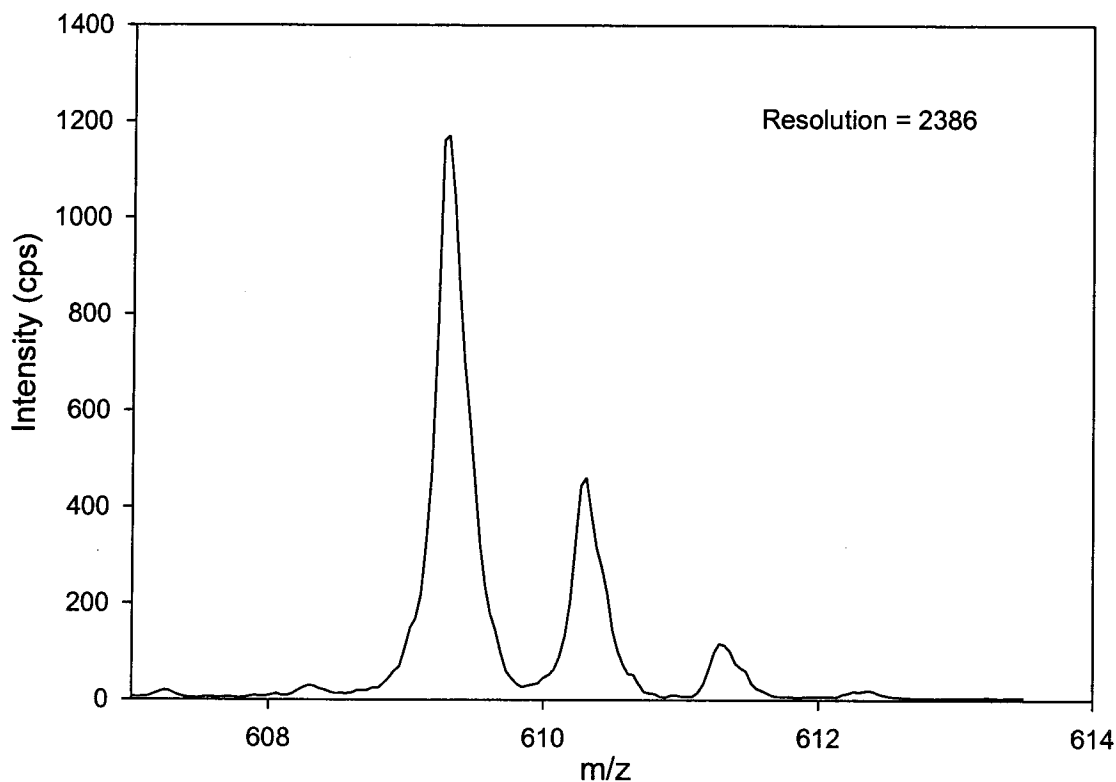
Figure 3.5 MSAE of reserpine ions at $q = 0.908$ with a scan speed of 0.8 Th/s. The rf is unbalanced so that the A-pole pair has 15% higher rf voltage than with balanced rf.

Hager found that it was necessary to apply the higher voltage unbalanced rf to the pole pair with the negative resolving dc in order to obtain higher resolution and sensitivity. He argued that small amounts of resolving dc are needed to align the ion beam (positive ions in this case) with the pole pair that has the lower unbalanced rf voltage. Under these conditions ions aligned with this pole pair spend more time in the fringing field and receive higher axial kinetic energies [79]. Adding small amounts of resolving dc ($\approx \pm 3 - 5$ V) in conjunction with the unbalanced drive rf, which gave the best performance for Hager's experiments, did not prove to be as effective with our experimental set up for MSAE at $q = 0.908$. Figure 3.6 shows a spectrum from MSAE of

reserpine ions with +15% unbalanced rf applied to the B-pole pair (y rods) which has –3

V resolving dc.
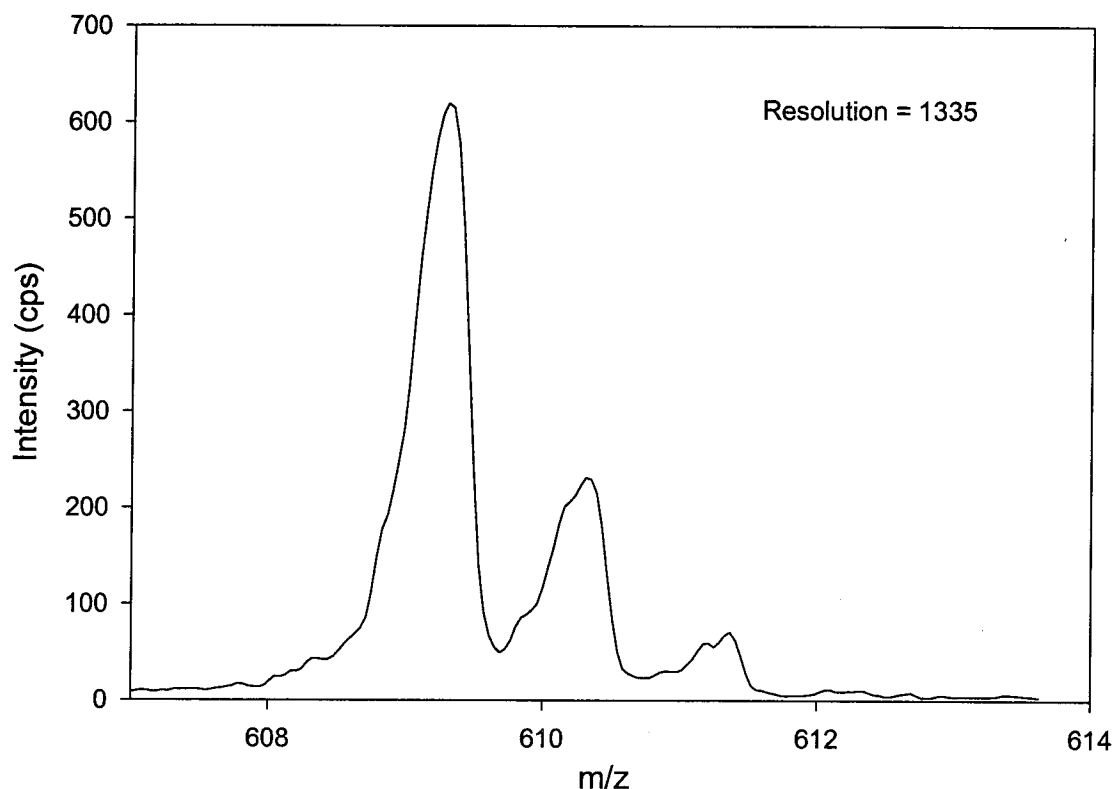
Figure 3.6 MSAE of reserpine ions at $q = 0.908$ with a scan speed of 0.8 Th/s. The rf is

unbalanced so that the B-pole pair has 15% higher rf voltage and –3V dc.

The resolution ($R_{1/2}$) is 1335. Adding the ± 3 V resolving dc decreases both peak

intensity and resolution. The reason for this difference from Hager's observations is

believed to be the differences in the experimental set up, including the exit lens aperture

size, distance from the rods, and the detector mounting.

Figure 3.7 shows the spectrum of reserpine ions axially ejected at q=0.908 when the

higher unbalanced rf voltage was applied to the A-pole pair which had +3V resolving dc.

As expected from Hager's results this mode of operation results in considerably poorer

peak shapes and lower ion intensity.
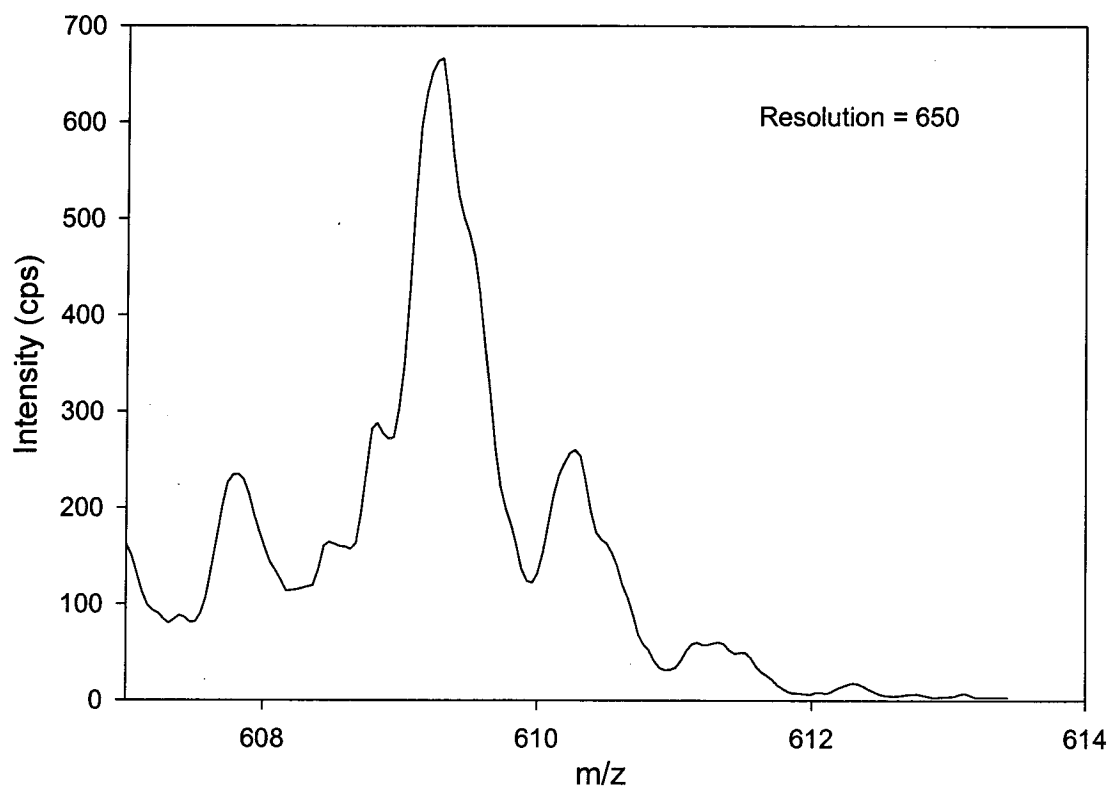
Figure 3.7 MSAE of reserpine ions at q = 0.908 with a scan speed of 0.8 Th/s. The rf is

unbalanced so that the A-pole pair has 15% higher rf voltage and +3V dc.

Figure 3.8 is a plot of ion intensity vs. the exit lens voltage for MSAE of reserpine

ions with a series of combinations of unbalanced rf and resolving dc conditions. It shows

that high exit energies are only observed when unbalanced rf is applied and a higher rf

voltage is applied to the A-pole pair (x rods).
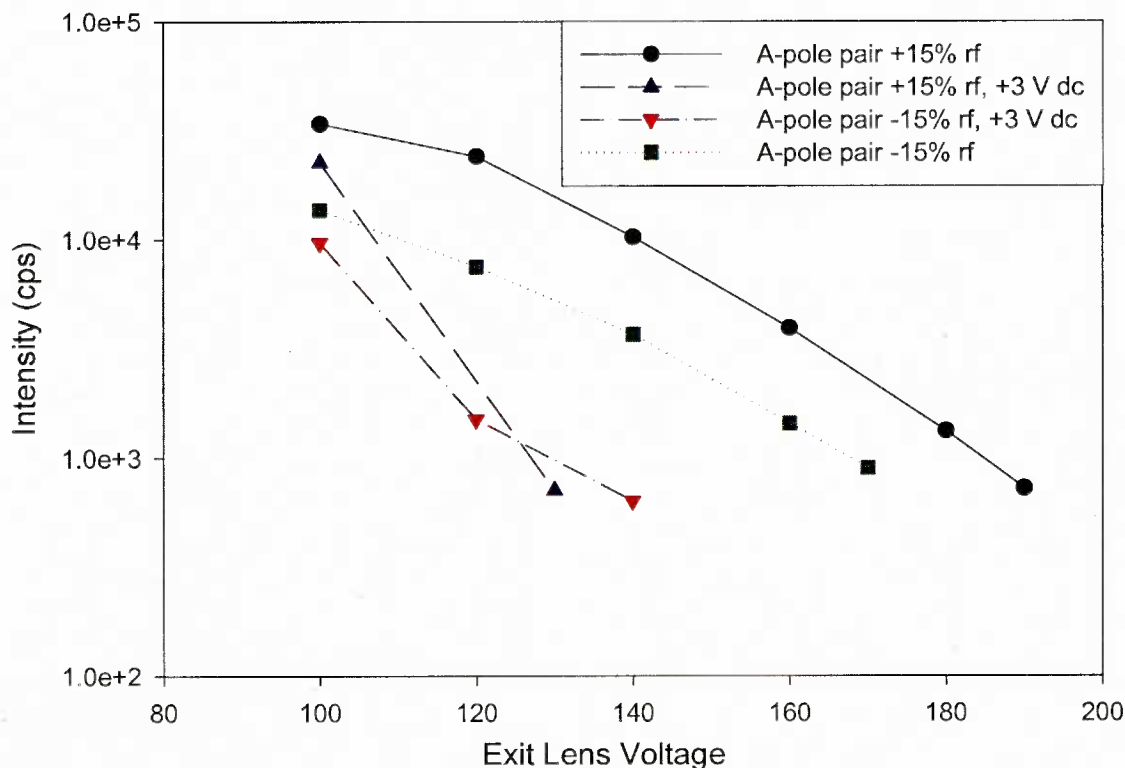
Figure 3.8 Intensity vs. the exit lens voltage for reserpine ions obtained using different combinations of unbalanced rf and added dc.

Hager found that the effect achieved by unbalancing the rf applied to the rods can also be achieved by applying a certain percentage of the drive rf with proper phase to the exit lens [80]. An unbalanced rf is equivalent to a balanced rf with an added axis potential between the quadrupole and exit lens [39]. This potential difference between the quadrupole and exit lens can be produced by applying some of the quadrupole rf to the exit lens without the need to unbalance the rf. MSAE experiments were also performed with balanced rf and 1.8-3.9 % of the drive rf applied to the exit lens. The resolution obtained with 50 V_{p-p} rf applied to the exit lens was $R_{1/2}$ = 1800. Figure 3.9 shows MSAE of reserpine ions obtained by applying 110 V_{p-p} rf to the exit lens. The resolution ($R_{1/2}$) is

1881. The resolution increases slightly with higher rf voltages on the exit lens. With the

set up at that time, it was not possible to add more than 110 V_{p-p} rf to the exit lens.
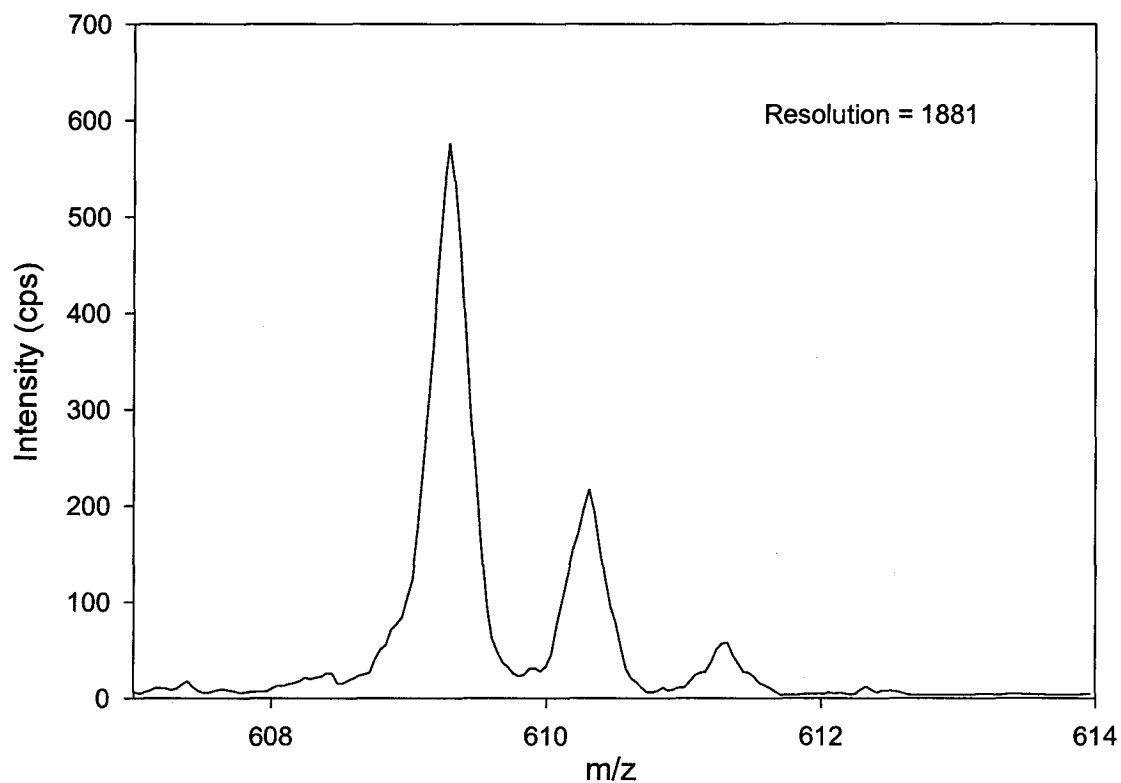
Figure 3.9 MSAE of reserpine ions at $q = 0.908$ with a scan speed of 0.8 Th/s. The rf

was balanced and 110 Vp-p rf applied to the exit lens.

3.3.2 Experiments with a Quadrupole Rod Set with a 2.6% Added Octopole Field

3.3.2.1 MSAE of ions at the stability boundary q = 0.908

Conventional rf/dc mass analysis- is possible with a quadrupole with 2.6% added octopole field when the positive dc voltage is applied to the smaller rods (for positive ions) [56]. Figure 3.10 shows a spectrum of reserpine ions obtained with this mode. The resolution ($R_{1/2}$) is 2500. MSAE experiments without trapping and ejection at $q = 0.908$ were then tried with this quadrupole. With balanced rf and no dc between the rods, a very broad peak with poor resolution (nominal $R_{1/2}=76$) was produced at about $m/z=607$, Figure 3.11.
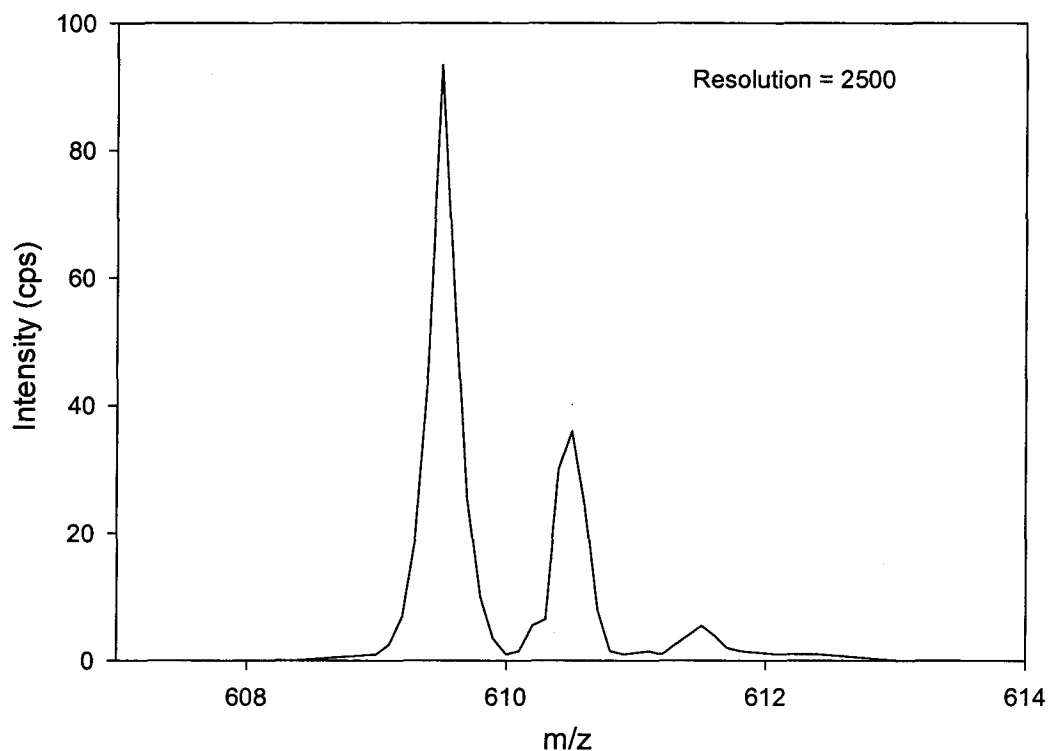
Figure 3.10 Conventional rf/dc mass analysis with a quadrupole with a 2.6% octopole field and a scan speed of 5 Th/s.

Combinations of unbalanced rf, dc between the rod pairs, and rf on the exit lens were tried, but the resolution could not be improved. Evidently with axial ejection at $q = 0.908$ and with excitation at the stability boundary, the quadrupole with 2.6% added octopole field produces much lower resolution than a conventional quadrupole.
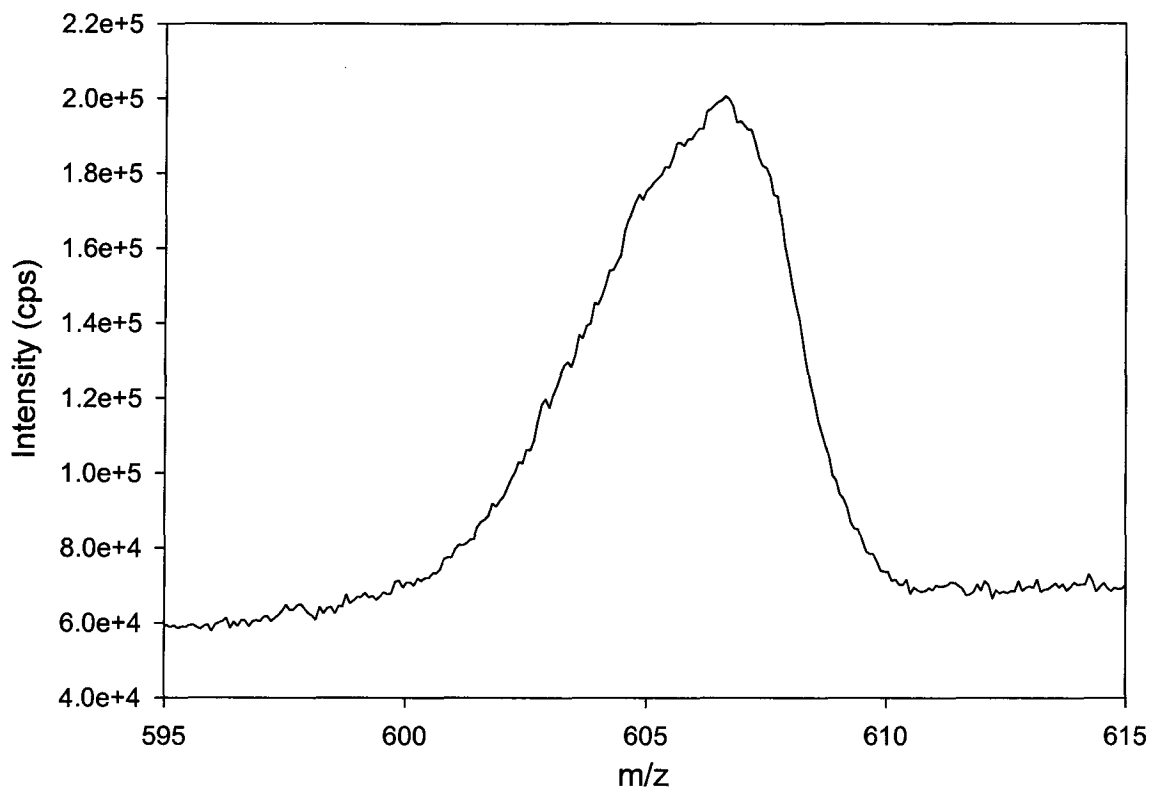
Figure 3.11 MSAE of reserpine ions from a quadrupole rod set with a 2.6% added octopole field at $q = 0.908$ and a scan speed of 0.8 Th/s.

The lower resolution may be a result of changes to the stability boundaries caused by the octopole field. With a conventional rod set, at the $a = 0$, $q = 0.908$ boundary, ion motion becomes unstable in the x and y directions simultaneously. The stability boundaries of a quadrupole with 2.6% octopole field are shown in Figure 3.12. The x and y motions have separate stability boundaries on the $a = 0$ axis. The x boundary is at $q = 0.908$, but the y boundary is at about $q = 0.931$. The y boundary is diffuse [56]. The octopole field couples the x and y motions. Excitation of ions in x near $q = 0.908$

may lead to excitation in the y direction where motion is stable, resulting in delayed

ejection and low resolution.
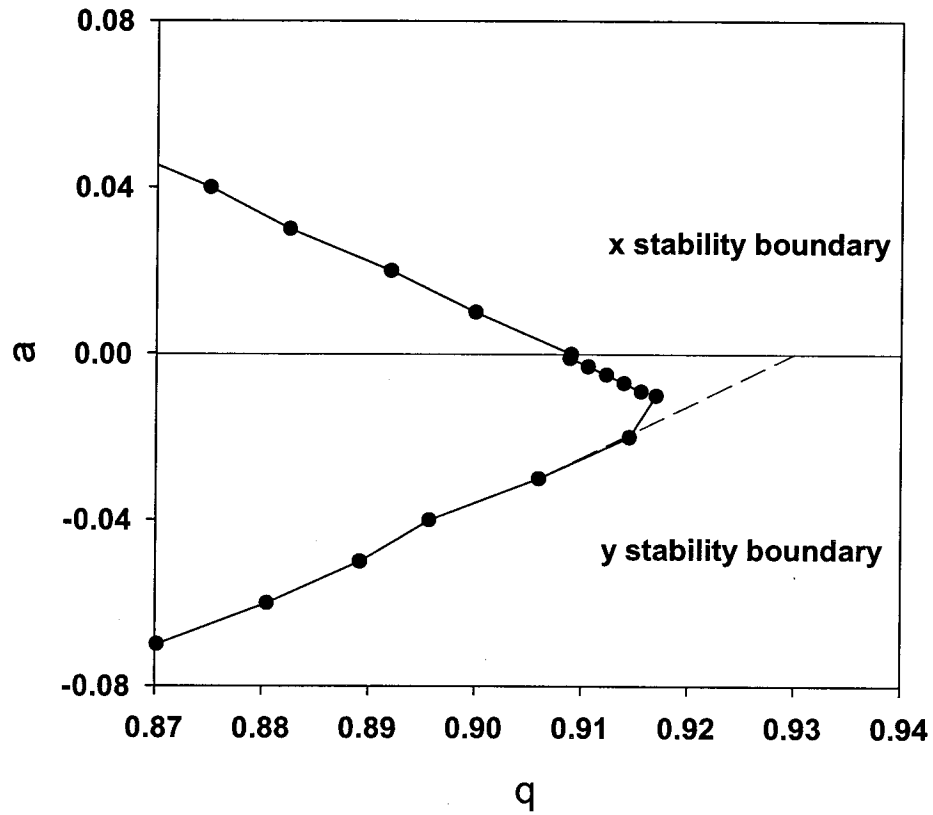
Figure 3.12 Calculated stability boundaries of a quadrupole with a 2.6% added octopole field (calculated by W. Xiao).

3.3.2.2 MSAE of ions with dipole excitation at q = 0.8765

When dipole excitation (4.0 V_{p-p}) at 500 kHz is applied between the larger rods, substantially better resolution is obtained. The isotopic peaks of reserpine could be resolved although not to baseline ($R_{1/2}$=758) (Figure 3.13). The same result could not be reproduced with dipole excitation between the smaller rods ($R_{1/2}$=200) (Figure 3.14). The scan speed with dipole excitation applied to the larger or the smaller rods was 0.8 Th/s and forward scans were used.
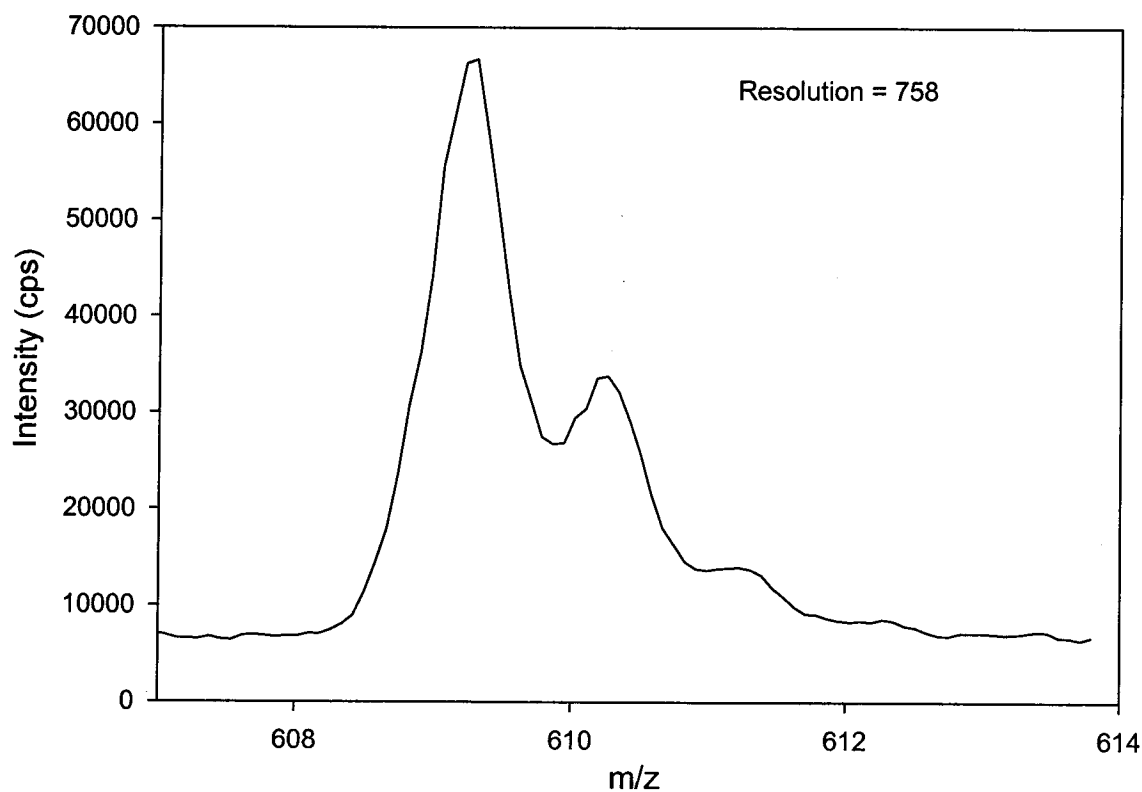
Figure 3.13 MSAE of reserpine ions at q = 0.8765 with 4.0 V_{p-p} dipole excitation applied to the larger rods.
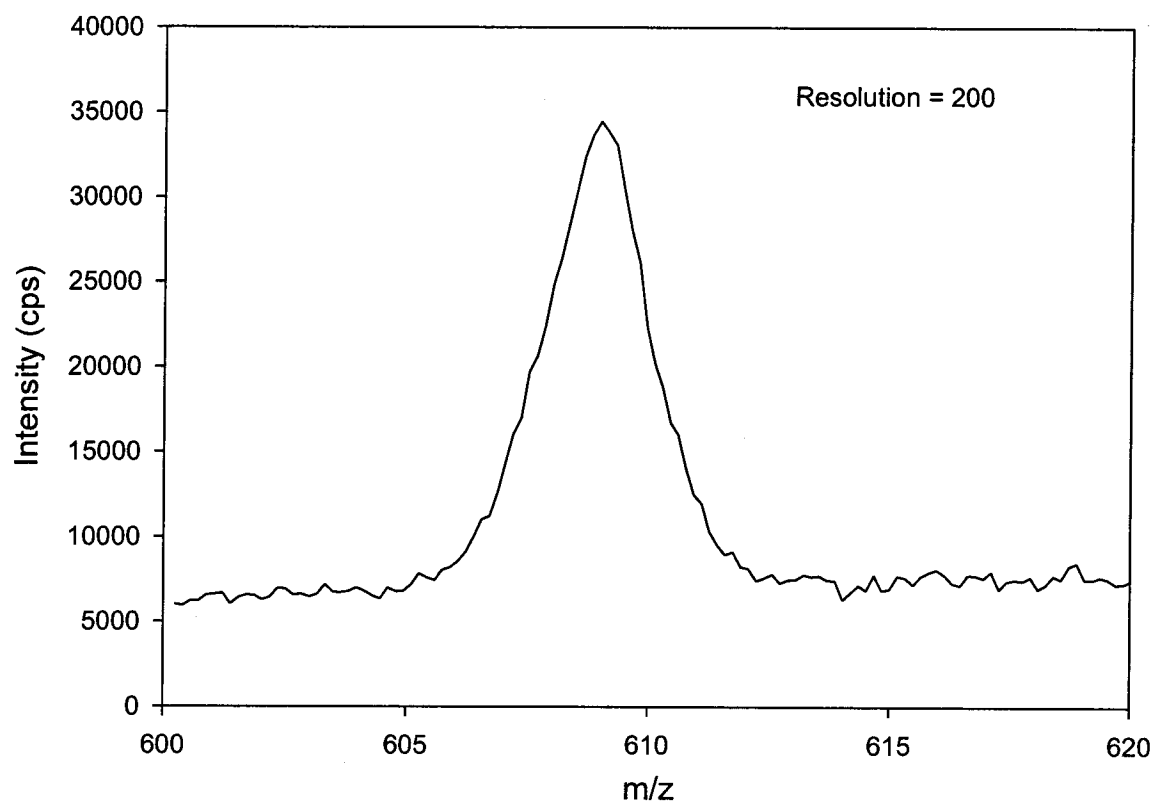
Figure 3.14 MSAE of reserpine ions at q = 0.8765 with 4.0 V_{p-p} dipole excitation applied to the smaller rods.

3.4 Summary

Resolution and peak shapes with MSAE of ions at the stability boundary $q = 0.908$ with a conventional round rod set were similar to those obtained by Hager, with some differences that were discussed in this chapter. MSAE of ions with a quadrupole with 2.6% added octopole field produced only a low-resolution spectrum with ejection at the stability boundary. Calculation of the stability diagram showed that the x and y motions have separate stability boundaries on the $a = 0$ axis. Results obtained when dipole excitation was applied between the larger rods and ions were ejected at $q = 0.8765$ were promising. Resolution was improved by an order of magnitude and isotopic peaks were resolved (not to baseline).

Chapter 4 Mass Selective Axial Ejection of Trapped Ions from a Linear Quadrupole

4.1 Introduction

In this chapter the MSAE of trapped ions from a conventional quadrupole rod set will be described. Different modes of excitation will be demonstrated. For each mode of excitation the optimum values of excitation amplitude and exit lens voltages were investigated. The effects of scan direction and scan speed on axial ejection of ions with each mode of excitation were explored.

4.1.1 Review of the Theoretical Treatment of MSAE of Ions from Linear Ion Traps

Londry and Hager [81] studied the electric fields responsible for MSAE of ions trapped in a linear ion trap using a combination of analytic theory and computer simulations. The decay of the two dimensional quadrupole potential in the fringing region near the ends of the rods was described by a function $f(z)$ so that the potential in the fringing regions, Φ_{FF} can be written as

$$\Phi_{FF} = \Phi(x, y) f(z) \tag{4.1}$$

where $\Phi(x, y)$ is the quadrupole potential described in equation (1.1). The axial component of the electric field due to the decay of the quadrupole field is

$$E_{z,quad} = -\Phi(x, y) \frac{\partial f(z)}{\partial z} \tag{4.2}$$

In trapping mode there is no dc component to the quadrupole potential. Therefore the Dehmelt [82] approximation for ion motion can be adapted and $\Phi(x, y)$ and consequently $E_{z,quad}$ can be approximated by a pseudo or effective potential. The effective potential for the time dependent potential of equation (1.1) is given by

$$V_{eff} = \frac{e|\vec{E}|^2}{4m\Omega^2}$$ (4.3)

For the potential of equation (1.1) the effective potential can be calculated using equation (4.3)

$$V_{eff}(x, y) = \frac{qA_2^2 V}{4}(\frac{x^2 + y^2}{r_0^2})$$ (4.4)

which gives

$$E_{z,quad} = \left|\frac{\partial f(z)}{\partial z}\right|\frac{m\Omega^2}{16e}q^2(x^2 + y^2)$$ (4.5)

where m is the mass of a singly charged ion, e is the electronic charge and Ω is the angular frequency of the drive rf. Equation (4.5) shows that as a result of a decreasing quadrupole potential in the fringing region ($f(z)$ decreasing with z), ions will experience a net positive axial electric field. To a first approximation, this field is proportional to the square of the radial displacement, the square of the q value and the mass to charge ratio of the ion.

In order to eject ions in a mass selective fashion the positive electric field described by equation (4.5) must be balanced by a negative electric field, which decreases in strength with increasing ion radial displacement. This can be achieved by applying a static potential to the exit lens. Londry and Hager [81] obtained the electric field

$E_{z,lens}$ arising from the exit lens potential, by differentiating a numerical solution to the Laplace equation. Plotting the contribution of $E_{z,lens}$ to the total electric field in the $x - z$ plane, for a specific exit lens potential showed that the $|E_{z,lens}|$ decreases with increasing x.

The two contributions to the axial component of the electric field, $E_{z,quad}$ and $E_{z,lens}$ were summed to obtain the total axial field experienced by an ion, $E_{z,rf}$. When the resulting $E_{z,rf}$ was plotted as a function of axial position for most values of radial displacement x, there was a value of z for which $E_{z,rf} = 0$. The locations of these zero crossings were marked in the $x - z$ plane. These points defined a surface on which the net axial force acting on an ion is zero. The shape of this surface is similar to a cone and for this reason it was called the "cone of reflection". Only ions with sufficient radial amplitude are able to penetrate this surface and be ejected axially, while others are reflected.

Londry and Hager [81] discussed the impacts of different parameters like the q-value and exit lens potential on the cone of the reflection. The calculations were consistent with their experimental results. The effects of the exit lens potential are discussed below.

For MSAE to be effective, the exit lens potential must be chosen carefully. When it is reduced below optimum, resolution is degraded. If increased above optimum, sensitivity is reduced. The mapping of cones of reflection for different exit lens potentials confirmed this. When the exit lens potential is too low, the cone of reflection is further from the exit lens. As a result, the cone can be penetrated by ions with only moderate

radial amplitude and the resolution is degraded. With increasing exit lens potential, the cone moves toward the ends of the rods, and ions require higher radial amplitudes to penetrate the cone and be detected.

In this thesis a theoretical treatment of this kind is not attempted. Nevertheless the experimental results are consistent with Londry and Hager's theoretical results, both for MSAE of ions from a conventional linear quadrupole, and a linear quadrupole with a 2.0% added octopole field.

4.2 Experimental

The single quadrupole instrument described in chapter 2 was used to perform MSAE experiments with a conventional linear quadrupole. The instrument was operated in trapping mode as described in chapter 2. Briefly, as shown in the schematic of the scan function provided in Figure 2.8, ions are injected into the linear ion trap and cooled. These ions can be ejected axially in a mass selective way by ramping the amplitude of the rf drive, to bring ions into resonance with a single frequency dipole, dipole-dipole or quadrupole auxiliary signal. The ions gain radial amplitude until they are ejected axially or neutralized on the rods.

4.3 Results and discussion

4.3.1 Dipole Excitation

Dipole excitation was used to excite ions in a conventional rod set at $q = 0.80$ (excitation frequency 413.14 kHz, amplitude 0.03 V_{p-p}). For the experiments described

here for scan speeds of 15 Th/s there was no resolving dc added to the rods. For all the other reported scan speeds there was 7 V dc added between the rods to eliminate the background and to increase sensitivity with faster scans. As Hager [83] argued, the problem of an underlying continuum background could be significant for MSAE experiments with ions introduced from atmospheric pressure ion sources like ESI. These devices can produce ionic clusters of varying sizes and energies. Higher mass ions with q-values lower than the ejection q-value can also pass the exit lens barrier if their kinetic energies are sufficient. These ions do not gain significant energy in the fringing field and they will be observed as a background contribution to the mass spectrum. It was found that the application of a low level of resolving dc to the quadrupole rod set could significantly reduce this background by allowing the quadrupole to act as a low pass filter [83].

Hager and Londry showed that applying some of the trapping rf to the exit lens can improve the resolution, with no loss of ion signals [79]. Thus in all experiments with trapped ions the drive rf was balanced and, as shown in chapter 2, approximately 23% of the rf was added to the exit lens.

With dipole excitation applied to either pair of rods, MSAE of reserpine ions with forward and reverse scans at low scan speed (15 Th/s) and an excitation amplitude of 0.03 V_{p-p} gave similar spectra, with resolutions of up to 4900 (Figure 4.1).
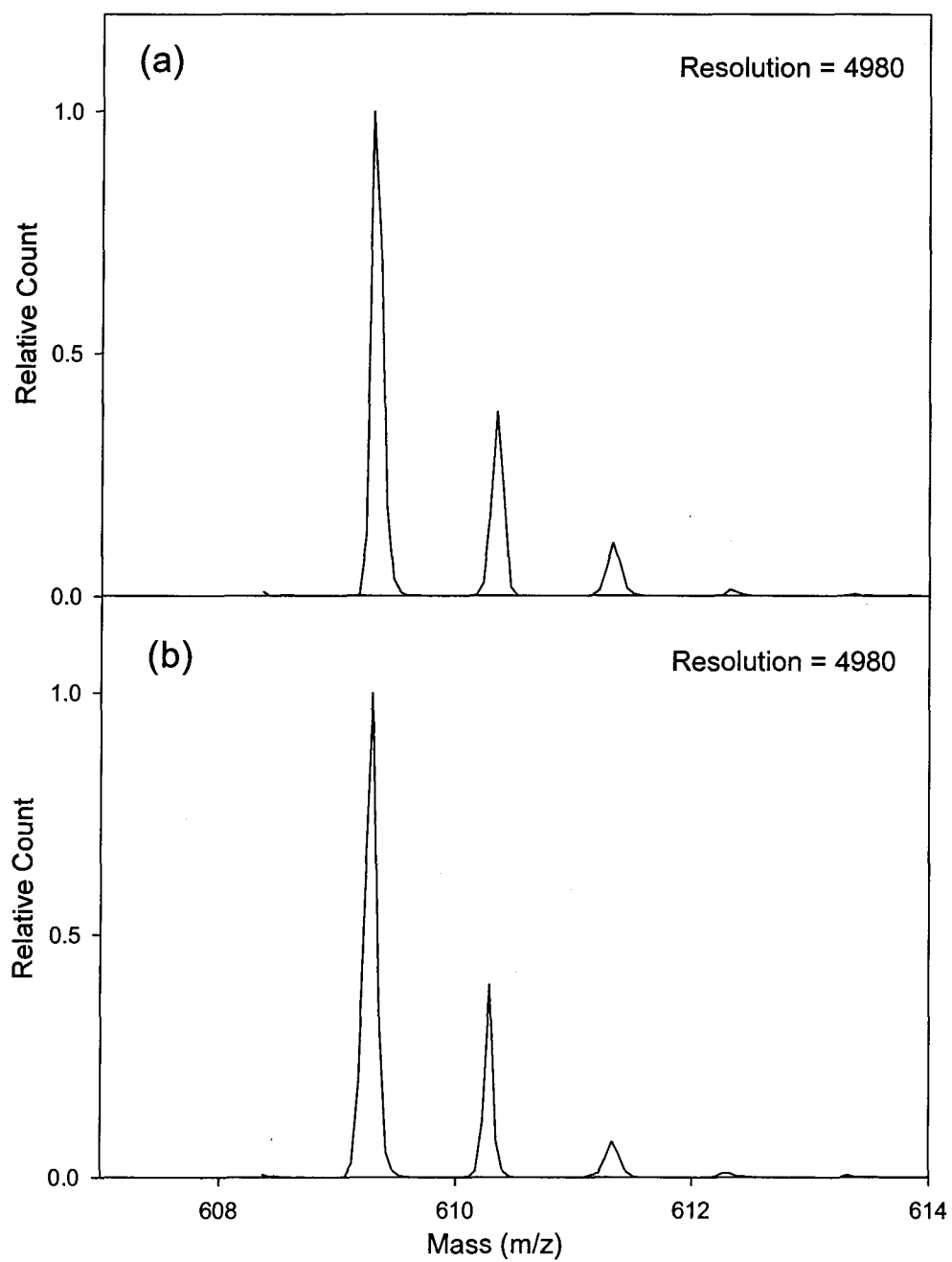
Figure 4.1 Peak shapes and resolution with axial ejection of trapped ions, and dipole excitation. a) forward scan, ejection at $q = 0.80$, 15 Th/s b) reverse scan, ejection at $q = 0.80$, 15 Th/s.

As expected forward and reverse scans with a conventional quadrupole linear ion trap produced similar resolution spectra. With forward and reverse scans, at 1500 Th/s (excitation amplitude 0.6 V_{p-p}) spectra with a resolution of about 3000 were obtained.

With forward scans, at 3300 Th/s (excitation amplitude1.0 V_{p-p}), the resolution was 2350. For the same scan speed and excitation amplitude and with a reverse scan, resolution of 2400 was obtained. With forward scans at 5000 Th/s (excitation amplitude 2.0 V_{p-p}), peaks showed mass shifts and unequal spacings. To calculate the resolution in this case, the peak width of the most abundant peak (the monoisotopic peak) was compared to the spacing between the two most abundant isotopic peaks, taken as 1 mass unit. The resolution, calculated as described above, was 1970. With reverse scans at 5000 Th/s a similar resolution, 2000, (same method of calculation) was achieved. Spectra are shown in Figure 4.2. The unequal peak widths and spacings are likely a result of a limitation of the quadrupole power supply, which was designed for scan speeds of ca. 100 Th/s with step sizes of 0.1 Th.
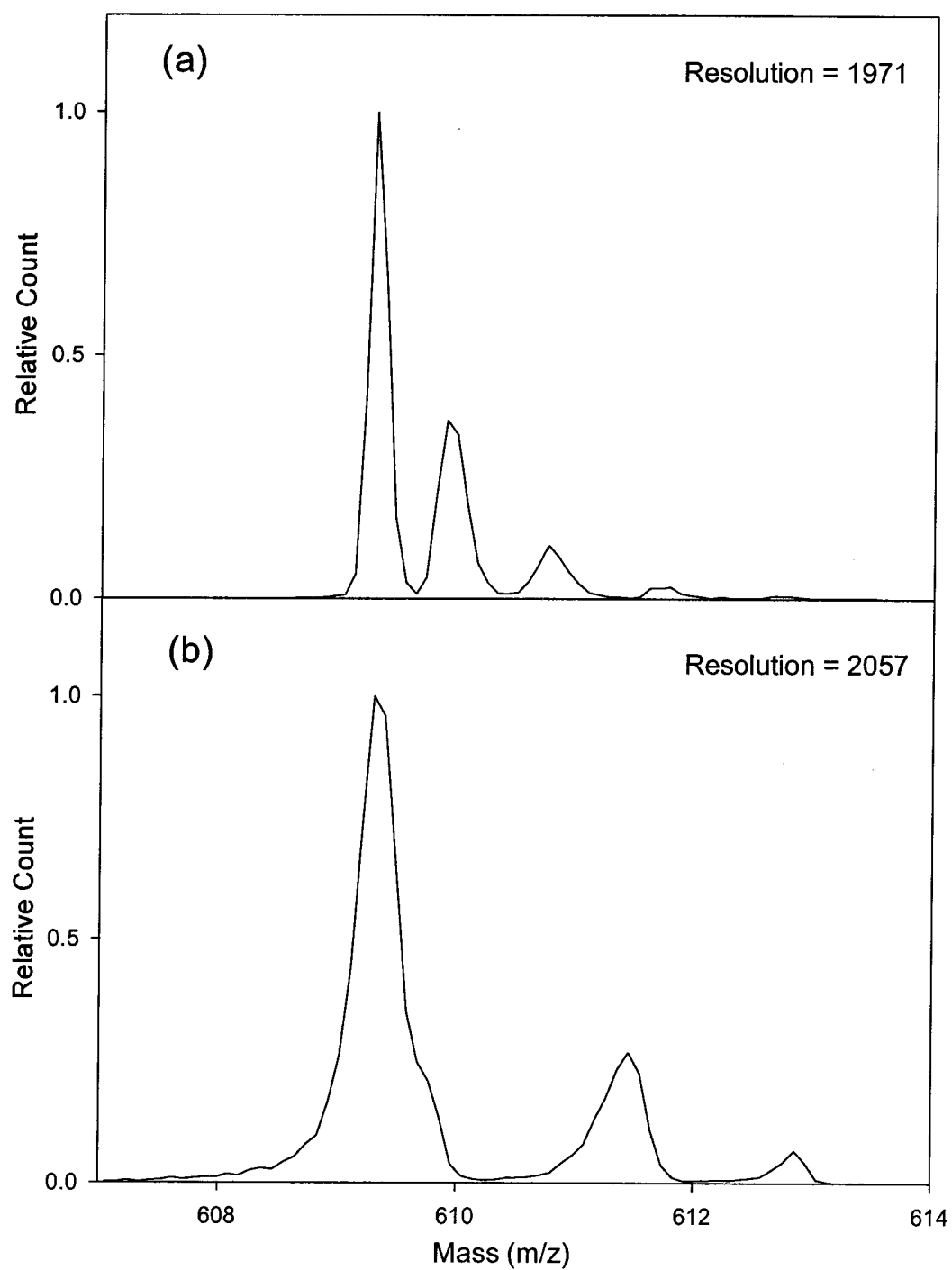
Figure 4.2 Peak shapes and resolution with axial ejection of trapped ions, and dipole excitation. a) forward scan, ejection at $q = 0.80$, 5000 Th/s b) reverse scan, ejection at $q = 0.80$, 5000 Th/s.

4.3.2 Quadrupole Excitation

Auxiliary quadrupole excitation was applied to the conventional quadrupole rods to give parametric excitation at twice the fundamental frequency of ion oscillation. Due to an electronics limitation, the higher auxiliary voltages at the higher frequencies needed for quadrupole excitation at $q = 0.80$ could not be applied, so experiments were performed with ions trapped at $q = 0.7002$ (excitation frequency 676.00 kHz).With quadrupole excitation (0.90 V_{p-p}) and with a scan speed of 15 Th/s, both forward and reverse scans gave a resolution of 4300-4700. High scan speed was also possible with both forward and reverse scanning. With 7 V dc added between the rods, forward scanning (3.76 V_{p-p}) and a scan speed of 3800 Th/s, the resolution was 1580, and with reverse scanning (3.65 V_{p-p}) and a scan speed of 3300 Th/s, resolution of 1500 was possible. Scan speeds higher than 3300 - 3800 Th/s in each scanning direction resulted in poor peak shapes. Reverse scanning gave somewhat better peak shapes and slightly higher resolution. Figure 4.3 shows MSAE of Agilent tune mix m/z =622 with reverse scanning at two different scan speeds.
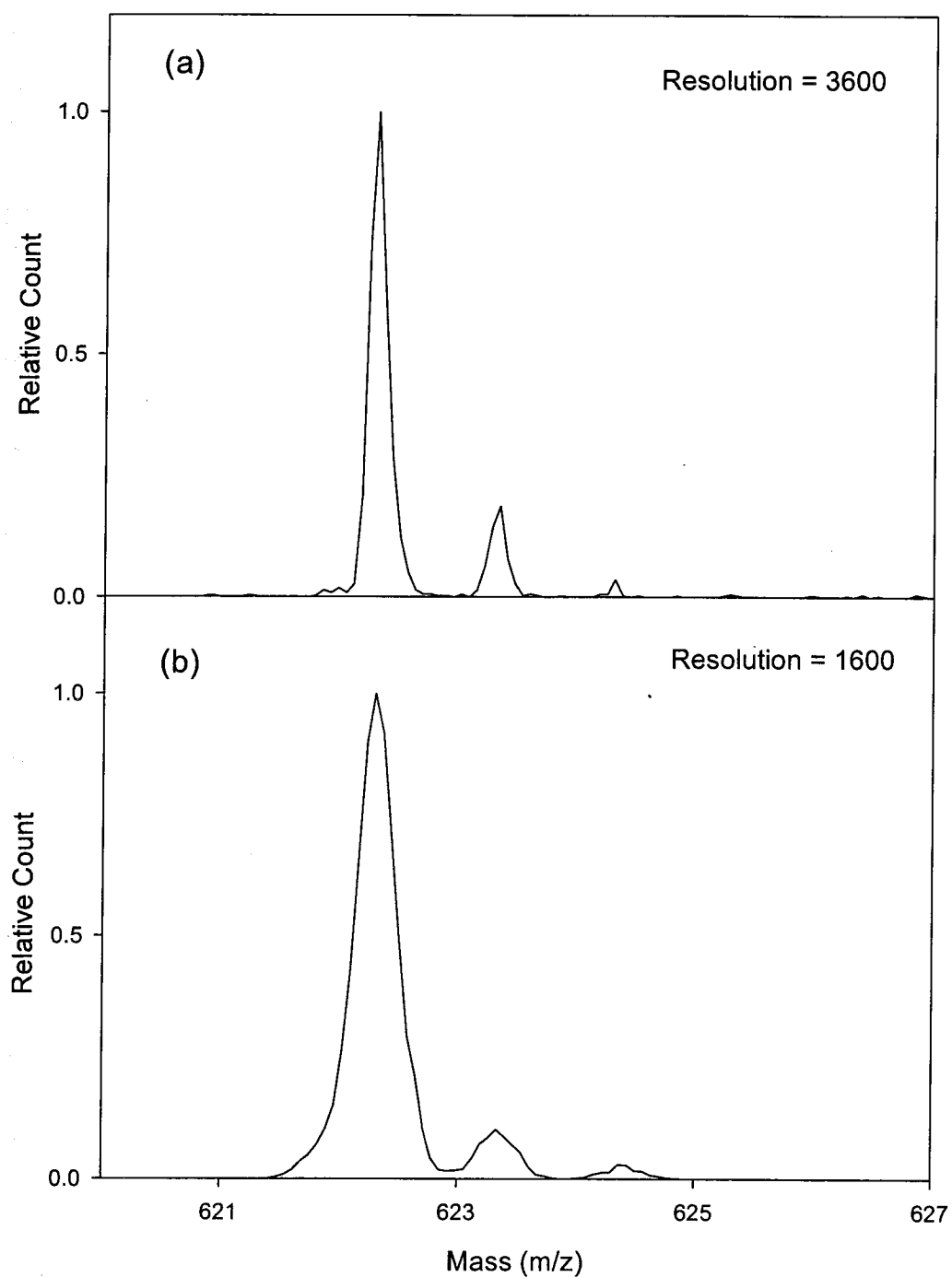
Figure 4.3 Peak shapes and resolution with axial ejection of trapped ions, and quadrupole excitation. a) reverse scan, ejection at $q = 0.7002$, 15 Th/s b) reverse scan, ejection at $q = 0.7002$, 3300 Th/s.

4.3.3 Dipole-Dipole Excitation

Experiments were done with dipole excitation applied simultaneously to both pairs of rods. The optimal excitation amplitudes for different scan speeds ranged from 0.05 V_{p-p} at 15 Th/s to 3.5 V_{p-p} at 5000 Th/s. With forward scans, low scan speeds (15 Th/s) gave a resolution of around 4600. With increasing scan speed, about 3000 Th/s, a resolution of 2100 was possible, and with a scan speed at 5000 Th/s, the resolution was 1500. Dipole-dipole excitation resulted in lower resolution at higher scan speeds than single dipole excitation. No improvements in scan speed or resolution were found with dipole-dipole excitation.

4.4 Summary

High resolution and high scan speeds were possible with MSAE experiments with a conventional round rod quadrupole ion trap. Different excitation modes with different scan direction and scan speeds were tested. With dipole excitation with either forward or reverse scanning directions at scan speeds of 5000 Th/s resolution of 2000 is possible. With quadrupole excitation maximum achievable scan speed was about 3300 – 3800 for forward and reverse scanning respectively. In this case resolution was 1500 Th/s. With dipole-dipole excitation resolution of 1500 was possible with a scan speed of 5000 Th/s. Dipole excitation yields higher resolution than quadrupole or dipole-dipole excitation.

Chapter 5 Mass Selective Axial Ejection of Trapped Ions from a Quadrupole with a 2.0% Added Octopole Field

5.1 Introduction

In this chapter the MSAE of trapped ions from a quadrupole with 2.0% added octopole field will be described. Different modes of excitation will be discussed. For each mode of excitation the optimum values of excitation amplitude and exit lens voltage were investigated. The effects of scan direction and scan speed on axial ejection of ions with each mode of excitation were explored.

5.1.1 Octopole Potential and Frequency Shifts

The electric potential within the rod sets with a 2.0% octopole field is given to a good approximation by

$$\Phi(x,y,t) = \left(A_0 + A_2 \frac{x^2 - y^2}{r_0^2} + A_4 \frac{x^4 - 6x^2 y^2 + y^4}{r_0^4} \right)(U - V \cos\Omega t) \tag{5.1}$$

where x is the distance from the centre towards a smaller rod, y is the distance from the centre towards a larger rod, U and V are the amplitudes of dc and rf voltages applied from pole to ground, A_0, A_2 and A_4 are the dimensionless amplitudes of a constant potential, the quadrupole potential and the octopole potential respectively. For these rod

sets $A_2 \approx 1.00$ and $A_0 \approx -A_4$. Use of round rods adds other multipoles to the potential

(Table 2.2) [53, 56].

For the potential of equation (5.1) the effective potential can be calculated using

equation (4.3) as [57]

$$V_{eff} = \frac{qA_2^2 V}{4}\left(\frac{x^2 + y^2}{r_0^2}\right) + \frac{qA_2 A_4 V}{1}\left(\frac{x^4 - y^4}{r_0^4}\right) + \cdots \qquad (5.3)$$

where q is given by equation (1.6). The first term in equation (5.3) is the effective

potential for a linear rf-only quadrupole, and the second term describes the modifications

caused by the octopole field. Terms in $x^m y^n$ have not been included in equation (5.3)

since only the excitation of the x motion when $y = 0$ is considered and the y motion

when $x = 0$. In the direction of the x rods the effective potential increases more rapidly

with distance from the center than that of a pure quadrupole potential, and in the y

direction increases less rapidly than that of a pure quadrupole potential.

Motion of a singly charged ion in the x direction in the effective potential of

equation (5.3) is described by

$$m\frac{d^2 x}{dt^2} = F_x = -e\frac{\partial V_{eff}}{\partial x} = -\frac{eqA_2^2 V 2x}{4r_0^2} - \frac{4eqA_2 A_4 V x^3}{r_0^4} \qquad (5.4)$$

Equation (5.4) can be written

$$\frac{d^2 x}{dt^2} + \omega_0^2 x = -\frac{4eqA_2 A_4 V x^3}{mr_0^4} \qquad (5.5)$$

where

$$\omega_0^2 = \frac{eqA_2^2 V 2}{4mr_0^2} \qquad (5.6)$$

which can be written as

$$\omega_0 = \frac{qA_2\Omega}{\sqrt{8}} \tag{5.7}$$

Equation (5.7) is the secular frequency of the ion which can be calculated using equations (1.10) and (1.11).

Equation (5.5) resembles the equation of motion for an anharmonic oscillator described by Landau and Lifshitz [84]

$$\frac{d^2x}{dt^2} + \omega_0^2 x = -\alpha x^2 - \beta x^3 \tag{5.8}$$

where $\alpha = 0$ and $\beta = -\frac{4eqA_2A_4V}{mr_0^4}$. The anharmonic terms on the right of equation (5.8)

cause shifts in the resonant frequency from ω_0, given by [84]

$$\Delta\omega = \left(\frac{3\beta}{8\omega_0} - \frac{5\alpha^2}{12\omega_0^3}\right)b^2 \tag{5.9}$$

where b is the amplitude of oscillation. Therefore the frequency shift caused by the octopole field is

$$\Delta\omega = \frac{3eqA_2A_4V}{2mr_0^4\omega_0}b^2 \tag{5.10}$$

Equation (5.10) can be rewritten substituting V from equation (5.6)

$$\Delta\omega = 3\frac{A_4}{A_2}\left(\frac{b^2}{r_0^2}\right)\omega_0 \tag{5.11}$$

5.1.2 Mass Resolution and Frequency Resolution

Mass resolution and frequency resolution in the ion trap can be related by proceeding from the fundamental equation [85],

$$m = \frac{\sqrt{2}eV}{\omega_0 r_0^2 \Omega} \qquad q_u < 0.4 \qquad\qquad (5.12)$$

Differentiating equation (5.12) gives

$$dm = \left(\frac{\sqrt{2}eV}{\omega_0 r_0^2 \Omega}\right)_{\omega_0,\Omega} dV - \left(\frac{\sqrt{2}eV}{\omega_0^2 r_0^2 \Omega}\right)_{V,\Omega} d\omega_0 - \left(\frac{\sqrt{2}eV}{\omega_0 r_0^2 \Omega^2}\right)_{\omega_0,V} d\Omega \qquad (5.13)$$

Equation (5.13) indicates that a small change in the amplitude of the drive rf or in the secular frequency or the drive frequency is linearly related to a small deviation in mass. Consequently, mass analysis by resonance ejection can be achieved by ramping the rf voltage level, by varying the frequency of the supplementary excitation, or by sweeping the drive rf frequency. Setting dV and $d\Omega$ to zero in equation (5.13), dividing by equation (5.12), and making the assumption that $d\omega_0 \approx \Delta\omega_0$ and $dm \approx \Delta m$ yields

$$\frac{\omega_0}{\Delta\omega_0} = \frac{m}{\Delta m} \qquad\qquad (5.14)$$

This indicates that mass resolution is numerically equal to the frequency resolution for $q_u < 0.4$. Substituting the expression $\omega_0 = \dfrac{q_u \Omega}{2\sqrt{2}}$ into equation (5.14) gives

$$\frac{m}{\Delta m} = \frac{q_u \Omega}{2\sqrt{2}\Delta\omega_0} \qquad\qquad (5.15)$$

Equation (5.15) shows the relation of mass resolution to the fundamental operating parameters and the frequency resolution. For a given $\Delta\omega_0$, the mass resolution increases with q.

5.2 Experimental

The single quadrupole instrument operated in trapping mode as described in chapter 2 was used to perform MSAE experiments with the quadrupole with a 2.0% added octopole field. Different modes of applied rf, excitation and applied dc are possible and are summarized in Table 5.1. In principle, any of the three rf modes can be combined with any of the excitation modes and with any of the methods of applying dc (36 combinations).

Table 5.1 Modes of applied rf, excitation and dc.

rf	Excitation Mode	dc between Rods
balanced	none	none
unbalanced	dipole (smaller or larger rods)	+ smaller rods
~ 20% on exit lens	dipole-dipole	+ larger rods
	quadrupole	

5.2.1 Mass Calibration

The rf and dc levels of the voltages applied to the quadrupole rods with conventional analysis are set by and are linearly proportional to a mass command voltage between 0 and 10.0 V. To mass calibrate the spectra shown here, the quadrupole was first run

conventionally with rf/dc and calibrated so that the monoisotopic reserpine peak appeared at m/z 609.3. In this case the rf level corresponds to the tip of the stability diagram where $q = 0.70600$ [7]. Ions were then mass selectively ejected at various q values, and the voltage at which they were ejected was determined from the MCS ramp parameters. The apparent mass was calculated from

apparent mass= (ejection voltage) * 609.3/ (voltage with conventional analysis).

The apparent mass did not correspond exactly to that expected from the q value selected for ejection (see below). For the spectra of Figures 2-6, the masses were recalculated so that the monoisotopic peak appeared at the correct mass (e.g. 609.3 for reserpine).

5.3 Results and Discussion

5.3.1 Dipole Excitation with a Quadrupole with a 2.0% Added Octopole Field

Initial experiments with trapped ions and a quadrupole with a 2.0% added octopole field were tried with ejection at the stability boundary near $q = 0.908$. As with experiments without trapping, only very low resolution was found. Therefore all subsequent experiments with trapped ions used auxiliary ac voltages to excite ions for axial ejection.

Axial ejection experiments with dipole excitation between the larger or smaller rods were done with a quadrupole with a 2.0% added octopole field. When the quadrupole is used as either a mass filter or a linear trap in a triple quadrupole system [72], it is necessary to operate the rod set as both a conventional rf/dc mass analyzer and a linear

ion trap with axial ejection. Operation as a mass filter requires that the positive dc be applied to the smaller rods [56]. As mentioned in section 3.3.1 applying some of the trapping rf (balanced) to the exit lens can improve the resolution, with no loss of ion signals [79]. Thus in all experiments with trapped ions the drive rf was balanced (23% applied to the exit lens) and the positive dc was applied to the smaller rods. The polarity of the dc applied between the rods was reversed and it was found that this gave no improvements in resolution. With low scan speeds (10-15 Th/s), no resolving dc was added to the rods. Adding dc did not improve the resolution. With high scan speeds (>300 Th/s) adding the low and optimum levels of dc that are indicated below helped to improve the ejection efficiency and resolution.

5.3.1.1   Comparison of Ejection at Different q Values

Initially, ejection with excitation frequencies corresponding to q values of 0.4, 0.5, 0.6, 0.7 and 0.8 was tested. Figures 5.1 and 5.2 show results of ejection at $q = 0.40$ and $q = 0.80$ respectively, with excitation between the larger rods (reverse scans) and smaller rods (forward scans) respectively. No resolving dc was added. Higher q values result in higher resolution. With dipole excitation applied to the larger rods and reverse scanning, excitation amplitudes of $0.03 - 0.1$ V_{p-p} at scan speeds of 10-15 Th/s gave the best peak shape and resolution. With dipole excitation applied to the smaller rods and forward scanning, an excitation amplitude of 0.30 V_{p-p} at scan speeds of 10-15 Th/s, was optimal.

Figure 5.1 Peak shapes and resolution with axial ejection of trapped ions, and dipole excitation between the larger (y) rods. a) reverse scan, ejection at $q = 0.40$, 10 Th/s b) reverse scan, ejection at $q = 0.80$, 10 Th/s.

Figure 5.2 Peak shapes and resolution with axial ejection and dipole excitation between the smaller (x) rods. a) forward scan, ejection at $q = 0.40$, 10 Th/s b) forward scan, ejection at $q = 0.80$, 15 Th/s.

Three factors may contribute to the higher resolution at higher q values. First, ions

have higher oscillation frequencies at higher q. According to equations (5.14) and (5.15)

for a given $\Delta\omega_0$, the frequency resolution $\omega_0 / \Delta\omega_0$ and hence mass resolution, $m / \Delta m$

increases with q. Second β, and hence the resonant frequency of an ion, is a nonlinear

function of q and increases more rapidly with q at higher q values. This increases the

rate of change of frequency with mass, ($\dfrac{df}{dm} = \dfrac{df}{dq}\dfrac{dq}{dm} = -\dfrac{q}{m}\dfrac{df}{dq}$) which may also increase

mass resolution. Third, the strength of $E_{z,quad}$ increases with the square of q (equation

(4.5)). Higher values of $E_{z,quad}$ mean that higher stopping potentials can be used on the

exit lens and these higher potentials give higher resolution.

5.3.1.2   Comparison of Forward and Reverse Scans

Figure 5.3 shows a comparison between forward and reverse scans with excitation

between the larger rods (15 Th/s). No dc was added between the rods. Higher resolution

is possible with reverse scans. Figure 5.4 compares forward and reverse scans with

excitation between the smaller rods (15 Th/s). No dc between the rods was added. In this

case forward scans give higher resolution. These results are as expected from the

frequency shifts caused by the added octopole field [86]. The shift of oscillation

frequency, $\Delta\omega$, in a quadrupole with an added octopole is given by equation (5.11).

When $A_4 > 0$, the x motion shifts to higher frequencies. The shift is proportional to

A_4 and to the square of the amplitude of ion oscillation. For the y motion there is a shift

to lower frequency of the same magnitude for the same amplitude of oscillation. With

excitation between the smaller rods and forward scanning, as the rf amplitude increases,

the oscillation frequencies of the ions increase. As the ions come into resonance their frequencies are further increased by the octopole component. These frequency shifts drive the ions faster toward the frequency of the auxiliary ac, which in turn causes the ion oscillation amplitudes to grow more rapidly until ions are ejected from the trap. With excitation between the smaller rods and reverse scanning, as the rf amplitude decreases the oscillation frequencies of the ions decrease. As the ions come into resonance their frequencies are increased by octopole component. These frequency shifts causes the ions to move away from the frequency of the auxiliary ac, which in turn causes the oscillation amplitudes to grow more slowly, and this degrades mass resolution. For similar reasons, reverse scans give higher resolution with excitation between the larger rods.

The apparent masses at which ions of m/z 609.3 are ejected are consistent with this explanation and are shown in Table 5.2. With forward scans, and excitation between the smaller rods, ions are ejected at an apparent mass of 685.56. With the ejection between the larger rods, the ions are ejected at 686.15, showing that ejection is delayed and the quadrupole must scan up to a somewhat higher rf voltage before the ions are ejected. With a reverse scan and excitation between the larger rods, ions are ejected 689.32. With excitation between the smaller rods, the ions are ejected at 688.53, showing again that ejection is delayed and the quadrupole must scan down to a lower rf voltage before the ions are ejected.
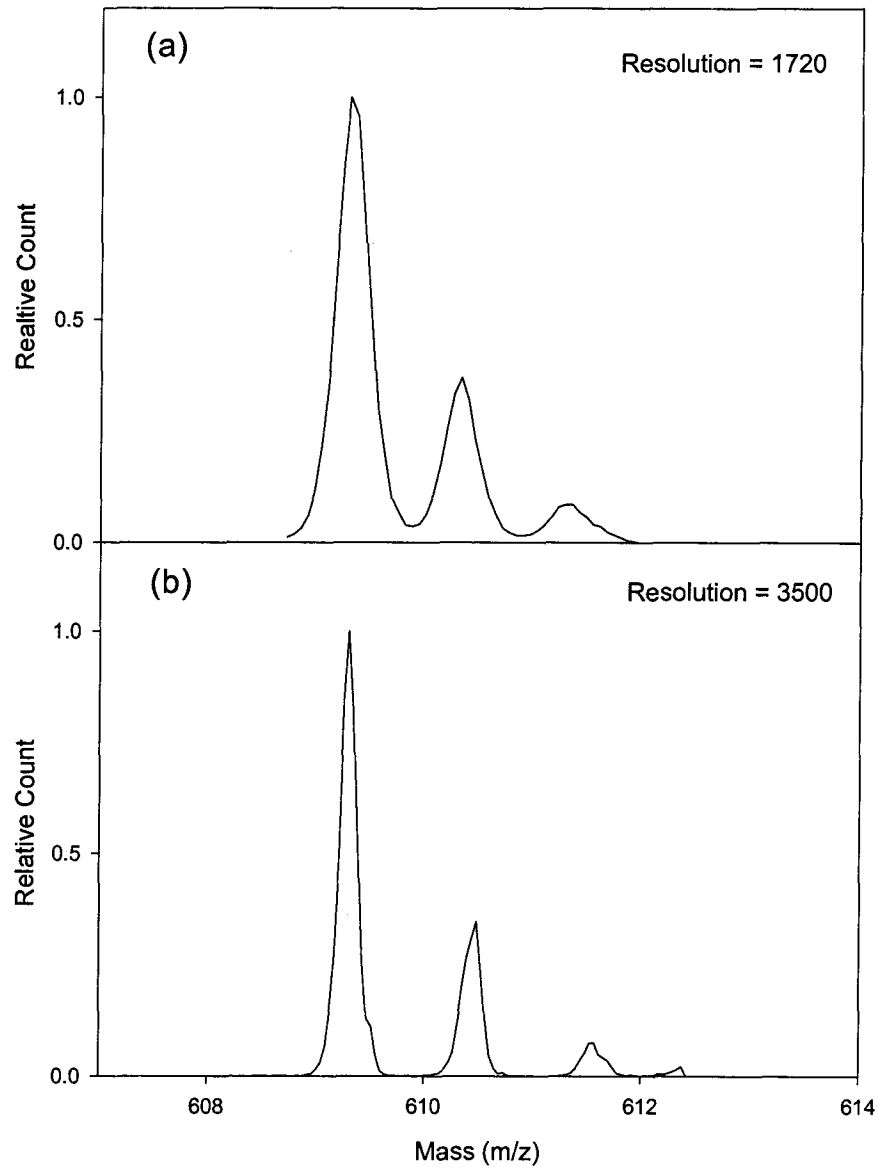
Figure 5.3 Peak shapes and resolution with axial ejection of trapped ions, and dipole excitation between the larger (y) rods. a) forward scan, ejection at $q = 0.80$, 15 Th/s b) reverse scan, ejection at $q = 0.80$, 15 Th/s.
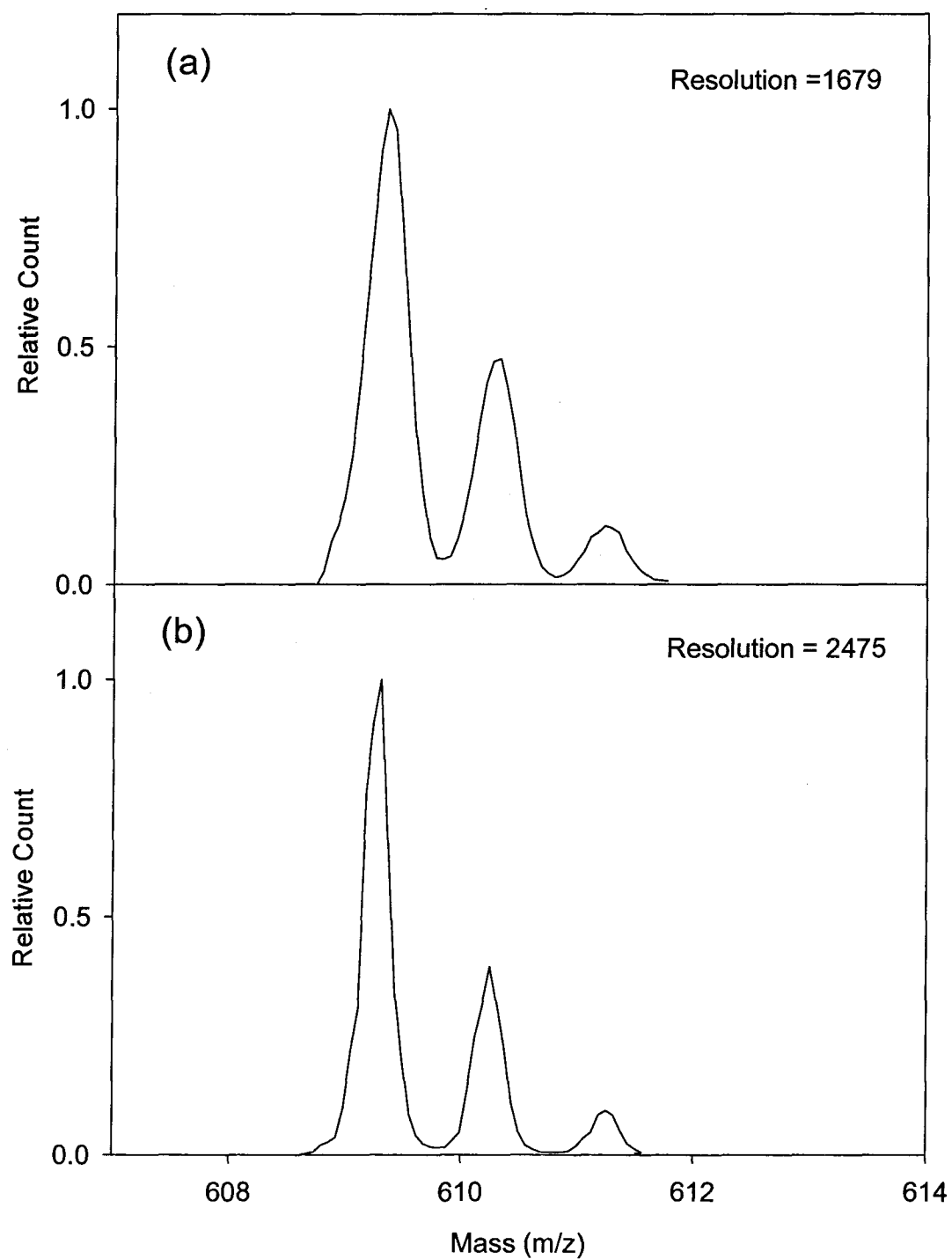
Figure 5.4 Peak shapes and resolution with axial ejection and dipole excitation between the smaller (x) rods. a) forward scan, ejection at $q = 0.80$, 15 Th/s b) reverse scan, ejection at $q = 0.80$, 15 Th/s.

Table 5.2 Apparent mass of reserpine with different scan directions with trapped ions excited between the smaller and larger rods at $q \approx 0.8$ and a scan speed of 10 Th/s.

Scan direction	rod pair with applied excitation	Apparent mass of m/z 609.28
forward	smaller	685.56
forward	larger	686.15
reverse	larger	689.32
reverse	smaller	688.53

5.3.1.3   Comparison of Different Scan Speeds

The effects of higher scan speeds were investigated. Figure 5.5 shows spectra of

reserpine ions with excitation between the larger rods and scan speeds of 1570 and 5000

Th/s respectively (reverse scans). There was 10 V dc added between the rods. At higher

scan speeds, with dipole excitation applied to the larger rods and reverse scanning, an

excitation amplitude of 0.55 – 1.0 V_{p-p} at scan speeds of 3000-5000 Th/s gave the best

peak shape and resolution. Figure 5.6 shows spectra of reserpine ions with excitation

between the smaller rods at scan speeds of 1500 Th/s (with 7 V dc) and 5000 Th/s (with

10 V dc) respectively (forward scans). With dipole excitation applied to the smaller rods

and forward scanning, an excitation amplitude of 10 V_{p-p} at scan speeds of 3000-5000

Th/s was optimal. At scans speeds of ca.1500 Th/s (Figures 5.5a and 5.6a) the resolution

is about 1500. At 5000 Th/s (Figures 5.5b and 5.6b) the peak widths and spacing are not

constant, particularly with reverse scans, Figure 5.5b. The resolution in this case, was

calculated as described in section 4.3.1. Resolutions of ca. 1000 (Figure 5.5b) and 1600 (Figure 5.6b) are calculated.

Figure 5.5 Peak shapes and resolution with axial ejection of trapped ions, and dipole excitation between the larger (y) rods. a) reverse scan, ejection at $q = 0.80$, 1570 Th/s b) reverse scan, ejection at $q = 0.80$, 5000 Th/s.
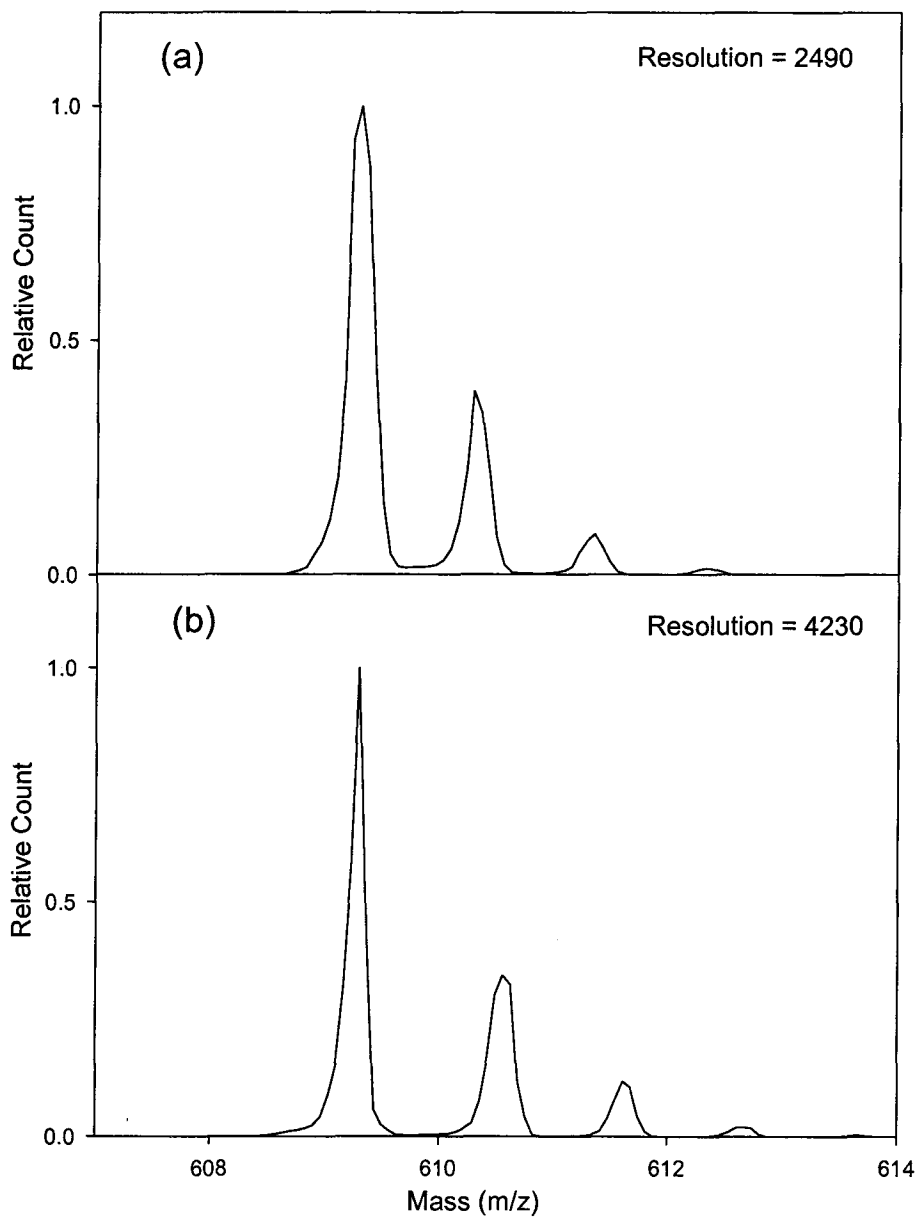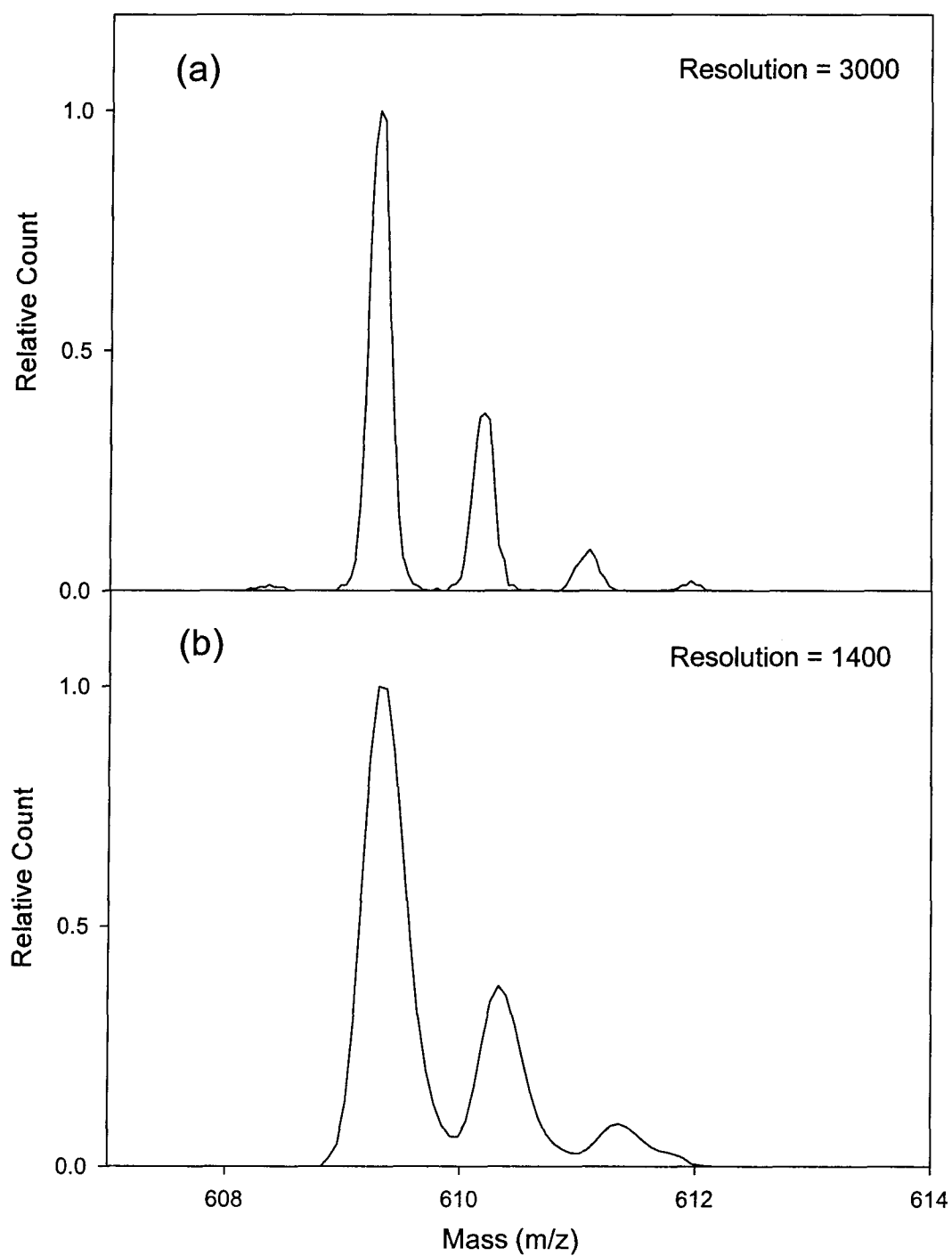
Figure 5.6 Peak shapes and resolution with axial ejection and dipole excitation between the smaller (x) rods. a) forward scan, ejection at $q = 0.80$, 1500 Th/s b) forward scan, ejection at $q = 0.80$, 5000 Th/s.

5.3.2 Quadrupole Excitation with a Quadrupole with a 2.0% Added Octopole Field

Auxiliary quadrupole excitation was applied to the quadrupole rods with a 2.0% added octopole field to give parametric excitation at twice the fundamental frequency of ion oscillation. As with a conventional rod set (section 4.3.2) ions were trapped at $q = 0.7002$ (excitation frequency 676.00 kHz). The optimal excitation amplitude for low scan speeds (10-15 Th/s) was 1.14 Vp-p and the highest possible excitation amplitude for higher scan speeds (3000-5000 Th/s) was 3.64 Vp-p.

With forward scans at 15 Th/s, a resolution of about 1800 was obtained. With reverse scans at 15 Th/s a resolution of about 3100 was possible (Figure 5.7). In both cases no resolving dc was added to the rods. These resolutions are similar to those obtained with dipole excitation between the larger rods. Quadrupole excitation excites ion motion between both the smaller and larger rods. It appears as if the motion between the larger rods dominates the ejection process. Most experiments with quadrupole excitation investigated reverse scanning because this yields higher resolution. With reverse scans at 1200 Th/s and 7.0 V dc between the rods, a resolution of 2300 was obtained, and at 4200 Th/s, a resolution of 1200 was achieved (Figure 5.8). Overall, no advantage to using quadrupole excitation was found.
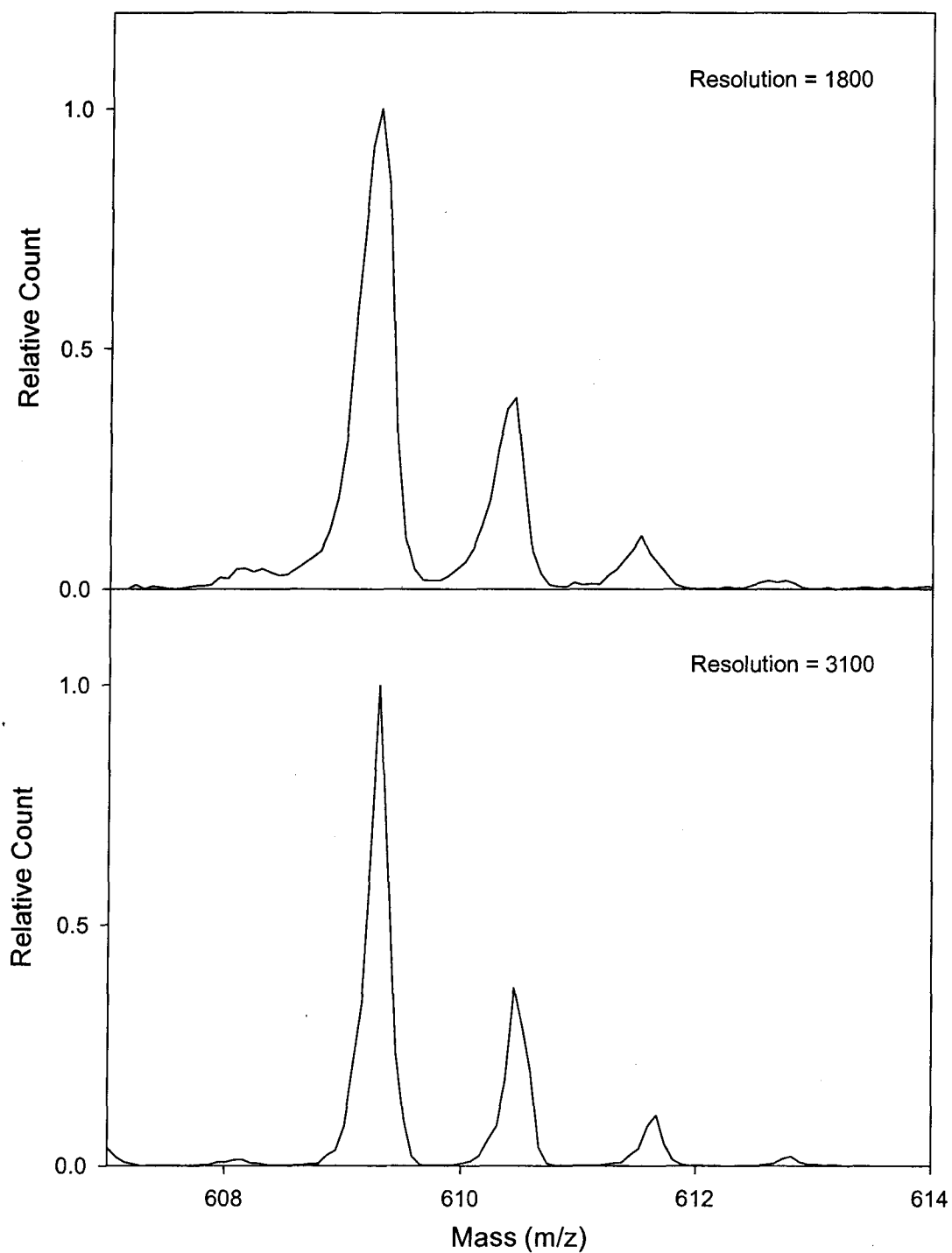
Figure 5.7 Peak shapes and resolution with axial ejection of trapped ions, and quadrupole
excitation between the rods. a) forward scan, ejection at $q = 0.7002$, 15 Th/s b) reverse
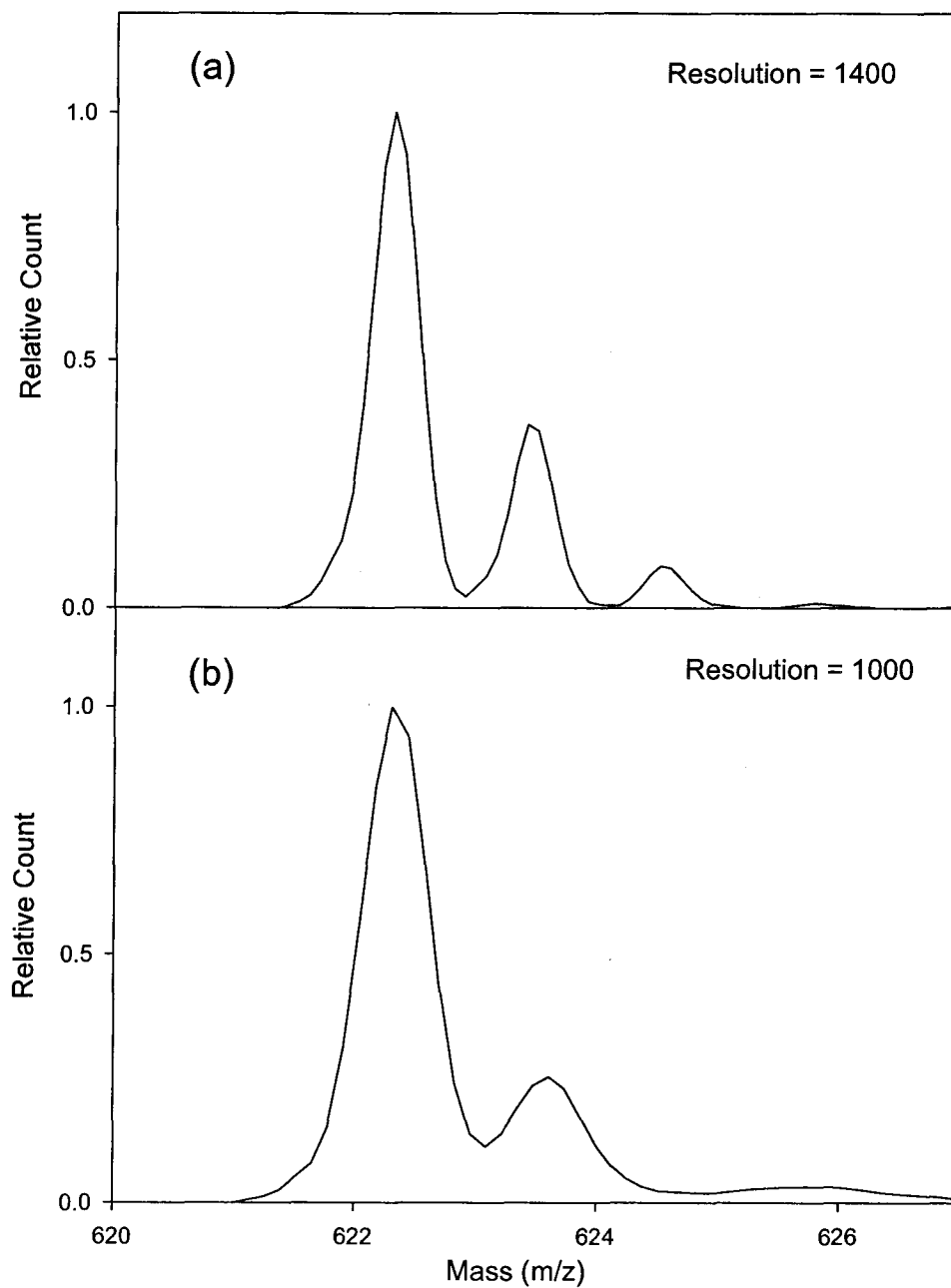scan, ejection at $q = 0.7002$, 15 Th/s.
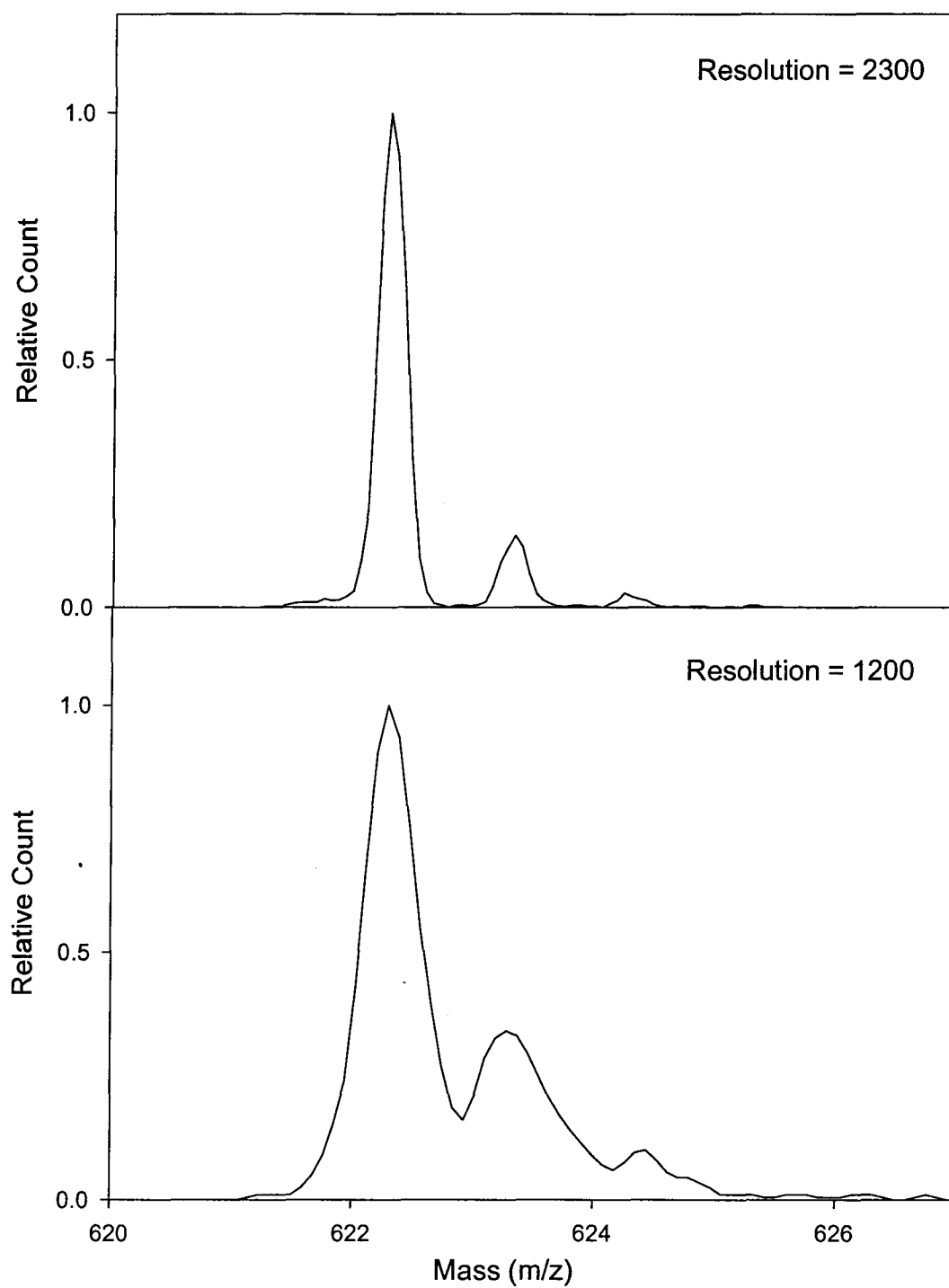
Figure 5.8 Peak shapes and resolution with axial ejection of trapped ions, and quadrupole excitation between the rods. a) reverse scan, ejection at $q = 0.7002$, 1800 Th/s b) reverse scan, ejection at $q = 0.7002$, 4200 Th/s.
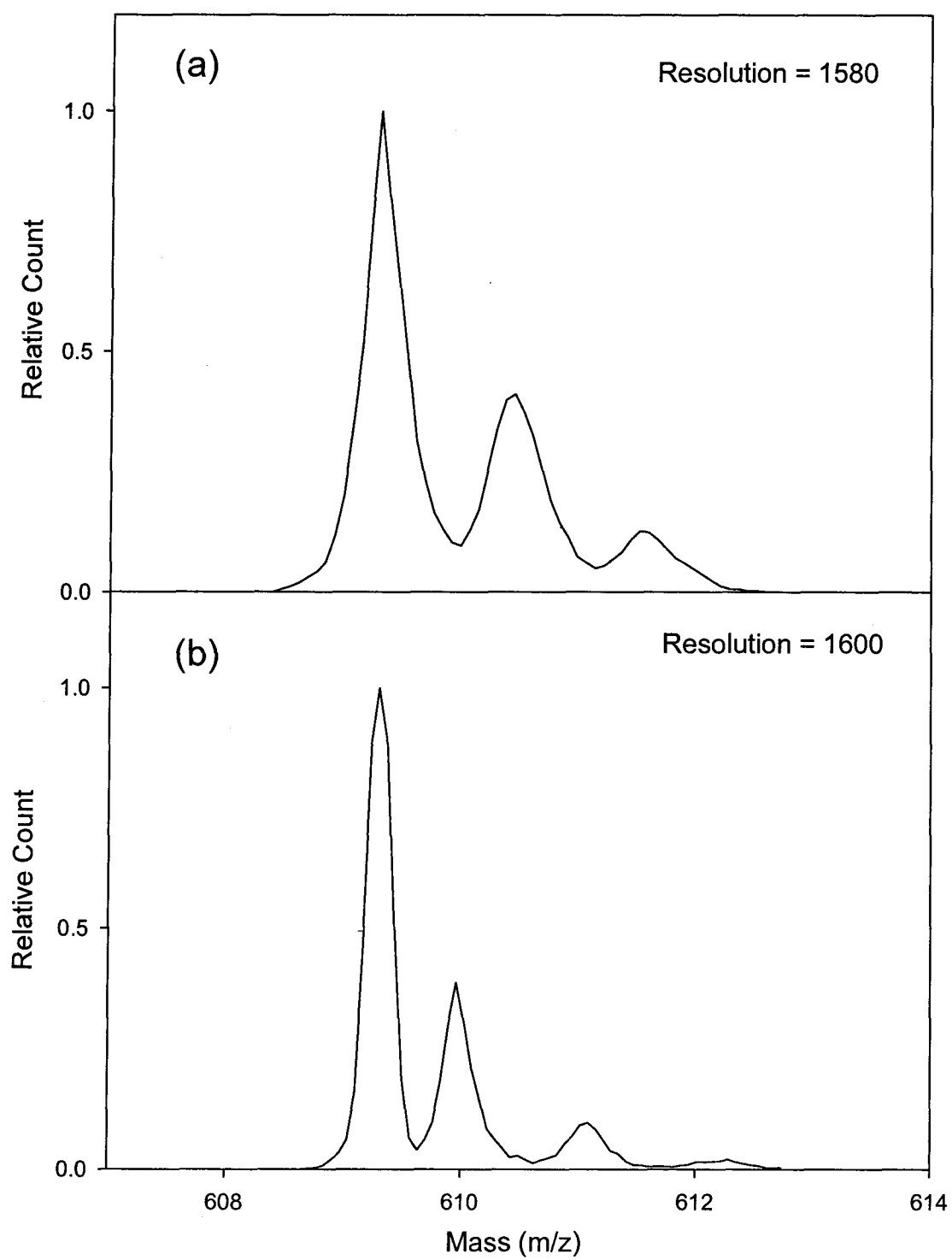
5.3.3 Dipole - Dipole Excitation with a Quadrupole with a 2.0% Added Octopole Field

Experiments were tried with dipole excitation applied simultaneously between the smaller and larger rods with no resolving dc added to the rods, and with scan speeds of 10 Th/s. When the same excitation frequency and amplitude (413.14 kHz and 0.2 Vp-p) were applied to both rod pairs, with forward and reverse scanning the ions were ejected mainly at the apparent masses of m/z= 686.15 and m/z=689.32 respectively. These are the apparent masses at which ions are ejected with excitation between the larger rods alone. Approximately 10% of the ejected ions appeared at the apparent masses corresponding to excitation between the smaller rods, m/z=685.56 and m/z=688.53 for forward and reverse scans respectively. The excitation frequency applied to the smaller rods was then increased to 413.9 kHz, so that ions were ejected at the apparent masses corresponding to excitation between the larger rods. With reverse scanning and a scan speed of 10 Th/s, a resolution of 2000 was possible. This gave resolution lower than that with dipole excitation between the larger rods alone. With forward scanning the resolution decreased to 1200. Thus no improvements were obtained by applying dipole excitation simultaneously between both rod pairs and no additional experiments with faster scans were done.

Figure 5.9 shows a comparison of scan speeds and resolutions achieved with each mode of excitation for a conventional quadrupole and a quadrupole with a 2.0% added octopole field. In general, increasing scan speed decreases resolution. The quadrupole with a 2.0% added octopole field shows somewhat lower resolution than a conventional

rod set at a given scan speed. In all cases resolutions of 1000 or more can be obtained a

scan speeds up to 5000 Th/s.
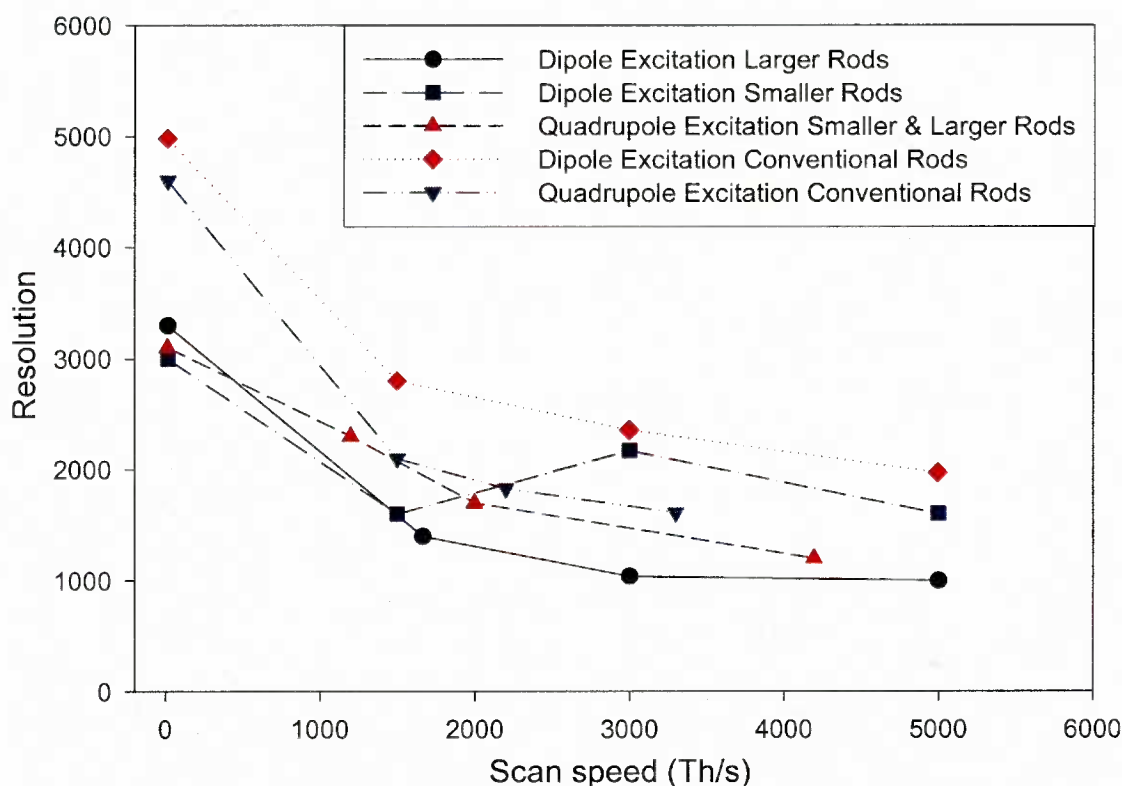
Figure 5.9 Resolution vs. scan speed with different excitation modes, with a conventional quadrupole and a quadrupole with a 2.0% added octopole field.

5.3.4 Optimum Operating Mode with a Quadrupole with a 2.0% Added Octopole field

Mass selective axial ejection of trapped ions that have a broad range of mass to

charge ratios requires ejection at a high q value with forward scans. In this case, dipole

excitation between the smaller rods gives the highest resolution and is the preferred mode

of operation. Conversely, with reverse scans, a broad range of mass to charge ratios can be mass analyzed with ejection at low q. For reverse scans, excitation between the larger rods gives higher resolution and is preferred. However any gain in resolution from exciting between the larger rods is offset by ejecting at lower q. Forward scans with ejection at $q = 0.80$ were compared to reverse scans with ejection at $q = 0.20$, with the +3 ions of renin substrate tetradecapeptide with a conventional quadrupole rod set and a rod set with a 2.0% added octopole field. In all cases 10 V dc was added between the rods. Figure 5.10a shows the resolution achieved with a conventional rod set with forward scanning and ejection at $q = 0.80$, at 3000 Th/s scan speed and a step size of 0.08 mass units. The resolution is just sufficient to separate the isotopic peaks. Figure 5.10b shows the peak shape and resolution with the quadrupole with a 2.0% added octopole field, dipole excitation between the smaller rods, ejection at $q = 0.80$, a forward scan at 3000 Th/s, and step size of 0.08 mass units. Although the resolution is slightly lower than with a conventional rod set, the isotopic peaks are (just) resolved. With dipole excitation between the larger rods, reverse scanning and ejection at $q = 0.20$ at 3000 Th/s and a step size of 0.08 mass units, it was not possible to resolve the isotopic peaks, Figure 5.10c. Thus, of all the operating modes investigated here, dipole excitation between the smaller rods with ejection at high q is preferred when ions of a broad range of m/z are to be mass analyzed.
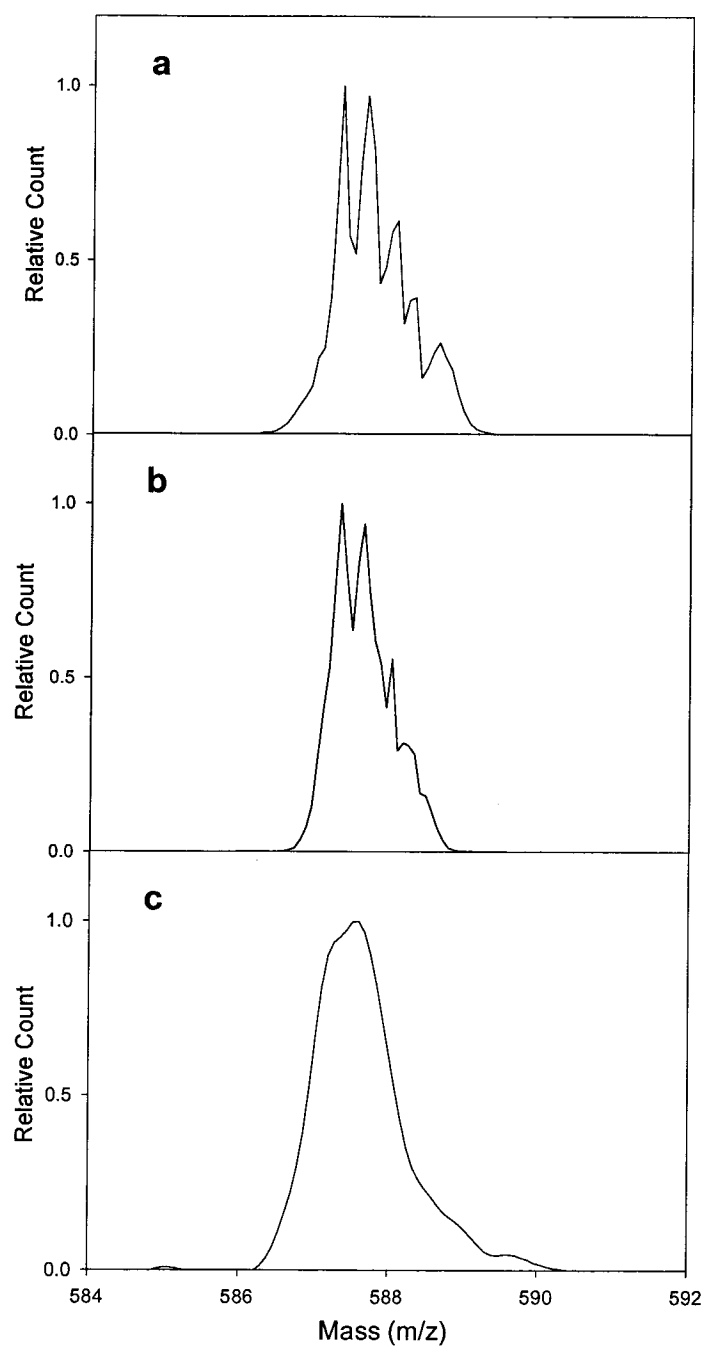
Figure 5.10 Axial ejection of +3 ions of renin substrate tetradecapeptide with dipole excitation applied to a) conventional rods with a forward scan and ejection at $q = 0.80$, b) the smaller rods of a quadrupole with a 2.0% octopole field with a forward scan and ejection at $q = 0.80$ and c) the larger rods of a quadrupole with a 2.0% octopole field with a reverse scan and ejection at $q = 0.20$. The scan speed in all cases is 3000 Th/s.

5.3.5 Ejection Efficiencies

With trapped ions, the operating conditions can be chosen to give the highest resolution or to give the highest sensitivity at each scan speed. Lowering the exit barrier increases sensitivity but decreases resolution. The ejection efficiencies of the conventional rod set and the rod set with a 2.0% added octopole field were measured with the results shown in Table 5.2. Here the system was optimized for the highest resolution with dipole excitation to eject ions at $q = 0.80$ with forward scans. The ejection efficiency decreases as the scan speed increases. The two rod sets show similar efficiencies. The system was then optimized for the highest ejection efficiency while keeping $R_{1/2} \approx 1000$ at each scan speed, and the ejection efficiencies with the quadrupole with a 2.0% added octopole field were re-measured, with the results shown in Table 5.3. The ejection efficiencies here are higher, with the greatest increases at the higher scan speeds. Hager found efficiencies of 2-18% with ejection of ions from q2 of a triple quadrupole system with operating pressures of ca. $1x10^{-4}$ Torr to $2x10^{-3}$ Torr [72]. Higher pressures gave higher efficiencies. Because of the much higher operating pressures in those experiments, the results cannot be compared directly to the experiments here.

Table 5.3 Ejection efficiencies (%) with the system optimized for the highest resolution.

Scan speed Th/s	Conventional quadrupole	Quadrupole with a 2.0% added octopole field
15	30	60
600	2.3	2.0
1500	2.0	1.8
3000	1.3	1.0
5000	0.5	0.4

Table 5.4 Ejection efficiencies with a quadrupole with a 2.0% added octopole field and the system optimized for the highest sensitivity at $R_{1/2} \approx 1000$.

Scan speed (Th/s)	Ejection efficiency (%)
15	67
267	38
671	5.6
1706	3.7
2542	2.5
3917	2.4

5.4 Summary

Mass selective axial ejection of ions with a quadrupole with a 2.0% added octopole field is possible. With low scan speeds of 10-15 Th/s, resolution of several thousand was achieved. At higher scan speeds, up to 5000 Th/s, at least unit resolution is possible. Comparison of different excitation modes shows that the optimum operating mode of MSAE with this quadrupole is forward scanning and ejection at $q = 0.80$ with dipole excitation applied to the smaller rods. Nevertheless for some applications where a large mass range need not be scanned, reverse scanning with dipole excitation applied to the larger rods and ejection at $q = 0.80$ can also be used to give high resolution.

Chapter 6 Mass Analysis Using an Island of Stability with a Quadrupole with a 2.0% Added Octopole Field

6.1 Introduction

This chapter describes experimental investigations of mass analysis using an "island of stability" with a linear quadrupole with 2.0% added octopole field. The theory behind this method of mass analysis will be explained briefly. Experimental settings and methods specific to these experiments will be discussed. Results from these experiments are compared to previous simulation studies.

6.1.1 Theory and Background

Mass analysis with linear quadrupoles is also possible using islands of stability [76, 87]. These islands are formed by parametric excitation of ions, either with an auxiliary quadrupole rf field [76] or by amplitude modulation of the rf voltage [87]. In a pure quadrupole field the potential is described by equations (1.1) and (1.2).

With quadrupole excitation, the time dependent potential applied to the electrodes, $\varphi(t)$, is given by

$$\varphi(t) = U - V\cos(\Omega t - \gamma) - V'\cos(\omega t - \gamma') \qquad (6.1)$$

where V' is the amplitude of the quadrupole excitation voltage with angular frequency ω. With the initial phase angles γ and γ' set to zero for simplicity, motion of an ion in the potential of equations (1.1) and (6.1) is determined by

$$\frac{d^2x}{d\xi^2} + [a - 2q\cos(2\xi) - 2q'\cos(2\upsilon\xi)]x = 0 \qquad (6.2)$$

$$\frac{d^2y}{d\xi^2} - [a - 2q\cos(2\xi) - 2q'\cos(2\upsilon\xi)]y = 0 \qquad (6.3)$$

where the dimensionless parameters are defined as:

$$\xi = \frac{\Omega t}{2} \qquad a = \frac{8zeU}{m\Omega^2 r_0^2} \qquad q = \frac{4zeV}{m\Omega^2 r_0^2}$$

$$(6.4)$$

$$\nu = \frac{\omega}{\Omega} \qquad q' = \frac{4zeV'}{m\Omega^2 r_0^2} = q\frac{V'}{V}$$

where ν is the ratio of excitation angular frequency to drive rf angular frequency and q' is the ratio of excitation voltage to rf voltage of the specific m/z multiplied by its q-value.

The angular frequencies of ion motion, ω_u, (with $u = x$ or y) are given by equation (1.11). The excitation frequencies of ions with quadrupole excitation are described in section 1.3.3 through equation (1.14) ($\omega_{ex} = |l + \beta_u|\frac{\Omega}{K}$ where $K = 1,2,3...$ and

$l = 0, \pm 1 \pm 2,...$). If $\nu = \frac{Q}{P}$ where Q and P are integers, ions are excited when their β values satisfy

$$\frac{Q}{P} = \frac{|l + \beta_u|}{K} \qquad (6.5)$$

103

The stability diagram splits into islands, with multiple operating tips available for mass analysis [76, 87]. Figure 6.1 and Figure 6.2 (adapted from reference 77) show the stability boundaries and islands of stability calculated for a quadrupole with a 2.0% added octopole field when a>0 and a<0 respectively. Ions can be mass analyzed by adjusting the applied rf and dc voltages to place the ions at the tip of an island. A mass scan is performed by changing the rf and dc voltages with fixed ratio U/V to bring ions of different m/z to the tip of the stability island. At the same time, the excitation amplitude, V', can be scanned to keep q' constant [76, 77, 87]. The excitation parameters v and q' are adjusted to give islands spaced such that a scan line passes through the tip of an island without intersecting other islands.
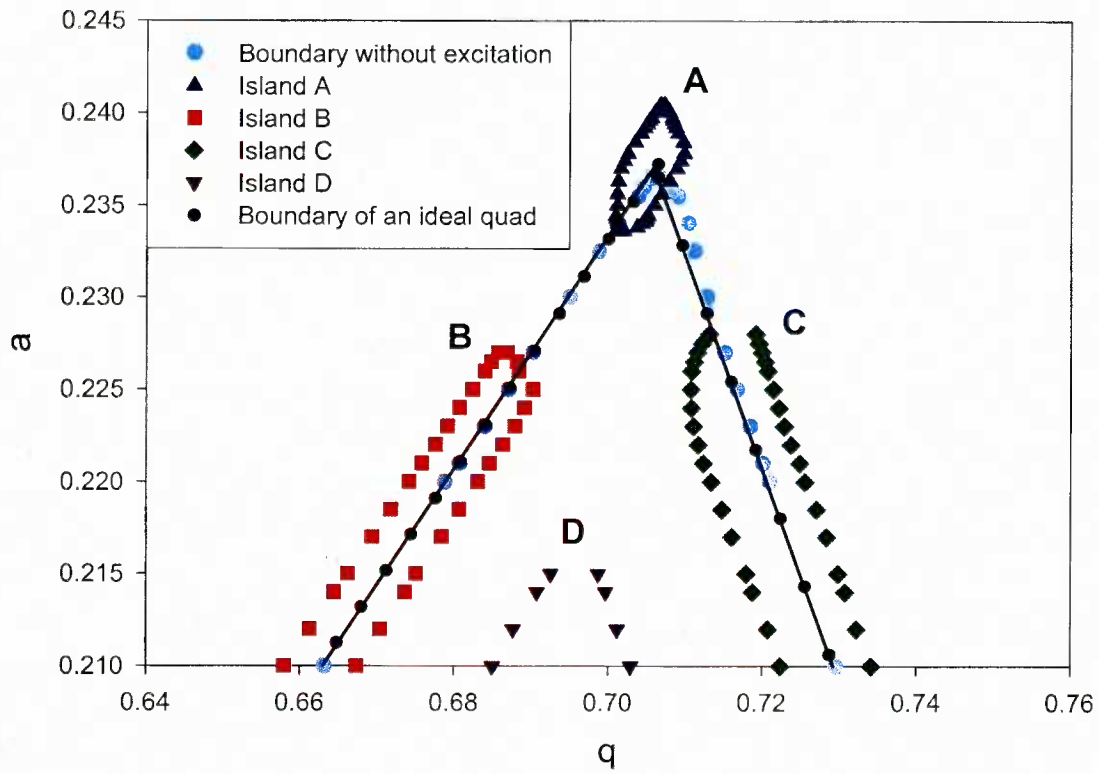
Figure 6.1 Stability boundaries and islands of stability ($q' = 0.02$, $\nu = 9/10$) for a quadrupole with 2.0% added octopole field with $a > 0$.
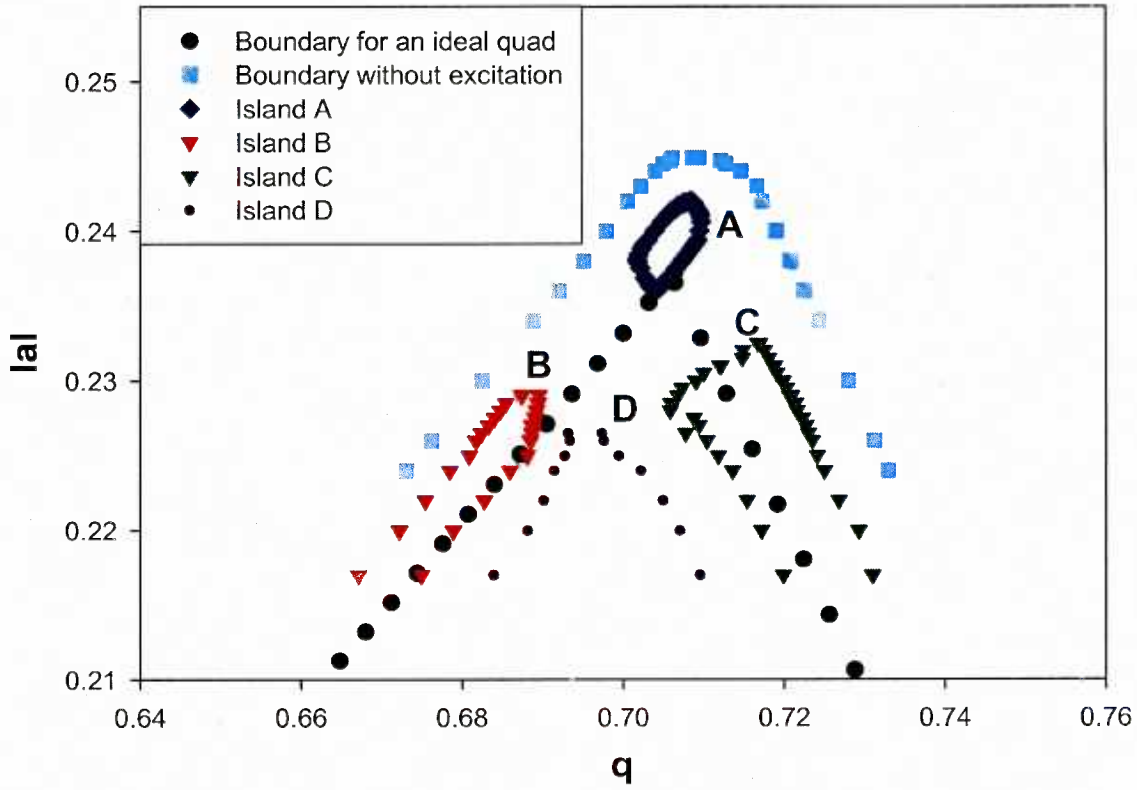
Figure 6.2 Stability boundaries and islands of stability ($q' = 0.02$, $v = 9/10$) for a quadrupole with 2.0% added octopole field with $a < 0$.

Recently, extensive computer simulations of mass analysis using islands of stability have been described for linear quadrupoles with added octopole fields [77]. Stability boundaries, island positions, peak shapes and ion transmission for linear quadrupoles with octopole fields of up to 4% were calculated. With an added octopole field, conventional mass analysis is possible with the dc voltage applied to the rods so that the Mathieu parameter $a > 0$; with the dc polarity reversed so that $a < 0$, conventional operation results in very low resolution [56]. However the computer simulations [77] suggest that when $a < 0$, mass analysis comparable to that with $a > 0$ should be possible, provided an island of stability is used with operation at the correct tip. In this case there is

little practical analytical advantage in running with $a < 0$, because adequate performance can be obtained with $a > 0$ and without use of an island. However the observation that use of an island allows mass analysis when a<0 demonstrates that islands might generally be useful to overcome at least some field imperfections in quadrupole mass filters.

6.2 Experimental

Experiments were performed using the single quadrupole instrument and the quadrupole rod set with 2.0% added octopole field described in section 2.1. Voltages applied to the various elements are shown in Table 6.1. With the positive dc applied to the smaller (x) rods, $a > 0$; with the positive dc applied to the larger (y) rods, $a < 0$. With this rod set, there is a dc axis potential $A_0 U$ in addition to the rod offset [56], where $A_0 = -0.020$ and $U = \pm 149$ V for $a > 0$ and $a < 0$ respectively. Thus the axis potential when $a > 0$ was +1.0 V and when $a < 0$, +4.0 V.

Table 6.1 Operating Voltages.

sprayer	+3700
curtain plate	+500
orifice	+50
Q0 rod offset	+2
interquad lens	-20
Q1 rod offset	$+1, a < 0; +4\ a > 0$
Exit lens 1	-100
Exit lens 2	-300

The quadrupole excitation circuit, Figure 6.3, was assembled in house and is similar

to that of Collings and Douglas [75]. The major difference is that capacitors that block

the dc of the quadrupole power supply from reaching Q1 were removed. For these

experiments the resolving dc of the quadrupole supply must be applied to the rods.

Removing the blocking capacitors increased the capacitive load on the quadrupole power

supply. To tune and balance the quadrupole power supply, the operating frequency was

lowered from 1.2 to 1.0 MHz and a 12.5 pF capacitor was added across the supply output.

Variable capacitors C_1 and C_2 (10-100 pF) were used to minimize the feedback from the

main rf into the auxiliary excitation electronics. The auxiliary rf was produced by the

SRS waveform generator described in section 2.1 and amplified by an rf power amplifier

(model 240L, ENI, Rochester, New York).
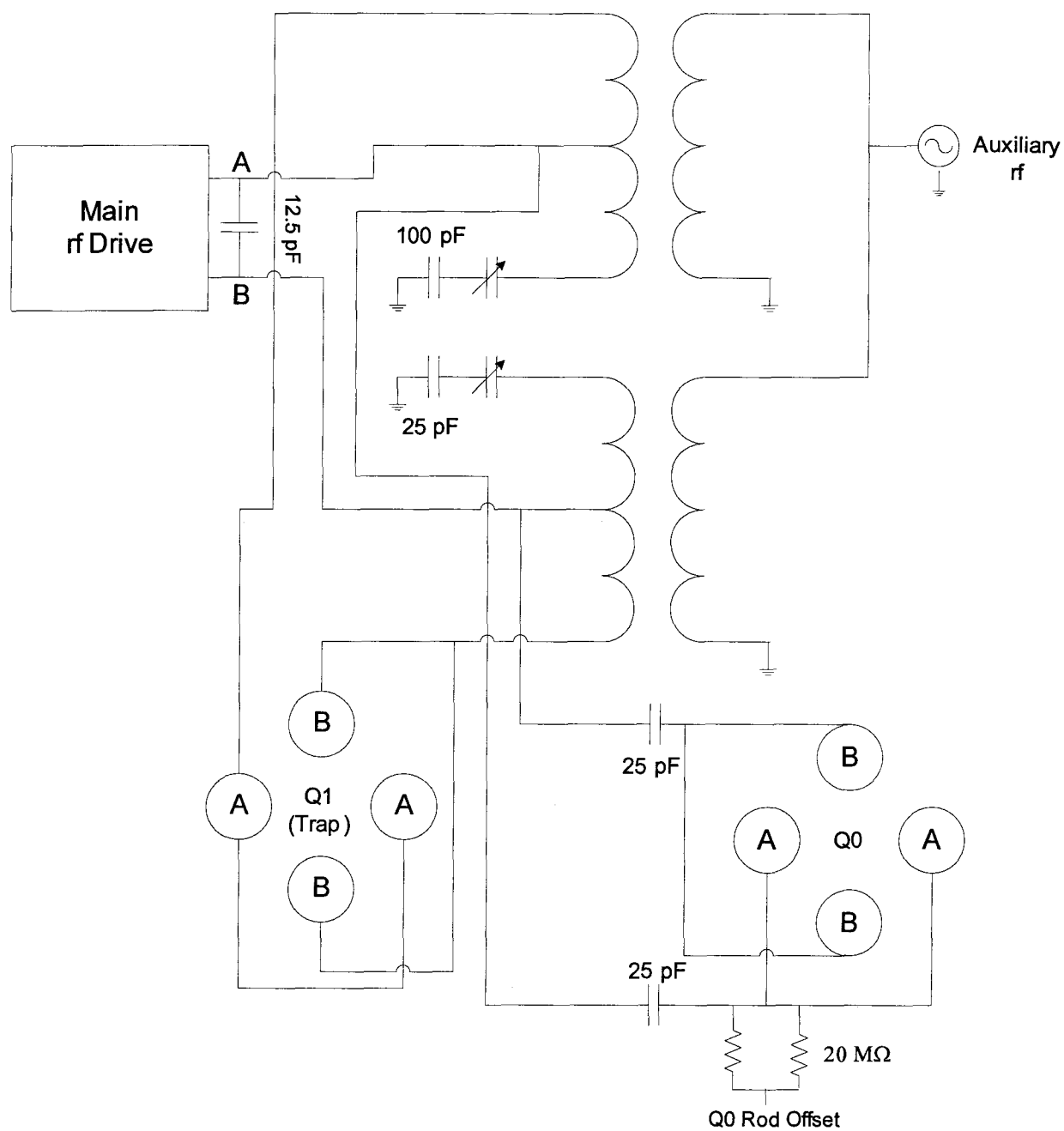
Figure 6.3 Quadrupole excitation circuit.

For these experiments, values of $q' = 0.020$ ($V' = 25$ V_{0-p} pole to ground) and

$v = 9/10$ were chosen because simulations show these values produce an island with a

scan line that does not intersect other islands. Because only a very limited mass range

was scanned in these experiments, V' was not scanned with mass. The island with the

greatest value of $|a|$ (termed "island A") was used. Mass analysis at the two tips of this

island with the greater and lesser values of $|a|$ was investigated. Scans over extended

mass ranges with different rf/dc ratios confirmed that scan lines through these tips do not

intersect other islands. The ratio of rf/dc voltages applied to the rods was set through

computer control by a software parameter RE1 with values between 1 and 255. The

numerical value of RE1 has no direct relation to mass resolution. For a given rf voltage,

the dc voltage, U, increases linearly with RE1. At m/z 609.28 and with the quadrupole

used here, the dc voltage pole to ground increased from 148.8 V at RE1=170

($a = 0.2358$) to 154.6 V at RE1=220 ($a = 0.2450$) to give ratios U/V from about

0.1694 to 0.1760. The system was mass calibrated with $a > 0$ and without excitation so

that the monoisotopic peak of protonated reserpine (exact mass 609.28) appeared at m/z

609.00. Spectra were then recorded with operation in the island with the dc applied to

give $a > 0$, and with and without the island and $a < 0$. The apparent m/z of the

monoisotopic peak shifts because the operating tips have q values that differ from the tip

without excitation and $a > 0$. Values of mass resolution are reported as resolution at half

height ($R_{1/2} = m/\Delta m_{1/2}$).

6.3 Results and Discussion

6.3.1 Positive a

Figure 6.4 shows spectra of reserpine ions recorded with $a > 0$ with and without excitation. With no excitation, (conventional mass analysis, Figure 6.4a) the resolution is about $R_{1/2} = 1500$. The resolution setting was RE1 = 170. With the excitation applied, a scan at the upper tip (greater $|a|$) of the stability island produces a similar spectrum (Figure 6.4b) with $R_{1/2} \approx 1100$. Here RE1 = 187, giving a greater slope to the scan line, demonstrating that the upper tip of this stability island is located above the tip of the stability diagram, as shown in simulations [77] and Figure 6.1. With this setting of RE1, and a conventional scan, no ions are detected because the scan line is outside the stability region. A scan at the lower tip of the stability island (lesser $|a|$) can be produced by reducing RE1 to 163. In this case a broad peak is produced, Figure 6.4c, and the isotopic peaks are not resolved. Lowering the resolution setting causes signal losses but does not improve the resolution. Thus the tip with the greater $|a|$ is necessary for mass analysis, as seen in the computer simulations [77]. The transmission and resolution in Figure 6.4a and 6.4b are comparable. With $a > 0$, there is little advantage in using the island of stability for mass analysis.

Figure 6.4 Mass analysis with $a > 0$ and (a) with no excitation (b) with the stability island at the tip with the greater $|a|$ and (c) with the stability island at the tip with the lesser $|a|$.

Figures 6.5a to 6.5h show mass analysis of reserpine ions in different stability islands

with $a > 0$. The resolution setting was changed so the scan line crossed different islands.

This experiment confirms the positions of the islands predicted by the simulations [77].

In Figure 6.5a the reserpine peak is at the lower tip of the stability island A since

RE1=165 and as was shown in Figure 6.4c the lower tip (lesser $|a|$) of the stability island

A is at RE1=163. In Figure 6.5b where RE1 is decreased to 150, the slope of the scan line

is decreased, and a scan crosses island B. The peak around m/z=595 starts to appear.

Figure 6.5c with RE1=145, shows this more clearly. By lowering RE1 further to 115,

Figure 6.5d, the scan line crosses islands B and C but not island A, producing the peaks

m/z=587 and 616. Figure 6.5e, with RE1=105, shows that with a further decrease of

RE1, the scan line still crosses islands B and C. When RE1 is reduced to 90, Figure 6.5f,

the scan line begins to cross island D, and a low intensity peak appears at m/z=601.

Figures 6.5g and 6.5h with lower RE1 values show that with additional decreases of the

slope of the scan line, the scan line passes through three stability islands, B,C and D with

the peak of the stability island C giving the most intense peak which is saturating the

detector.
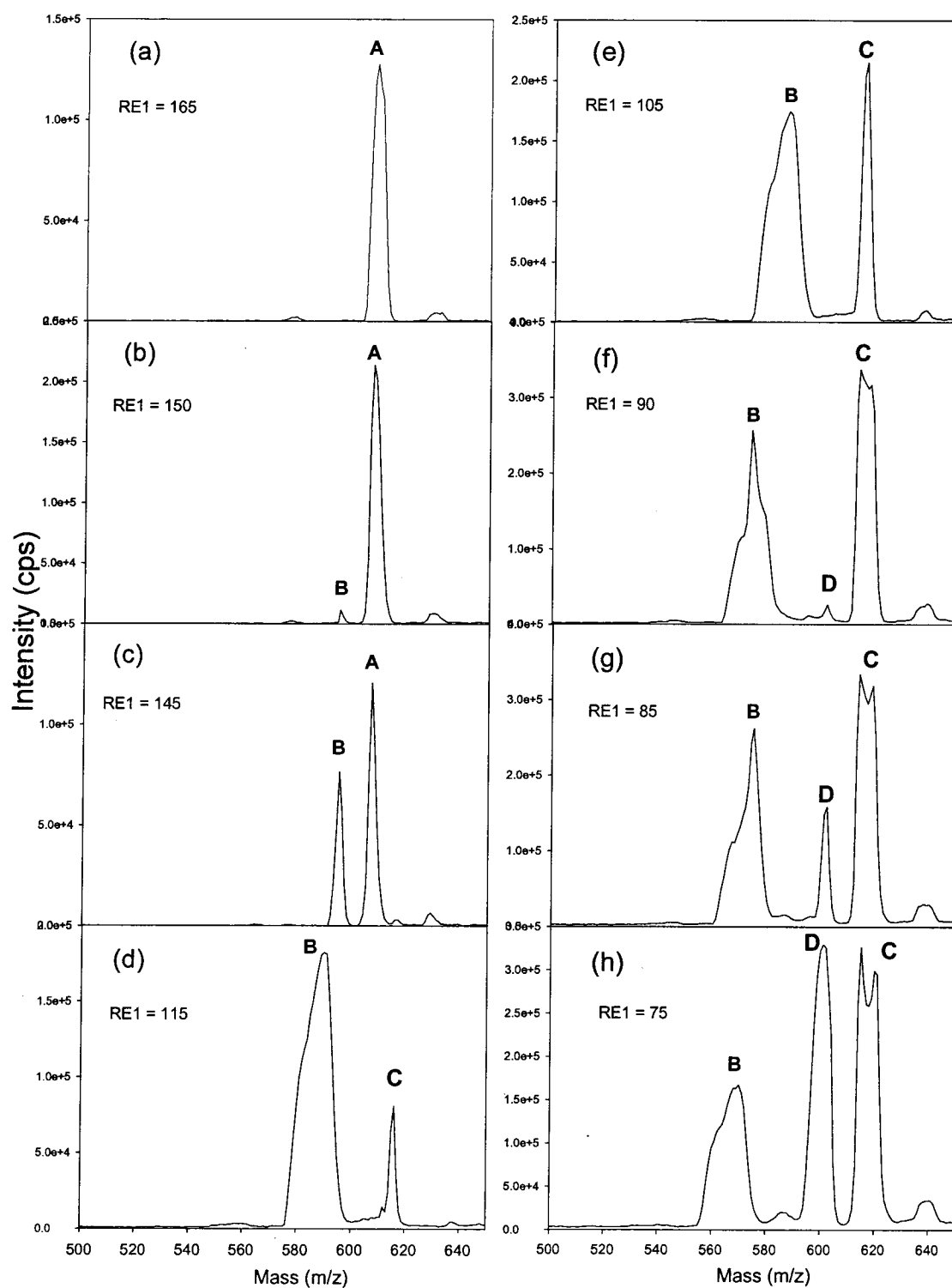
Figure 6.5 Mass analysis of reserpine ion in different stability islands with $a > 0$. Peaks are labeled with the name of the corresponding island used for mass analysis.

6.3.2 Negative a

Figure 6.6 shows spectra of reserpine ions with $a < 0$ recorded with and without excitation. With no excitation, Figure 6.6a, a broad peak (nominal $R_{1/2} = 125$) is produced and the isotopic peaks are not resolved. This is as expected and has been described previously [56]. For this scan RE1 = 220. An rf/dc ratio higher than that used for $a > 0$ is required because the stability boundaries shift out when $a < 0$ [56, 77]. With excitation, a scan at the tip with the greater $|a|$ results in a broad peak (nominal $R_{1/2} = 280$) (Figure 6.6b). Here RE1 = 194 which shows that the tip with greater $|a|$ is located under the tip of the stability diagram without excitation. With the excitation applied, and with scanning at the tip with the lesser $|a|$, the resolution is dramatically improved to $R_{1/2} \approx 1170$ (Figure 6.6c). The resolution in Figure 6.4c is comparable to that with conventional mass analysis with $a > 0$ and no excitation applied; the transmission is about six times less. This lower transmission was not seen in the simulations. At this tip, RE1 = 169, indicating the required rf/dc ratio is less than with no excitation and $a < 0$ and that the island tip is under the tip for operation without excitation. Therefore as predicted by the simulations, and as shown in Figure 6.2, with $a < 0$, the stability island is completely located under the tip of the stability diagram for a quadrupole with a 2.0% octopole field.
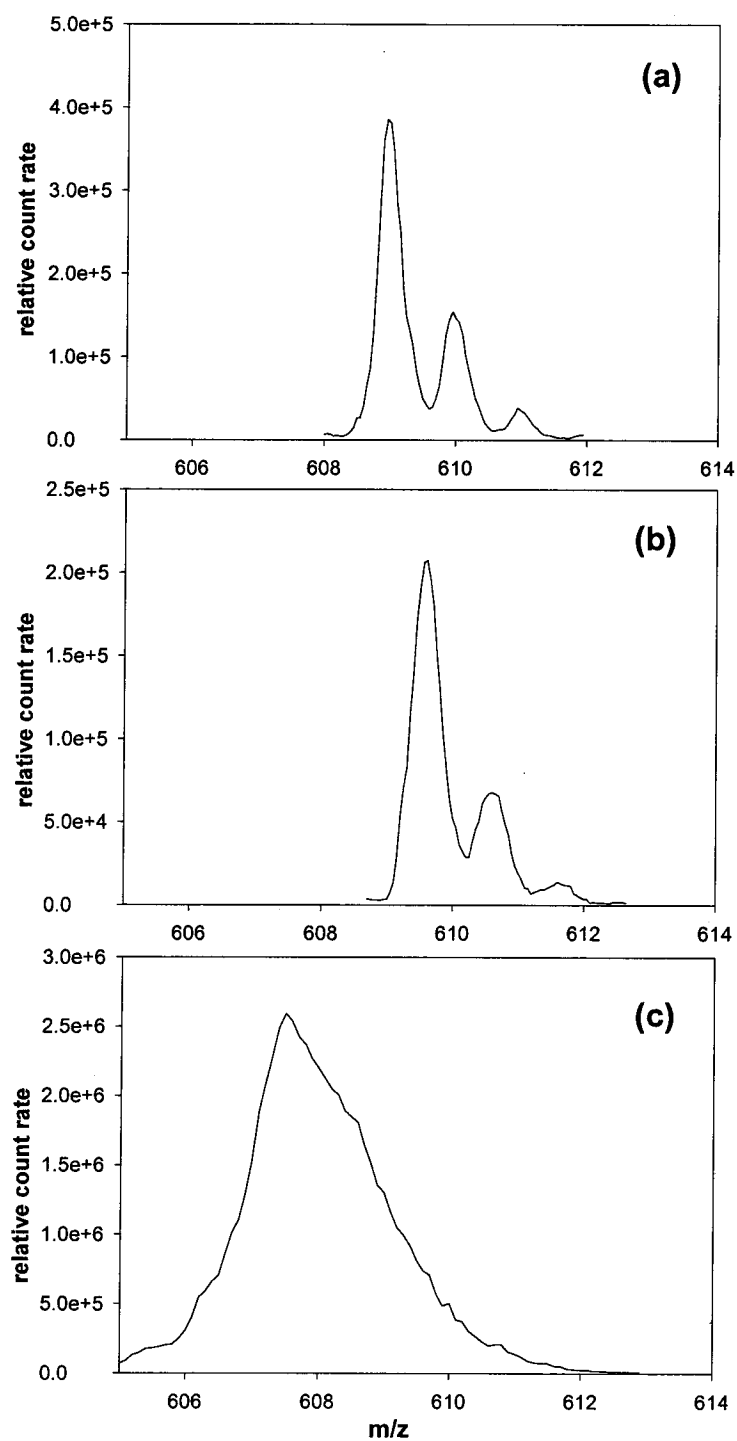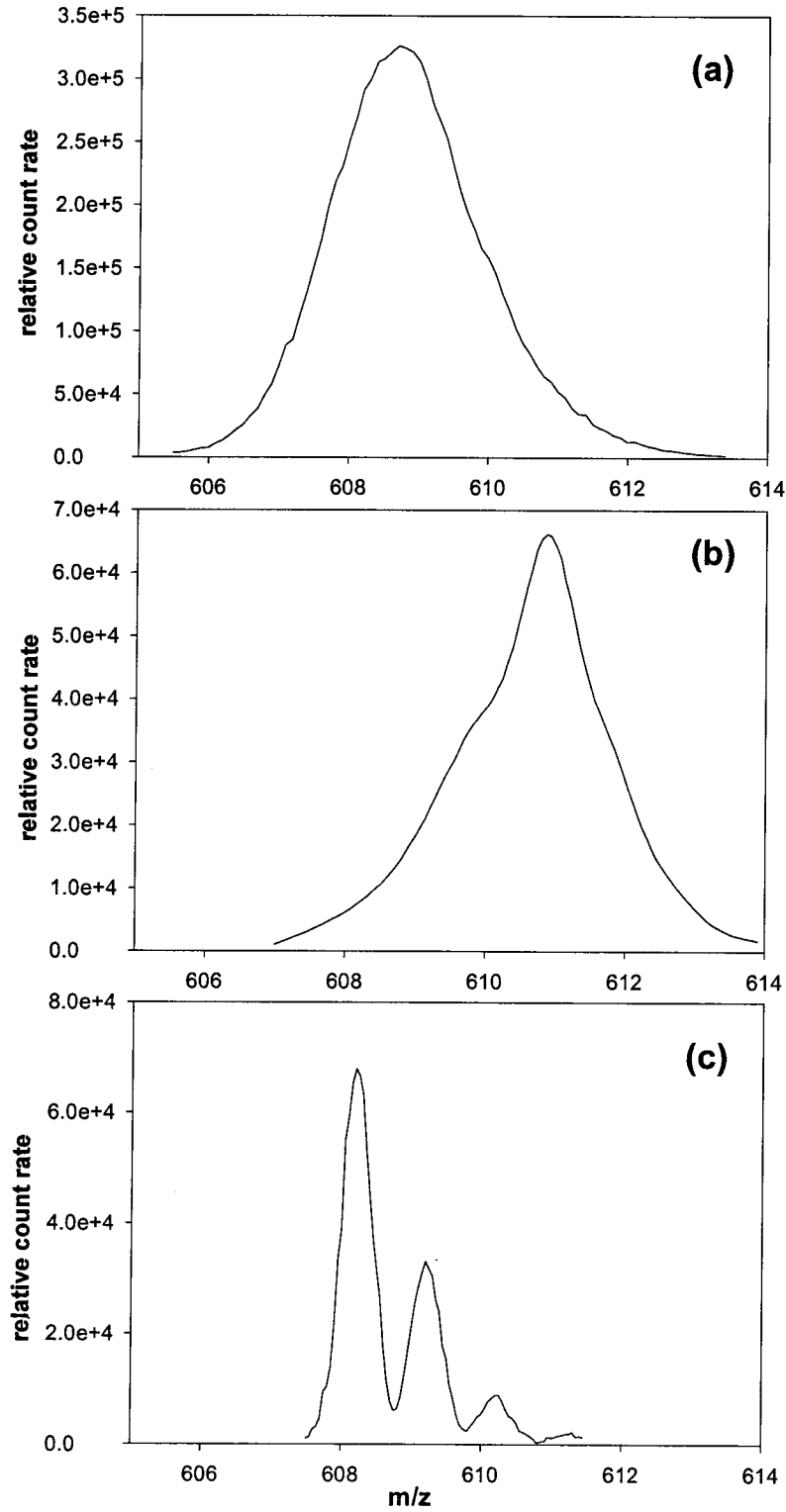
Figure 6.6 Mass analysis with $a < 0$ (a) with no excitation (b) with the stability island at the tip with the greater $|a|$ and (c) with the stability island at the tip with the lesser $|a|$.

6.3.3 Apparent Mass and Island Positions

The apparent m/z values of the peaks give approximately the q values of the operating tips. With $a > 0$ and without excitation, the stability diagram for a quadrupole with 2.0% added octopole field is very similar to that of a pure quadrupole field, and so the operating tip is at $q = 0.7060$ and $a = 0.237$ [7]. With other modes of operation, the q value of the operating tip can be calculated from

$$q = [(\text{apparent } m/z)/609.0]0.7060 \qquad (6.6)$$

and corresponding a values can be calculated using the instrumental parameters and measured dc voltages (U) during experiments as following

$$a = \frac{8 \times 1.602 \times 10^{-19} \times U}{(609.28/6.023 \times 10^{26}) \times (2 \times \pi \times 1.2 \times 10^{6})^{2} \times (4.5 \times 10^{-3})} \qquad (6.7)$$

These experimentally determined a and q values are shown in Table 6.2 and compared to the operating a and q values calculated in the simulations in ref 11. In some cases a range of q values is reported for the simulations because a rounded or poorly defined tip is formed. It is seen that the observed a and q values agree well with the a and q values of the simulations. Thus these experiments confirm the simulations, and show that the best resolution and peak shape are obtained with operation at the tip of the stability island with the greater $|a|$ with $a > 0$ and the tip with the lesser $|a|$ with $a < 0$.

Table 6.2 a and q values from experiments and simulation.

operating mode	apparent mass	experimental q	q from simulations	experimental a	a from simulations
a>0 tip with greater $|a|$	609.6	0.7067	0.7070	0.2392	0.2404
a>0 tip with lesser $|a|$	607.5	0.7043	0.7020-0.7040	0.2338	0.2336-0.2338
a<0 no excitation	608.6	0.7055	0.7040-0.7120	0.2451	0.2440-2450
a<0 tip with greater $|a|$	610.9	0.7082	0.7080-0.7086	0.2410	0.2419-2420
a<0 tip with lesser $|a|$	608.2	0.7051	0.7040	0.2353	0.2360

6.4 Summary

With a quadrupole with a 2.0% added octopole field, and with the dc applied to the rods so that the Mathieu parameter $a > 0$, mass analysis does not benefit greatly from the use of an island. However when $a < 0$, the added octopole severely limits the resolution with conventional mass analysis. By using the stability island when $a < 0$, the performance is greatly improved. In this case use of an island overcomes the deleterious effects of the added multipole field.

With mass analysis, the transmission of this rod set is very low (ca. 10^{-3}) compared to a conventional rod set. The reason is uncertain. Similar rod sets have shown transmission comparable to conventional rod sets up to $R_{1/2} = 2000$ [56]. Unfortunately, rod sets with added octopoles with this higher performance are no longer available here. Nevertheless, the results here qualitatively confirm the predictions of computer simulations of the position of stability boundaries without excitation, and island tip positions. Most importantly these experiments show that use of an island of stability may allow improved resolution or peak shape under conditions where an added multipole field, in this case an octopole field, otherwise degrades performance.

Chapter 7 Summary and Future Work

The increasing role of linear quadrupole ion traps and their advantages were discussed in chapter one of this thesis. Linear ion trap mass spectrometers were described in section 1.5. These instruments provide high resolution and scan speeds and have already been incorporated in several commercial instruments. It is well established that 3-D traps benefit from stretched or other geometries that introduce field distortions, described by the addition of higher order multipoles to the potential [40]. Douglas and co-workers [53, 55] were first to explore the addition of 2-12% higher order multipole fields to linear quadrupole ion traps. They reported higher MS/MS efficiencies and new methods of mass analysis with linear quadrupole ion traps with added multipole fields [56, 57, 77, 78]. These rod sets have the potential to become improved ion traps. Nevertheless, much work remains to investigate the effects of these multipoles on the performance of linear quadrupole rod sets operated as traps and mass filters. The work presented in this thesis was part of this investigation.

In this thesis different mass analysis methods for a quadrupole with a 2.0% added octopole field were described and experimental results were presented. Experiments using islands of stability confirm the results of previous computer simulations and demonstrate the possibility of mass analysis under conditions where the octopole term in the potential severely degrades conventional mass analysis.

Comparison of MSAE with a conventional quadrupole rod set and a quadrupole with a 2.0% added octopole field with different modes of excitation shows similar resolutions and ejection efficiencies, with somewhat higher resolution obtained with a conventional quadrupole rod set. Mass selective axial ejection with quadrupoles with added octopole

fields is possible with a resolution of several thousand and scan speeds of at least 2000 Th/s. Thus quadrupoles with added octopole fields can be used as rf/dc mass filters, demonstrate higher efficiency in MS/MS experiments, and can eject ions axially in a mass selective manner with high resolution and scan speed. Quadrupoles with added octopole fields show promise as improved ion traps, particularly for instruments where a linear trap is used as Q3 of a triple quadrupole.

In future, similar experiments like MSAE and mass analysis with islands of stability could be performed with quadrupoles with 2.6 and 4.0% octopole fields. To understand the ion motion during MSAE process, it might also be useful to simulate the fringing field region of these quadrupoles. As part of ongoing projects in this lab different methods of mass analysis with quadrupoles with 4-12% added hexapole fields are also under investigation.

References

1.   Paul, W.; Steinwedel, H. *Z. Naturforsch.* **1953**, *8a*, 448-450.

2.   Paul, W.; Reinhard, H. P.; Zahn, V. *Z. Physik* **1958**, *152*, 143-182.

3.   Paul, W.; Steinwedel, H. German Patent 944,900, 1956.

4.   Fischer, E. *Z. Physik* **1959**, *156*, 1-26.

5.   Fenn, J. B.; Mann, M.; Meng, C. K.; Wong, S. F.; Whitehouse, C. M. *Science* **1989**, *246*, 64-71.

6.   Karas, M.; Hillenkamp, F. *Anal. Chem.* **1988**, *60*, 2299-2301.

7.   Dawson, P. H. *Quadrupole Mass Spectrometry and Its Applications*; AIP Press: Woodbury, N.Y., 1985.

8.   March, R. E.; Hughes, R. J. *Quadrupole Storage Mass Spectrometry*; John Wiley & Sons: New York, 1989.

9.   Denison, D. R. *J. Vac. Sci. Technol.* **1971**, *8*, 266-269.

10.   Austin, W. E.; Holme, A. E.; Leck, J. H. In *Quadrupole Mass Spectrometry and its Applications*; Dawson, P. H., Ed.; Elsevier: Amsterdam, 1976, pp 121-151.

11.   Titov, V. V. *J. Am. Soc. Mass Spectrom.* **1998**, *9*, 70-87.

12.   Brubaker, W. M. *Advan. Mass Spectrom.* **1968**, *4*, 293-299.

13.   Dawson, P. H. *Adv. Electron. Electron Phys.* **1980**, *53*, 153-208.

14.   Dawson, P. H. *Int. J. Mass Spectrom. Ion Process.* **1977**, *25*, 375-392.

15.   Ehlert, T. C. *J. Phys. E* **1970**, *3*, 237-239.

16.   Hunter, K. L.; McIntosh, B. J. *Int. J. Mass Spectrom. Ion Process.* **1989**, *87*, 157-164.

17.   Brinkmann, U. *Int. J. Mass Spectrom. Ion Phys.* **1972**, *9*, 161-166.

18.   Stafford, G. C.; Kelley, P. E.; Syka, J. E. P.; Reynolds, W. E.; Todd, J. F. J. *Int. J. Mass Spectrom. Ion Process.* **1984**, *60*, 85-98.

19.   Church, D. A. *J. Appl. Phys.* **1969**, *40*, 3127-3134.

20.   Douglas, D. J.; Frank, A. J.; Mao, D. M. *Mass Spectrom. Rev.* **2004**, *23*, 1-29.

21.   Dolinkowski, G. G.; Kristo, M. J.; Enke, C. G.; Watson, J. T. *Int. J. Mass Spectrom. Ion Process.* **1988**, *82*, 1-15.

22.   Beaugrand, C.; Jaouen, D.; Mestdagh, H.; Rolando, C. *Anal. Chem.* **1989**, *61*, 1447-1453.

23.   Chen, Y. L.; Campbell, J. M.; Collings, B. A.; Konermann, L.; Douglas, D. J. *Rapid Commun. Mass Spectrom.* **1998**, *12*, 1003-1010.

24.   Prestage, J. D.; Dick, G. J.; Maleki, L. *J. Appl. Phys.* **1989**, *66*, 1013-1017.

25.   Prestage, J. D.; Dick, G. J.; Maleki, L. *IEEE Trans on. Instrum. and Meas.* **1991**, *40*, 132-136.

26.   Douglas, D. J. US Patent 5,179,278, 1993.

27.   Cha, B. C.; Blades, M.; Douglas, D. J. *Anal. Chem.* **2000**, *72*, 5647-5654.

28.   Voyksner, R. D.; Lee, H. *Rapid Commun. Mass Spectrom.* **1999**, *13*, 1427-1437.

29.   Dresch, T.; Gulcicek, E. E.; Whitehouse, C. M. US Patent 5,689,111, 1997.

30.   Hardman, M.; Makarov, A. A. *Anal. Chem.* **2003**, *75*, 1699-1705.

31.   Senko, M. W.; Hendrickson, C. L.; Emmett, M. R.; Shi, S. D. H.; Marshall, A. G. *J. Am. Soc. Mass Spectrom.* **1997**, *8*, 970-976.

32.   Sannes-Lowery, K.; Griffey, R. H.; Kruppa, G. H.; Speir, J. P.; Hofstadler, S. A. *Rapid Commun. Mass Spectrom.* **1998**, *12*, 1957-1961.

33.   Campbell, J. M.; Collings, B. A.; Douglas, D. J. *Rapid Commun. Mass Spectrom.* **1998**, *12*, 1463-1474.

34.   Collings, B. A.; Campbell, J. M.; Mao, D. M.; Douglas, D. J. *Rapid Commun. Mass Spectrom.* **2001**, *15*, 1777-1795.

35.   Whitehouse, C. M.; Dresch, T.; Andrien, B. A. US Patent 6,011,259, 2000.

36.   Sudakov, M.; Konenkov, N.; Douglas, D. J.; Glebova, T. *J. Am. Soc. Mass Spectrom.* **2000**, *11*, 10-18.

37.   Feynman, R. P.; Leighton, R. B.; Sands, M. *The Feynman Lectures on Physics V2*; Addison-Wesley, 1963.

38.   Szilagyi, M. *Electron and Ion Optics*; Plenum Press: New York, 1988.

39.   Douglas, D. J.; Glebova, T. A.; Konenkov, N. V.; Sudakov, M. Y. *Tech. Phys.* **1999**, *44*, 1215-1219.

40.   Franzen, J.; Gabling, R.-H.; Schubert, M.; Wang, Y. In *Practical Aspects of Ion Trap Mass Spectrometry Volume I. Fundamentals of Ion Trap Mass Spectrometry*; March, R. E., Todd, J. F. J., Eds.; CRC Press: Boca Raton FL, 1995, pp 49-167.

41.   Titov, V. V. *Int. J. Mass Spectrom. Ion Process.* **1995**, *141*, 37-43.

42.   Gibson, J. R.; Taylor, S. *Rapid Commun. Mass Spectrom.* **2000**, *14*, 1669-1673.

43.   Gibson, J. R.; Taylor, S. *Rapid Commun. Mass Spectrom.* **2003**, *17*, 1051-1055.

44.   Douglas, D. J.; Konenkov, N. V. *Rapid Commun. Mass Spectrom.* **2002**, *16*, 1425-1431.

45.   Louris, J.; Stafford, G.; Syka, J. E. P.; Taylor, D., *Proceedings of ASMS Conference on Mass Spectrometry and Allied Topics*, Washington D.C., 31 May - 5 June **1992**.

46.   Franzen, J.; Gabling, R.-H.; Heinen, G.; Weiss, G.: US Patent 5,028,777, 1991.

47.   Wang, Y.; Franzen, J. *Int. J. Mass Spectrom. Ion Process.***1992**, *112*, 167-178.

48.   Wang, Y.; Franzen, J.; Wanczek, K. P. *Int. J. Mass Spectrom. Ion Process.* **1993**, *124*, 125-144.

49.   Wang, Y.; Franzen, J. *Int. J. Mass Spectrom. Ion Process.* **1994**, *132*, 155-172.

50.   Sudakov, M. *Int. J. Mass Spectrom.* **2001**, *206*, 27-43.

51.   Franzen, J. *Int. J. Mass Spectrom. Ion Process.* **1994**, *130*, 15-40.

52.   Soudakov, M.; Douglas, D. J.; Ding, C. F.: US Patent 6,897,438, 2005.

53.   Sudakov, M.; Douglas, D. J. *Rapid Commun. Mass Spectrom.* **2003**, *17*, 2290-2294.

54.   Douglas, D. J.; Ding, C. F.; Londry, F. US Patent 7,141,789, 2006.

55.   Konenkov, N.; Londry, F.; Ding, C. F.; Douglas, D. J. *J. Am. Soc. Mass Spectrom.* **2006**, *17*, 1063-1073.

56.   Ding, C. F.; Konenkov, N. V.; Douglas, D. J. *Rapid Commun. Mass Spectrom.* **2003**, *17*, 2495-2502.

57.   Michaud, A. L.; Frank, A. J.; Ding, C.; Zhao, X. Z.; Douglas, D. J. *J. Am. Soc. Mass Spectrom.* **2005**, *16*, 835-849.

58.   Senko, M. W.: US Patent 6,403,955, 2002.

59.   Welling, M.; Schuessler, H. A.; Thompson, R. I.; Walther, H. *Int. J. Mass Spectrom.* **1998**, *172*, 95-114.

60. Bier, M. E.; Syka, J. E. P. US Patent 5,420,425, 1995.

61. Schwartz, J. C.; Senko, M. W.; Syka, J. E. P. *J. Am. Soc. Mass Spectrom.* **2002**, *13*, 659-669.

62. Ouyang, Z.; Wu, G. X.; Song, Y. S.; Li, H. Y.; Plass, W. R.; Cooks, R. G. *Anal. Chem.* **2004**, *76*, 4595-4605.

63. Dawson, P. H.; Meunier, M. *Int. J. Mass Spectrom. Ion Process.* **1979**, *29*, 269-299.

64. Dawson, P. H. *Int. J. Mass Spectrom. Ion Process.* **1985**, *67*, 267-276.

65. Holme, A. E. *Int. J. Mass Spectrom. Ion Process.* **1976**, *22*, 1-5.

66. Holme, A. E.; Sayyid, S.; Leck, J. H. *Int. J. Mass Spectrom. Ion Process.* **1978**, *26*, 191-204.

67. Weaver, H. E.; Mathers, G. E. *Dyn. Mass Spectrom.* **1978**, *5*, 41-54.

68. Dawson, P. H.; Meunier, M.; Tam, W. C. *Adv. Mass Spectrom.* **1980**, *8B*, 1629-1637.

69. Yang, J.; Leck, J. H. *Vacuum* **1982**, *32*, 691-694.

70. Ross, D. N.; Leck, J. H. *Int. J. Mass Spectrom. Ion Process.* **1983**, *49*, 1-9.

71. Hager, J. W. *Rapid Commun. Mass Spectrom.* **1999**, *13*, 740-748.

72. Hager, J. W. *Rapid Commun. Mass Spectrom.* **2002**, *16*, 512-526.

73. Hopfgartner, G.; Husser, C.; Zell, M. *J. Mass Spectrom.* **2003**, *38*, 138-150.

74. Le Blanc, J. C. Y.; Hager, J. W.; Ilisiu, A. M. P.; Hunter, C.; Zhong, F.; Chu, I. *Proteomics* **2003**, *3*, 859-869.

75. Collings, B. A.; Douglas, D. J. *J. Am. Soc. Mass Spectrom.* **2000**, *11*, 1016-1022.

76. Konenkov, N. V.; Cousins, L. M.; Baranov, V. I.; Sudakov, M. Y. *Int. J. Mass Spectrom.* **2001**, *208*, 17-27.

77. Konenkov, N.; Zhao, X. Z.; Xiao, Z. L.; Douglas, D. J. *J. Am. Soc. Mass Spectrom.* **2007**, *18*, 826-834.

78. Moradian, A.; Douglas, D. J. *Rapid Commun. Mass Spectrom.* **2007**, *21*, 3306-3310.

79. Hager, J. W.; Londry, F. A. US Patent 7,019,290, 2006.

80. Hager, J. W. US Patent 6,028,308, 2000.

81. Londry, F. A.; Hager, J. W. *J. Am. Soc. Mass Spectrom.* **2003**, *14*, 1130-1147.

82. Dehmelt, H. G. *Adv. Atom. Mol. Phys.* **1967**, *3*, 53-72.

83. Hager, J. W. US Patent 5,998,787, 1999.

84. Landau, L. D.; Lifshitz, E. M. *Mechanics*; Pergamon Press: New York, NY, 1960, pp 74-93.

85. Goeringer, D. E.; Whitten, W. B.; Ramsey, J. M.; McLuckey, S. A.; Glish, G. L. *Anal. Chem.* **1992**, *64*, 1434-1439.

86. Williams, J. D.; Cox, K. A.; Cooks, R. G.; McLuckey, S. A.; Hart, K. J.; Goeringer, D. E. *Anal. Chem.* **1994**, *66*, 725-729.

87. Konenkov, N. V.; Korolkov, A. N.; Machmudov, M. *J. Am. Soc. Mass Spectrom.* **2005**, *16*, 379-387.